Electronic Thesis and Dissertation Repository

6-26-2019 2:00 PM

Remote Navigation and Contact-Force Control of Radiofrequency Ablation Catheters

Daniel Gelman
The University of Western Ontario

Supervisor
Drangova, Maria
The University of Western Ontario

Graduate Program in Biomedical Engineering
A thesis submitted in partial fulfillment of the requirements for the degree in Doctor of Philosophy
© Daniel Gelman 2019

Follow this and additional works at: https://ir.lib.uwo.ca/etd

Part of the Biomedical Devices and Instrumentation Commons

Abstract

Atrial fibrillation (AF), the most common and clinically significant heart rhythm disorder, is characterized by rapid and irregular electrical activity in the upper chambers resulting in abnormal contractions. Radiofrequency (RF) cardiac catheter ablation is a minimally invasive curative treatment that aims to electrically correct signal pathways inside the atria to restore normal sinus rhythm. Successful catheter ablation requires the complete and permanent elimination of arrhythmogenic signals by delivering transmural RF ablation lesions contiguously near and around critical cardiac structures. These procedures are complex and technically challenging and, even when performed by the most skilled physician, nearly half of patients undergo repeat procedures due to incomplete elimination of the arrhythmogenic pathways. This thesis aims to incorporate innovative design to improve catheter stability and maneuverability through the development of robotic platforms that enable precise placement of reproducibly durable ablation lesions.

The first part of this thesis deals with the challenges to lesion delivery imposed by cardiorespiratory motion. One of the main determinants of the delivery of durable and transmural RF lesions is the ability to define and maintain a constant contact force between the catheter tip electrode and cardiac tissue, which is hampered by the presence of cardiorespiratory motion. To address this need, I developed and evaluated a novel catheter contact-force control device. The compact electromechanical add-on tool monitors catheter-tissue contact force in real-time and simultaneously adjusts the position of a force-

sensing ablation catheter within a steerable sheath to compensate for the change in contact force. In a series of *in vitro* and *in vivo* experiments, the contact-force control device demonstrated an ability to: a) maintain an average force to within 1 gram of a set level; b) reduce contact-force variation to below 5 grams (2-8-fold improvement over manual catheter intervention); c) ensure the catheter tip never lost contact with the tissue and never approached dangerous force levels; and importantly, d) deliver reproducible RF ablation lesions regardless of cardiac tissue motion, which were of the same depth and volume as lesions delivered in the absence of tissue motion.

In the second part of the thesis, I describe a novel steerable sheath and catheter robotic navigation system, which incorporates the catheter contact-force controller. The robotic platform enables precise and accurate manipulation of a remote conventional steerable sheath and permits catheter-tissue contact-force control. The robotic navigation system was evaluated *in vitro* using a phantom that combines stationary and moving targets within an *in vitro* model representing a beating heart. An electrophysiologist used the robotic system to remotely navigate the sheath and catheter tip to select targets and compared the accuracy of reaching these targets performing the same tasks manually. Robotic intervention resulted in significantly higher accuracy and significantly improved the contact-force profile between the catheter tip and moving tissue-mimicking material.

Our studies demonstrate that using available contact-force information within a robotic system can ensure precise and accurate placement of reliably transmural RF ablation lesions. These robotic systems can be valuable tools used to optimize RF lesion delivery techniques and ultimately improve clinical outcomes for AF ablation therapy.

Keywords

Summary for Lay Audience

Atrial Fibrillation (AF) is a common heart rhythm disorder often treated using catheters inserted in the heart to "burn" the tissue responsible for the arrhythmia (*i.e.* to make lesions). Radiofrequency (RF) catheter ablation strategies to treat AF are complex, technically challenging, and require a high degree of skill and physical effort. Furthermore, the motion of the heart as it beats and the patient breathes can affect the contact the catheter tip makes with the heart during the therapy delivery. This makes it very difficult for the physician to deliver lesions effectively. Because of these problems, it is not uncommon that lesions are delivered inadequately, leaving untreated tissue that can result in the recurrence of AF symptoms. Currently, nearly half of all patients return for a second procedure.

To avoid repeat procedures, ablation lesions must be precisely placed in specific locations within the heart chamber – lesions must be adjacent to one another and share a common border. Additionally, these lesions must be reliably durable and cover the entire heart-wall thickness. One key element that governs lesion production is stable contact force between the catheter tip and heart tissue. With the advent of force-sensing ablation catheters, physicians can monitor the amount of force the catheter makes with the tissue in real-time. However, physicians are limited in controlling the force and have no way to improve force stability and keep it constant during RF delivery.

My thesis describes the development and evaluation of two novel robotic technologies designed to address these problems. Specifically, I introduce the Catheter Contact-Force Controller (CFC) and the Steerable Sheath and Catheter Robotic Navigation System (SSC-RNS). These platforms are used in conjunction with standard, commercially available ablation instruments to provide automated catheter-tissue contact-force control and precise remote catheter navigation. I discuss their design and development as well as how these systems performed on a lab-bench and in pre-clinical studies. I show that the CFC is effective in stabilizing the force during lesion delivery, resulting in uniform lesions despite the presence of motion. Use of the SSC-RNS led to improved location accuracy of catheter navigation compared to manual procedures.

Co-Authorship Statement

The research presented in each chapter has been conducted and written primarily by the principal author, Daniel Gelman, and guided and supported by the research supervisor, Dr. Maria Drangova. This thesis is presented in an integrated article format, the chapters of which are based on the following publications that are either published, accepted for publication, or in preparation for submission:

The material presented in Chapter 2 has been published in:

Daniel Gelman, Mohammad A. Tavallaei, Allan C. Skanes, and Maria Drangova
"Design and Evaluation of a Catheter Contact-Force Controller
for Cardiac Ablation Therapy"
IEEE Transactions on Biomedical Engineering
vol. 63, no. 11, pp. 2301-2307, 2016

Daniel Gelman designed and developed the catheter contact-force controller, linear motion stage, and electronic systems; designed and implement the control algorithm, performed all *in vitro* experiments, collected and analyzed data. Dr. Mohammad A. Tavallaei assisted in designing the embedded electronic system, implementing the control algorithm, and preparing the manuscript. Dr. Allan C. Skanes was involved in generating the idea and assisted in preparing the manuscript. Dr. Maria Drangova was involved in generating the idea, analyzed the results, and assisted in the preparation of the paper. All authors approved the final manuscript.

The material presented in Chapter 3 is accepted for publication in:

Daniel Gelman designed, developed and implemented new control algorithms; designed and developed an RF-enabled linear motion phantom; developed software to integrate the catheter contact-force controller with the electro-anatomical mapping system; executed *in vitro* experiments; coordinated *in vivo* experiments; collected and analyzed data. Dr. Allan C. Skanes executed the *in vivo* experiments; analyzed the results; and assisted in preparing the manuscript. Dr. Douglas L. Jones executed the *in vivo* experiments and assisted in preparing the manuscript. Michael Timofeyev developed specialized software to enable integration between the catheter contact-force controller and electro-anatomical mapping system. Tal Baron was involved in project coordination and edited the manuscript. Dr. Maria Drangova coordinated *in vivo* experiments; assisted in collecting and analyzing data and assisted in preparing the manuscript. All authors approved the final manuscript.

The material presented in Chapter 4 is in preparation for submission in:

Daniel Gelman designed and developed the robotic system, the input device, and the linear motion phantom; designed and developed the electronic control system; designed, developed and implemented the control algorithms; coordinated the experiments, collected and analyzed the data. Dr. Allan C. Skanes executed the *in vitro* experiments, discussed the results, and assisted in preparing the manuscript. Dr. Maria Drangova coordinated the *in vitro* experiments; collected the data; and assisted in preparing of the manuscript.

This thesis has been written by Daniel Gelman under the supervision of Dr. Maria Drangova.

Acknowledgments

Foremost, I would like to start by expressing my sincere gratitude to my supervisor and mentor, Dr. Maria Drangova. The work presented in this thesis would not have been possible without her expertise, patience, support, and importantly, the immense effort she put to establish an academic infrastructure designed to allow her students thrive. Maria has been a source of guidance and direction; yet, gave me the freedom to explore new ideas and take advantage of the opportunities that presented itself. Maria led me to the door, taught me how to open it, and gave me the tools needed to walk through it. I am truly grateful and privileged to be one of her Ph.D. students.

I would also like to thank the members of my advisory committee for their guidance and support throughout my graduate studies. Dr. David Holdsworth and Dr. Allan Skanes challenged me with difficult questions, encouraged me to develop and improve my skills, and always showed interested and enthusiasm for my research. I am grateful to have David as a mentor and fellow nerd who appreciates the art of 3D printing, open-source hardware, and electronics. I am especially thankful for the opportunity that I had to work with my clinical supervisor, Dr. Allan Skanes. Allan has consciously and unconsciously opened many doors leading to opportunities that have paved a career path beyond my graduate work.

I would like to thank all my fellow graduate students in Dr. Maria Drangova's, Dr. Terry Peters', Dr. David Holdsworth's, and Dr. Aaron Fenster's lab for your thoughtful

discussions, helpful criticisms, and most of all, for your friendships. Amazing friends like Golafsoun, Allie, Adam, Patricia, Ali K., Ali T., Jiro, Kamyar and many others, thank you all for making my time as a graduate student so memorable. I am especially thankful to Goli for being a true friend, always being available for a chat and giving me moral support over these long years. I am particularly grateful to Ali T. who dedicated a considerable amount of his time to discuss ideas and approaches and taught me technical engineering skills in the early years of this project.

I cannot describe how thankful I am to the technical staff and basement dwellers of Robarts Research Institute. First, I would like to thank Hristo Nikolov, Steve Pollmann, Chris Norley, and Tom Chmiel. Although we wasted countless hours sharing stories and talking about nonsense, I could always look to them for helpful discussion, design approaches, and solutions. I would also like to thank Ivailo Petrov and Joy Dunmore-Buyze for the continued support and dedicating so much of their time helping me with my experiments. I would like to thank John Moore and Paul Picot for sharing their expertise and providing advice, assistance, and helpful conversation throughout my research. I would like to thank Jacques Montreuil, Kevin Barker, and Chris Blake for all the advice in the machine shop. After struggling and ruining so many of my parts time after time, I could always reach out to any of them for help on the mill or lathe. Lastly, I would like to thank all the undergraduate and high school students, which I had the pleasure of supervising, I am grateful to impact the lives of future engineers and scientists.

This research would not have been possible without the help of the clinical team at the Electrophysiology Laboratory at the London Health Sciences Centre. Specifically, Danielle Dean, who has been an incredible source of knowledge and guidance. She was always available and willing to spend her time to answer all my questions – I am incredible grateful for all her help. I would like to acknowledge electrophysiologists Dr. Peter Leong-Sit, Dr. Jaimie Manlucu, and Dr. Jason Roberts, who dedicated their valuable time with me

financially. I am lucky to have such a supportive family, standing behind me with their love and support. To my late grandmother, Dina Gelman, this is for you.

Lastly, to my loving wife, Joanne Gelman. After finishing my undergraduate degree, I decided to apply to one – and only one – university for my graduate studies. I did this because I knew early on that I wanted you to be my life. Not only do I have a promising career, but now I have a beloved wife, life partner, and soul mate; and together, we make a strong and unbreakable family unit. Thank you for coming along and letting me go on this crazy adventure. Thank you for the love, encouragement, unconditional support, and every little effort you do for me. I am truly blessed.

<div align="center">אני לדודי ודודי לי</div>

Contents

List of Tables

List of Figures

List of Abbreviations

3D   *Three Dimensional*

AF   *Atrial Fibrillation*

ANOVA   *Analysis of Variance*

ARM   *Advanced RISC Machine*

BPM   *Beats or Breathes Per Minute*

CF   *Contact Force*

CFC   *Contact-Force Controller*

CGCI   *Catheter Guidance Control and Imaging*

CS   *Coronary Sinus*

CT   *Computed Tomography*

DC   *Direct Current*

DOF   *Degrees of Freedom*

EAM   *Electro-Anatomical Map(ping)*

EP   *Electrophysiologist*

EP Lab   *Electrophysiology Laboratory*

FDA   *U.S. Food & Drug Administration*

FO   *Fossa Ovalis*

Fr   *Catheter French*

FTI	*Force-Time Integral*
g	*Grams Force*
gs	*Grams Seconds*
HFJV	*High-Frequency Jet Ventilation*
HPSD	*High-Power Short-Duration Ablation*
Hz	*Hertz*
ICE	*Intracardiac Echocardiography*
IVC	*Inferior Vena Cava*
kHz	*kiloHertz*
LA	*Left Atrium*
LIPV	*Left Inferior Pulmonary Vein*
LSPV	*Left Superior Pulmonary Vein*
LV	*Left Ventricle*
mm	*Millimeter(s)*
MNS	*Magnetic Navigation System*
MRI	*Magnetic Resonance Imaging*
ms	*Millisecond(s)*
PI	*Proportional-Integral Controller*
PID	*Proportional-Integral-Derivative Controller*
PVC	*Preventricular Contraction*
PVI	*Pulmonary Vein Isolation*
PWM	*Pulse-Width Modulation*
RA	*Right Atrium*
RF	*Radiofrequency*
RIPV	*Right Inferior Pulmonary Vein*

RMSE   *Root-Mean-Squared Error*

RNS   *Robotic Navigation System*

RSD   *Relative Standard Deviation*

RSPV   *Right Superior Pulmonary Vein*

s   *Second(s)*

SD   *Standard Deviation*

SSC-RNS   *Steerable Sheath and Catheter Robotic Navigation System*

SVC   *Superior Vena Cava*

T   *Tesla*

1 Introduction and Background

This introductory section provides a brief overview of relevant background information relating to the research described in the following chapters. This section also describes atrial fibrillation, cardiac catheter ablation, the current state-of-the-art tools and technologies used in the clinic. The proposed robotic systems designed to address the current challenges associated with current catheter ablation strategies are also discussed.

1.1 Atrial Fibrillation

Atrial fibrillation (AF), the most common and clinically significant cardiac arrhythmia, is a heart rhythm disorder characterized by chaotic electrical activity in the upper chambers (atria) of the heart. False electrical signals are generated from different parts within the atria causing abnormal contractions, resulting in a rapid and irregular heartbeat that can occur in episodes or last permanently [1]. During an AF episode, a surface electrocardiogram (ECG) will typically illustrate an irregular R-R interval and the absence of a distinct P-wave, as illustrated in **Figure 1.1** [2, 3]. AF is typically categorized as either: *paroxysmal* defined as recurrent that resolves within seven days; *persistent* defined as continuous AF that is sustained beyond seven days; *long-standing persistent* defined by continuous AF sustained beyond 12 months; or, *permanent* if treatment has failed or has been discontinued [4].
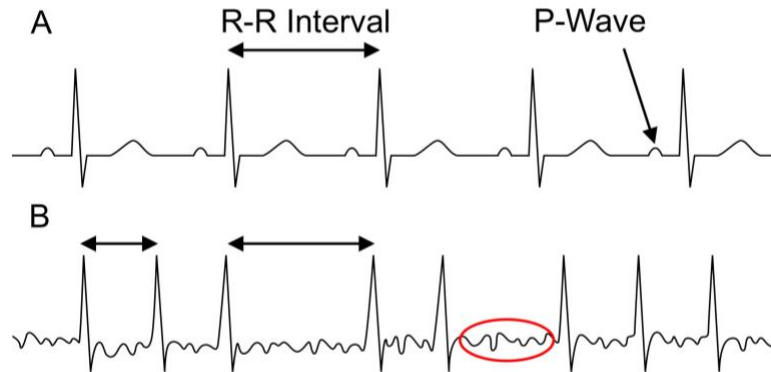
Figure 1.1. In comparison to a normal sinus rhythm **A**, a surface ECG of AF **B** will illustrate an irregular R-R interval and the absence of a distinct P-wave (red).

In North America, Europe, and Asia, the current estimated prevalence of AF is between 1% to 4% [5, 6]. In the ATRIA study, within a large and ethnically diverse population, they found that 1% of all adults were diagnosed with AF, and nearly 4% of individuals 60 years and older and 9% of individuals 80 years or older being diagnosed [7]. In addition to increasing age, the probability of developing AF is also influenced by inherited and acquired risk factors [8, 9]. Current estimates reveal that globally, 33 million people have some form of AF [10]. Reflecting the increasing proportions of the elderly, this number is projected to increase 2-4-fold by 2050 [7, 11, 12].

The healthcare burden associated with AF has increased and is expected to continue rising. In the United States, AF accounts for more than 479,000 hospitalizations yearly and has contributed to more than 130,000 deaths [13]. AF has been reported to increase the annual healthcare cost by USD 8,705 per patient resulting in between USD 6B and USD 26B per year in additional US healthcare costs [14]. In Canada, each AF patient costs CAD 6,718 attributing to CAD 815M [15]. The reported costs are based on databases collected between 2011 and 2013 and likely have increased significantly since its reporting. AF already has demonstrated tremendous implications on the global economy and public health [16] and this situation is rapidly becoming worse.

Clinically, the most critical complication associated with AF lies in the risk of cardiac thrombus formation. Because of this, AF is a strong independent risk factor for embolic strokes [17-19]. On average, AF increases the risk of stroke 5-fold [20], and strokes of AF-related etiology are twice as likely to be fatal in comparison to non-AF related strokes [21]. Estimates show that AF causes one-third of all strokes after the age of 60. In addition to age above 60, other significant risk factors of AF-related stroke include female sex, prior stroke, congestive heart failure, diabetes, and hypertension [22, 23].

The root causes of AF are unclear, but many concepts explaining its mechanism have been speculated: multiple re-entrant wavelets, rapidly discharging automatic foci, and a single re-entrant circuit with fibrillatory conduction [1]. Substantial progress has been made in understanding and defining the mechanisms underlying AF initiation and progression [24, 25]. It was recognized that AF is triggered or maintained by rapidly firing foci entering the left atrium (LA) originating from the cardiac muscle cells extending within the walls of the pulmonary veins (PVs). To this end, AF can be treated permanently with local catheter ablation near the PVs [26, 27].

1.2   Catheter Ablation

Cardiac catheter ablation is a minimally invasive curative treatment that aims to isolate the PVs from the atria electrically. Radiofrequency (RF) energy is delivered to cardiac tissue using an electrophysiology ablation catheter, resulting in the production of an ablation lesion.

A catheter ablation procedure begins with a small incision made in the groin, allowing a guidewire to be advanced to the right side of the heart via the femoral vein. A trans-septal puncture, guided by fluoroscopy and ultrasound, is performed through the fossa ovalis to gain access to the left atrium. An RF ablation catheter can then be introduced and manipulated within the cardiac chamber (**Figure 1.2**). Using a variety of modalities and

catheter navigation technologies (such as fluoroscopy and electromagnetic guidance), an electrophysiologist (EP) manipulates the catheter to specific targets in the LA and delivers numerous contiguous RF "applications" into the tissue.
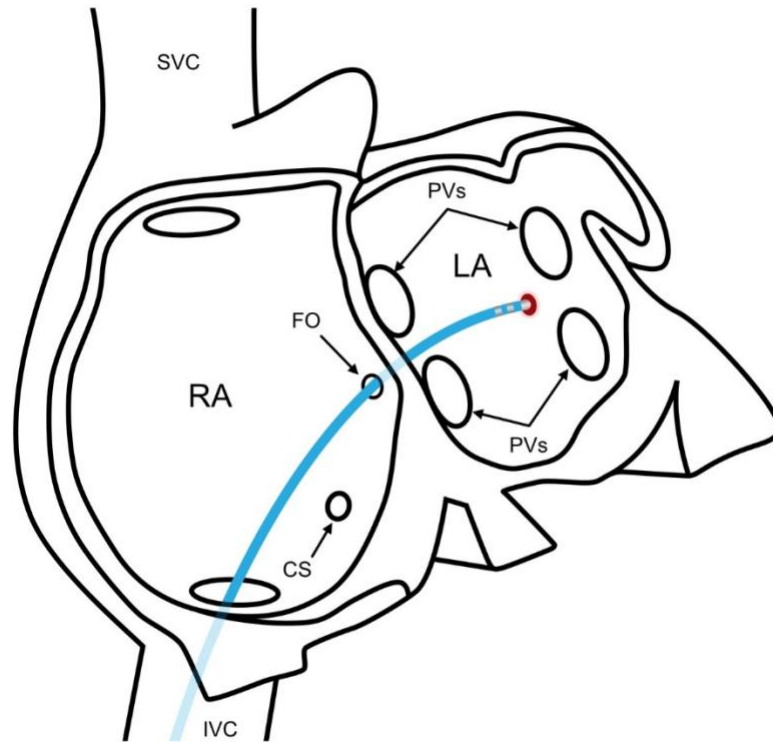
Figure 1.2. The catheter is introduced into the left femoral vein and fed up to the right atrium (RA) via the inferior vena cava (IVC). A transseptal puncture through the fossa ovalis (FO) allows the catheter to be introduced into the left atrium (LA) and deliver RF ablation lesions near the pulmonary veins (PV). The right and left ventricles (RV and LV, respectively) are not illustrated. This line drawing was adapted from Calkins *et al*. [1].

An ablation catheter is a long and flexible medical device consisting of a proximal handle, which allows the EP to insert, withdraw, and rotate an RF electrode tip within the patient's heart. A deflection mechanism on the handle applies tension to pull-wires within the catheter lumen resulting in the deflection (or bending) of the catheter tip along one, two, or four orthogonal angles, as illustrated in **Figure 1.3**.
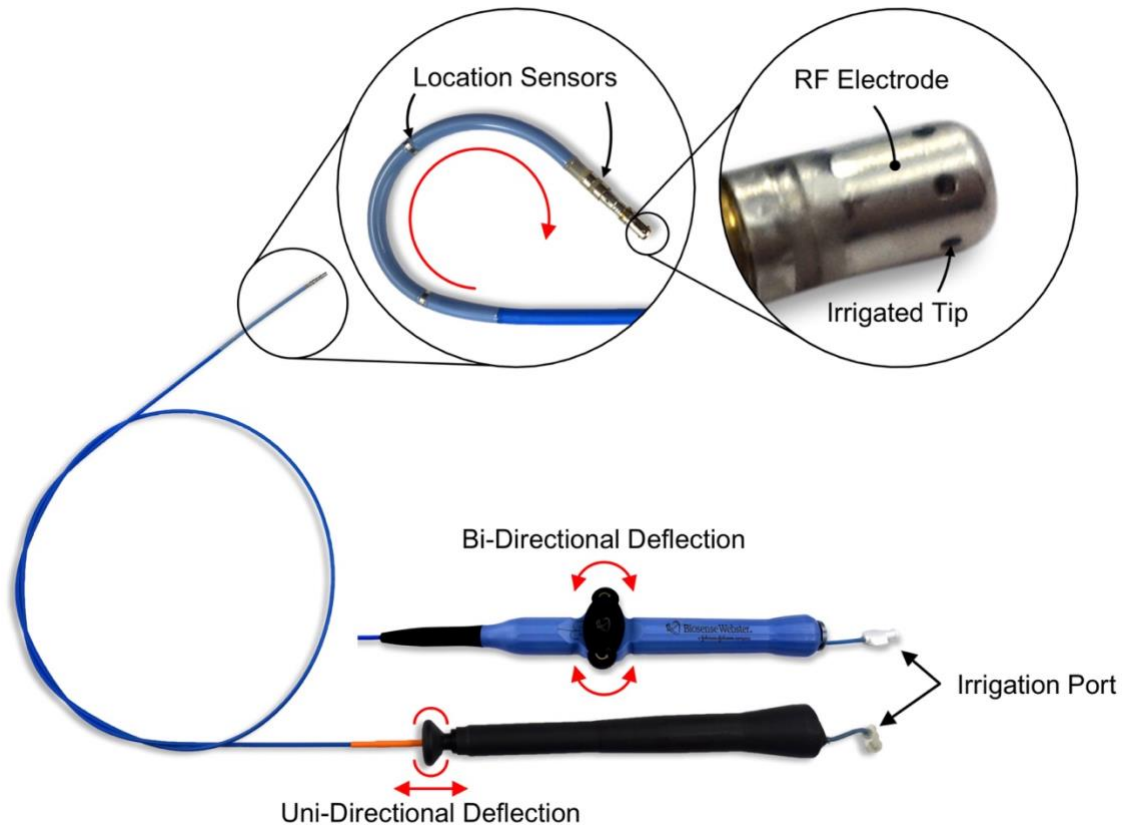
Figure 1.3. An ablation catheter consists of a proximal handle connected to a long and flexible tube, which houses various lumens, electrical wires, and pull-wires. An operator can insert, withdraw, and rotate an RF electrode (located at the very tip of the catheter) to make contact with cardiac tissue and deliver RF energy. A uni- or bi-directional mechanism on the handle deflects the distal tip (shown in red). The catheter tip incorporates electromagnetic location sensors, and electrodes used for delivering RF energy, recording intracardiac ECG, and cardiac pacing. Ablation catheters also include an irrigation line, which allows saline to be pumped continuously to cool the electrode during RF delivery.

Precisely placing transmural (across the thickness of the tissue) ablations lesions near the PVs blocks the electrical signals from disturbing the normal sinus rhythm of the heart. A common strategy employed in AF ablation is to deliver contiguous lesions encircling the ostia of the PVs. This procedure is known as pulmonary vein isolation (PVI), whose goal is to electrically isolate the left and right pairs of PVs from the LA [1]. The circumferential ablation lesions performed during PVI can be followed with additional ablation sets, as illustrated in **Figure 1.4**.
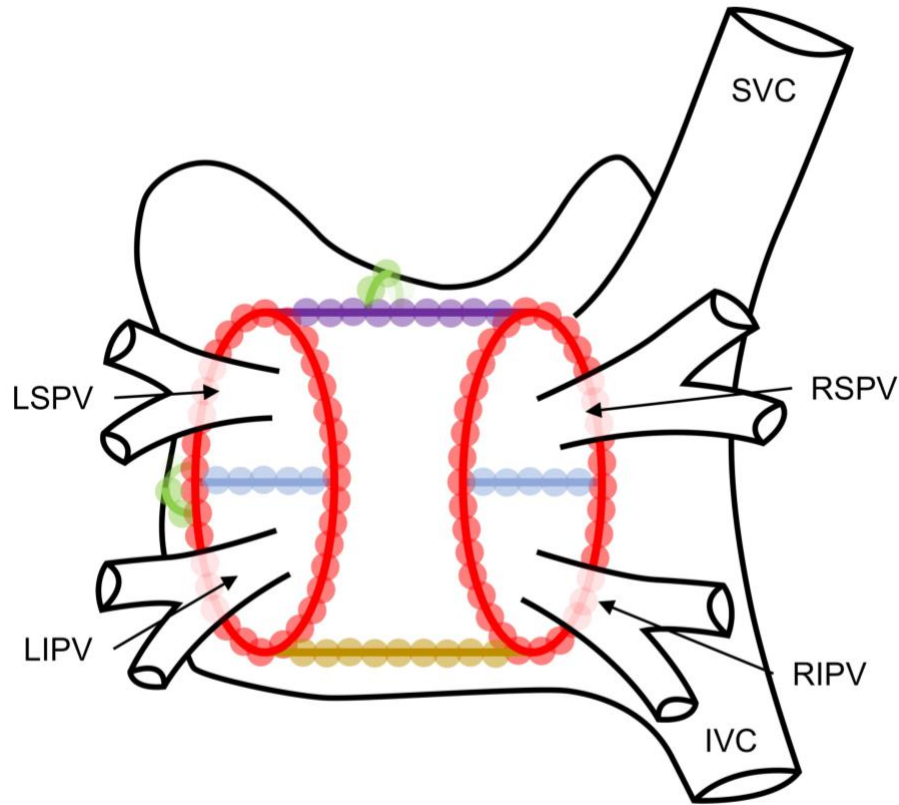
Figure 1.4. Line illustration represents the LA from the posterior perspective. PVI requires the precise placement of contiguous circumferential ablation lesions encircling the right and left PV pairs (red). The left PV pair includes left superior and inferior pulmonary veins (LSPV and LIPV, respectively), while the right PV pair consists of the right superior and inferior pulmonary veins (RSPV and RPIV, respectively). Other standard ablation lines include: a roof line connecting the left and right circumferential lesions (purple) and a corresponding inferior ablation line (yellow) resulting in a complete isolation the posterior wall; linear lesions between each PV pair (blue); and a mitral isthmus ablation line connect the left PV pair with the mitral valve (green). This line drawing was adapted from Calkins *et al*. [1].

To facilitate catheter navigation, modern catheter labs are equipped with electro-anatomical mapping (EAM) systems, which have led to a paradigm shift in treating patients with cardiac arrhythmia. EAM systems are used to define the mechanisms of arrhythmias, design ablation strategies, guide ablations, and improve safety by identifying critical cardiac structures. While manipulating the catheter in the cardiac chamber, its position and orientation are monitored by a low-field magnetic generator, which locates electromagnetic sensors incorporated within the catheter tip with sub-millimetre accuracy (**Figure 1.5**). In

addition to the primary ablation catheter, EPs can use a mapping catheter (taking the form of a lasso or paintbrush) to capture the 3D anatomical structure of the heart and determine the ECG at any mapped point in the cardiac chamber. By gating the acquisition of points to the cardiac electrical activity, points that represent both location and its corresponding electrical activity are acquired. A 3D representation is constructed and displayed to the EP. EAM systems allow for further understanding of arrhythmias and increase the safety, efficacy, and efficiency of catheter ablation, which has helped decrease procedural complexity and procedure time [28, 29].

Despite decades of intensive research and innovation, resulting in an arsenal of tools available to the EP, long-term results of catheter ablation demonstrate a high rate of recurrence following the first procedure. Early recurrences of AF, occurring after a 3-month blanking period post-ablation, have been reported in up to 50% to 70% of patients [30-33]. The low efficacy rate of first-procedure clinical success is likely due to the inability to create transmural and durable lesions in a contiguous fashion, ultimately resulting in the reconnection of the PVs with the LA. In these cases, a repeat procedure is performed in an attempt to re-isolate the PVs. With multiple procedures, the long-term success rate can be improved to 80% overall. It has been reported that, on average, each AF patient undergoes 1.5 ablation treatment to restore normal sinus rhythm [33].
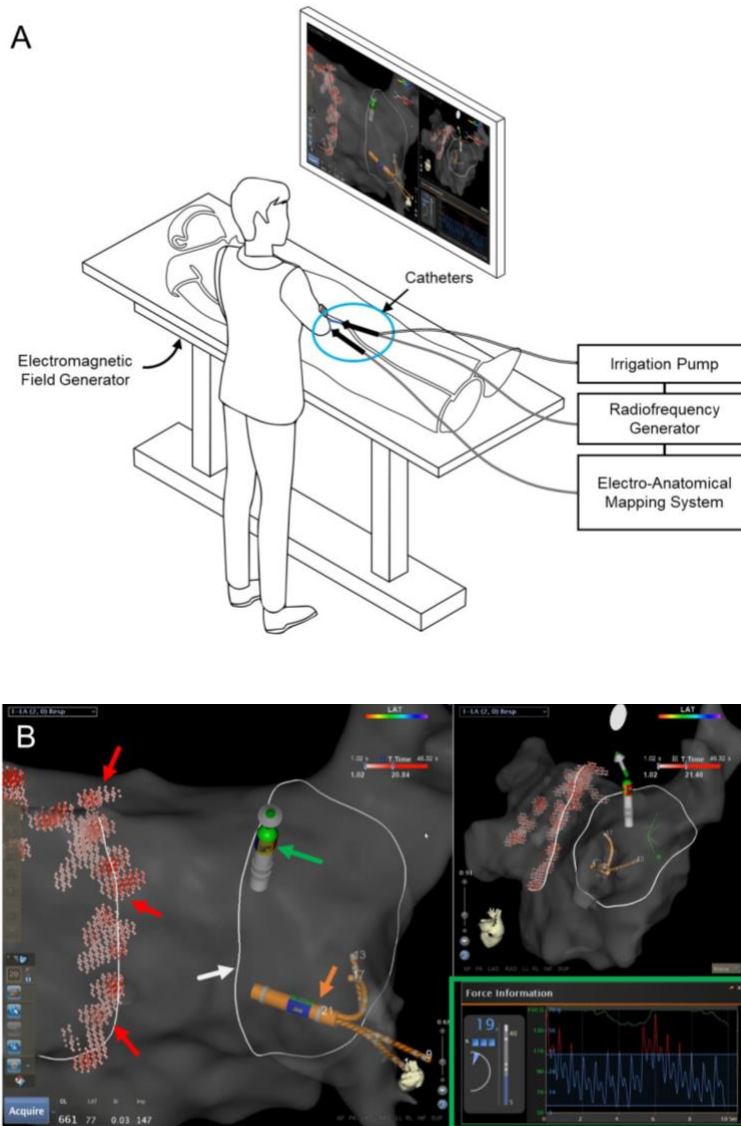
Figure 1.5. A typical modern EP lab is equipped with an EAM system which captures the location of the catheter tip using an electromagnetic field generator located under the chest of the patient **A**. Other equipment includes an RF generator and irrigation pump, a system for recording ECG signals, and fluoroscopic x-ray system (not shown). The EAM system is on display in front of the EP **B**. The EP can track the position of the tip of the ablation catheter (green arrow) in relation to a map of the patient's cardiac chamber and monitor the real-time catheter-tissue contact force (green square) between the tip and moving cardiac tissue. An additional mapping catheter (orange arrow), in the form of a paintbrush, is used to collect intracardiac ECG. The EAM system is also used to plan and guide ablation lines (white arrow) and track the locations of previously delivered lesions (red arrows).

Non-ablative strategies to treat AF includes the use of antiarrhythmic drugs. Three prospective randomized clinical trials have examined the efficacy of ablation as the first treatment versus antiarrhythmics [34-36]. A meta-analysis summarizing those trials [37], concluded that ablation was associated with significantly higher freedom from long-term AF recurrence in comparison to the pharmacological counterpart and provided the evidence to support AF ablation as first-in-line therapy. In the recent CABANA trial [38], involving over 2200 patients, they also demonstrated an association with lower AF recurrence rate using catheter ablation over drug therapy. The Cox-Maze procedure, an open-heart surgical approach to permanently treat AF, requires a cardiac surgeon to place a series of epicardial incisions (in a similar fashion to RF ablation) to interrupt the abnormal AF signals permanently. This procedure is routinely practiced and recommended at the time of simultaneous mitral and aortic valve operations and coronary artery bypass grafting.

Although this thesis focuses on AF, it is important to recognize that RF catheter ablation is used to treat other forms of supraventricular arrhythmias, such as atrial flutter and atrioventricular nodal re-entrant tachycardia, which require ablation in the RA, as well as ventricular tachycardia, which requires ablation in the LV.

1.2.1   Biophysics of Radiofrequency Lesion Formation

Radiofrequency energy is created by using alternating electrical current to generate an ablation lesion by electrical heating the cardiac tissue. Thermal energy deposited into the tissue is used to destroy the arrhythmogenic substrates by heating them to a lethal temperature; the 50°C isotherm determines the boundary of the lesion where tissue injury is irreversible. As electrical current passes through the tissue, the voltage drops, and heat is produced; this is called *resistive* heating. RF current is primarily delivered in a unipolar fashion with completion of the electrical circuit through an indifferent electrode placed on the skin (**Figure 1.6**). Typically, 500 to 750 kHz is used for efficient tissue heating while avoiding stimulating cardiac muscle and nerves.
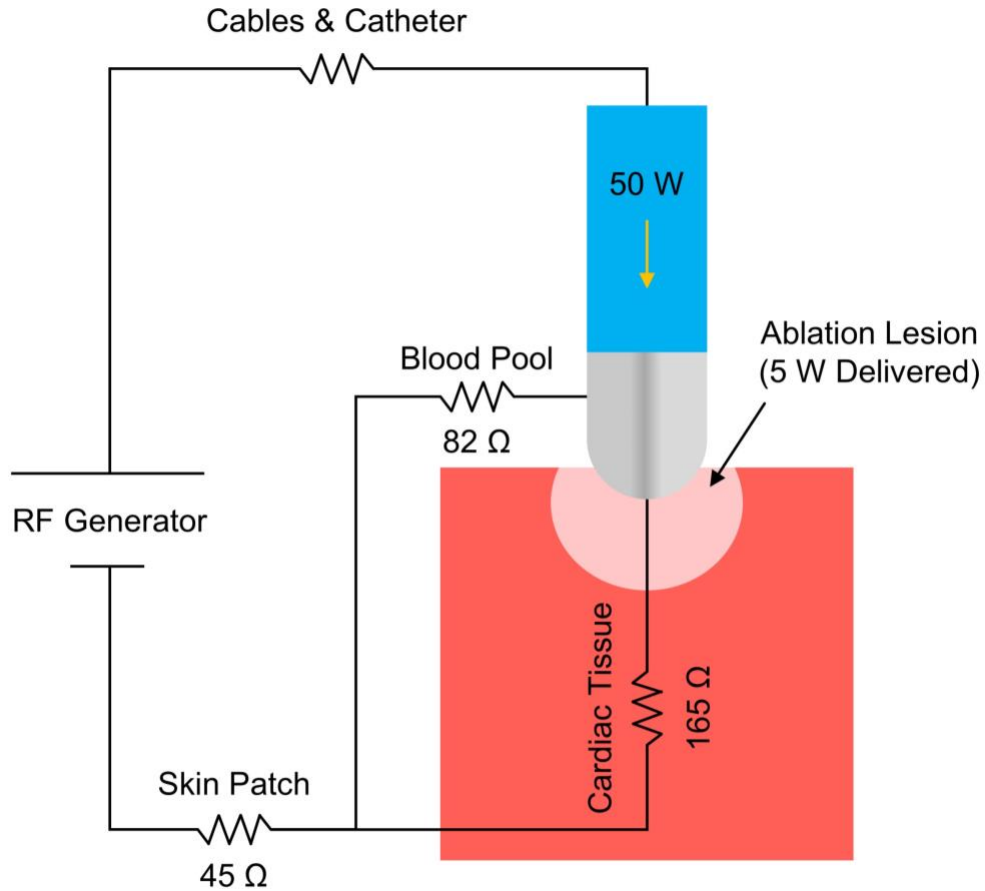
Figure 1.6. Circuit path for RF catheter ablation. Blood pool resistance is about half of that than cardiac tissue. Out of the 50 W of energy delivered from the catheter, only 5 W is deposited in the tissue because of power loss caused by the lower resistance (and impedance) of the blood pool. The amount of power delivered into the tissue is based on the amount of electrode surface in contact with the tissue, which is a function of electrode size, the orientation catheter in relation to the tissue surface, and the amount of electrode-tissue contact force. This illustration has been adapted from Huang & Miller [39].

Resistive heating decreases proportionally with the distance from the electrode to the fourth power. As a result, only a narrow rim of tissue in contact with the catheter electrode (approximately 2-3 mm) is heated. The majority of lesion production (and deep tissue heating) is a result of passive *thermal conduction* (**Figure 1.7**). Tissue temperature at any given distance from the electrode increases exponentially with proximity to the electrode.

The formation of coagulum at the electrode-tissue interface occurs when the temperatures exceed 100°C. As the blood and tissue in contact with the electrode begin to boil, denatured proteins stick to the surface of the electrode. Because coagulum electrically insulates the surface of the electrode, a concentration of power occurs over a reduced surface area. This positive feedback loop can cause a complete encasement of the electrode with coagulum within seconds. Modern RF generators use sharp increases in impedance, associated with coagulum encasement, to shut off RF energy. The formation of coagulum can cause micro embolisms, which have been shown to cause cerebral embolic lesions [40-42].

When deep tissue layers exceed 100°C, intramuscular water begins to boil and cause a sudden buildup of steam. High pressure is released, which can be heard or felt as a steam-pop [43]. Damage caused by steam pops ranges from superficial endocardial craters to full-thickness myocardial tears resulting in cardiac perforation and tamponade.

Active electrode irrigation is used to mitigate the effects of the electrode and tissue overheating. Continuous saline irrigation bathes and cools the RF electrode and superficial tissue layers (**Figure 1.7**), thereby allowing for longer RF application times and optimal RF power delivery, resulting in larger lesions. Modern catheters are designed with either closed-loop or open irrigation systems (catheter photographed in **Figure 1.3** uses an open system). Illustrated in **Figure 1.5A**, an irrigation pump – triggered with the RF generator – continuously pumps saline through to the electrode through the irrigation port of the catheter.
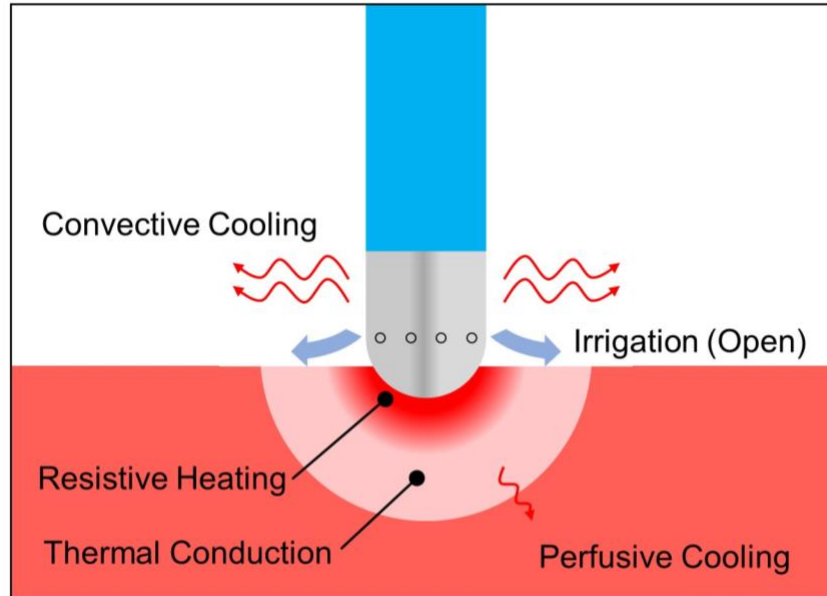
Figure 1.7. Drawing of RF catheter ablation on tissue demonstrating resistive and conductive heating. Continuous irrigation cools the electrode and tissue surface, allowing larger lesions to be formed by prolonging ablation time. Additional heat is lost passively through the blood pool (convective) and cardiac tissue (perfusive). This illustration has been adapted from Huang & Miller [39].

Several factors influence ablation lesion size includes: RF power, duration of RF energy delivery, *electrode-tissue contact force,* tissue composition, electrode temperature, peak tissue temperature, convective cooling, electrode size, ablation circuit impedance, electrode orientation, electrode geometry, electrode material, and characteristics of RF power. Electrode-tissue contact force is a novel concept and has emerged as a critical factor in RF catheter ablation – this thesis heavily focuses on this concept. For this reason, it is essential that thorough comprehension of catheter-tissue contact force is acquired.

1.2.2   Role of Contact Force in RF Catheter Ablation

Successful catheter ablation requires the complete and permanent elimination of arrhythmogenic substrates by delivering ablation lesions that are reliably transmural without collateral injury to other cardiac structures. RF energy creates resistive heating of the tissue that is in direct contact with the electrode tip, and therefore, sufficient catheter-

tissue contact is essential [44]. A major determinant of lesion size and depth is the amount of contact force (CF) between the catheter tip electrode and moving tissue. Greater CF increases lesion size by improving electrical coupling between the electrode and tissue. This increases the electrode surface area in contact with the tissue and reduces the shunting of current to the blood pool. Additionally, greater CF prevents the electrode from sliding with cardiac motion. To this end, manufacturers have developed ablation catheters with a force sensor integrated into the distal tip to measure real-time catheter-tissue CF during mapping and RF ablation. These force-sensing ablation catheters detect forces in 3D with high resolution (< 1 gram [g]) and display it visually on the EAM system (**Figure 1.5**). A large-scale clinical study has shown that force-sensing ablation catheters reduce gaps between adjacent lesions, steam pops, cardiac perforation, thrombus formation, and fluoroscopy time, while at the same time improving lesion formation and reducing AF recurrence rates [45].

Ablations lesions delivered with low levels of CF are superficial, increase the risk of intermittent contact (occasional complete loss of contact) is correlated with sites of PV reconnection [46-49]. In contrast, excessive CF is associated with deep tissue heating, increase the risk of steam-pop, perforation, thrombus formation, and collateral tissue damage to structures outside the heart, such as esophageal, pulmonary and phrenic nerve injury [50-56].

In an attempt to optimize durable PVI, clinical studies have provided CF guidelines. Notably, the EFFICAS II study (investigating 24 patients) demonstrated isolation of the PV using a CF target of 20 g, ranging between 10 g and 30 g, with a minimum Force-Time Integral (FTI, defined as the under the contact-force curve with respect to time [44]) of 400 grams-seconds (gs) [57]. In addition to the overall average CF, CF variability (or stability) is thought to be an essential parameter in determining RF lesion formation [44]. The SMART-AF trial, investigating 172 patients, showed an increase in clinical success when

more time was spent within a pre-defined CF range (*i.e.*, reduced CF variability) [58]. Specifically, investigators who stayed within a selected CF range more than 80% of the time during RF applications were more than four times more likely to have clinical success in comparison to those who did not. The study concluded that there is a non-linear relationship between CF and clinical success and that CF stability with sufficient average CF, rather than merely achieving higher average CF, is the key to creating durable ablation lesions. Contact quality (which includes catheter stability, cardiorespiratory motion and catheter drift), rather than absolute CF alone, has emerged as a critical element that governs lesion size and ablation outcomes. A meta-analysis summarizing all randomized controlled trials of CF ablation in AF (TOCATTA [59], EFFICAS I [45], EFFICAS II [57], SMART-AF [58], and TOCCASTAR [60]) reports ideal clinical outcomes appear when modest CF is reached while consistently staying within the CF target range during ablation [61].

Smaller clinical studies have looked at further quantifying CF variability to provide more context in lesion production and clinical success. Ullah *et al.* [62] demonstrated that lesions delivered with variability over 5 g are associated with a lower impedance drop (a surrogate for poor lesion production), despite delivering the same FTI. Additionally, Makimoto *et al.* [63], demonstrated that the relationship between the average and standard deviation of CF (relative standard deviation [RSD] or the coefficient of variation) correlates with PV reconnection. They show that ablation segments along the circumferential ablation lines delivered with lower average force and high variability are prone to form reconnection gaps. For instance, in the anterior portions of the left PVs, where the most frequent reconnection gaps are found, not only was the average CF low, but the variability was also very high (**Figure 1.8**). Additionally, although the roof and posterior segments of the right PVs have a typically adequate average CF, they have a high CF variability resulting in a high RSD – this may be the reason why reconnection gaps are found in these locations [64, 65]. This notion reinforced by Kumar *et al.* [66], where they demonstrated that the CF

variability was higher at the sites of reconnection than at non-reconnected sites. RF applications delivered with high CF variability result in lesions 30%-60% smaller in volume compared to constant CF, despite being delivered with the same power, duration, and maximum force [44]. The larger the dynamic range of CF, the less likely the lesion would reach an appropriate FTI and the longer the required duration of RF application. All these data suggest that CF variability, in addition to average CF, plays a vital role in durable ablation production.

In clinical practice, it is virtually impossible to reliably maintain stable CF between the catheter tip and moving tissue. Thousands of RF applications across hundreds of patients have been analyzed. In one study (+1600 RF applications across 22 patients), the average force among the interquartile range is between 6 g and 40 g [67]. In another study (+1400 RF applications across 20 patients performed by two operators), showed that one-in-five RF applications were delivered sub-optimally with less than 5 g on average, despite attempts to "optimize" CF [68]. In a final study (+900 RF application across 20 patients), 19% of RF applications were delivered with a variability of less than 10 g, while the rest remained highly variable greater than 20 g, despite further attempts to optimize CF [69]. Furthermore, average CF and variability also significantly differ depending on whether or not the patient is in sinus rhythm as well as anatomical regions within the LA [63, 67, 68, 70].
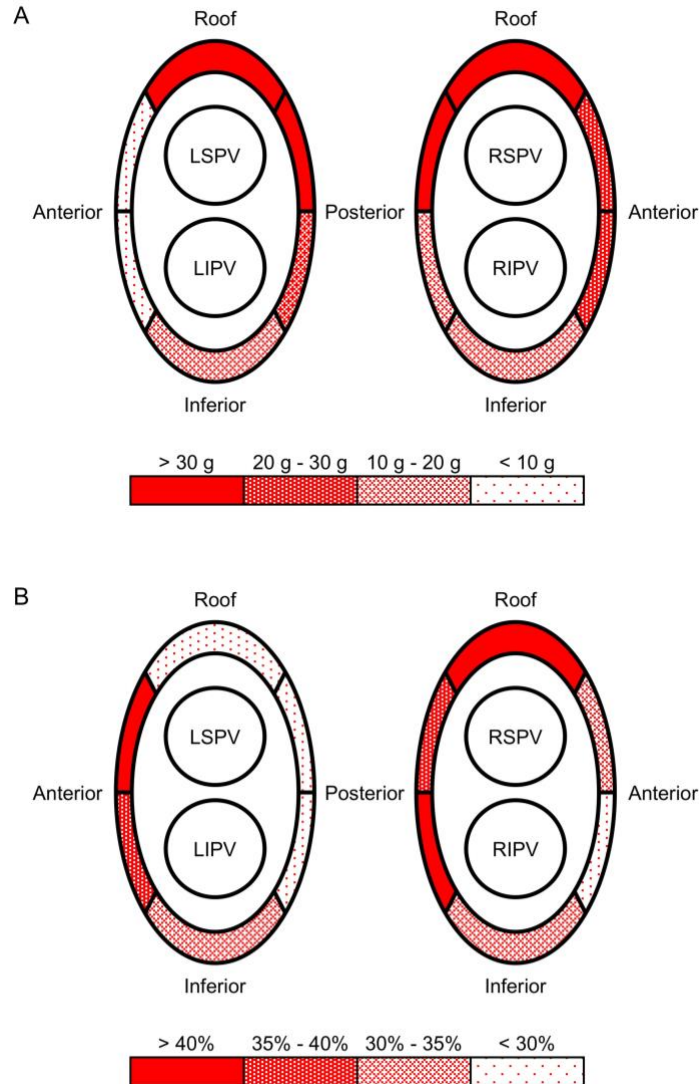
Figure 1.8. Maps of average CF **A** and relative standard deviation (RSD=[SD/Mean]∗100%) **B** acquired in partial segments along circumferential ablation lines during PVI. Areas of RSD over 40% are typically associated with regional locations where reconnection gaps occur. RSD regions less than 30% are generally non-problematic. Average CF was higher in the roof and posterior segments of LSPV and RSPV and lower in the anterior portion of the left PVs. Furthermore, roof and posterior segments of the RIPV and the anterior segment LSPV, RSD was significantly higher as compared to the other sections, implying a higher risk of reconnection. Figure created based on data from Makimoto *et al.* [63].

Systolic-diastolic cardiac motion and respiration are the primary contributors to variability in CF [66, 67, 69]. Given the need to minimize tissue movement to improve CF stability, techniques have been introduced clinically, which aim to decrease the amplitude of cardiac

and respiratory motion by increasing their corresponding frequencies. For example, rapid atrial pacing (increasing heart to over 120 BPM) improves catheter stability in the presence of cardiac motion [71]. However, the improvement in CF variability is minimal (less than 1 g) and is dependent on regional lesion location within the LA. Furthermore, patients can be sensitive to prolonged periods of rapid atrial pacing resulting in a quick drop in blood pressure. High-frequency jet ventilation (HFJV) which increases the ventilation rate to 100 cycles/minute, or inducing patient apnea (breath-hold) can be used to eliminate CF variability caused by respiratory motion [66, 72, 73]. HFJV may not be suitable for many patients due to adverse effects [74, 75]. Importantly, HFJV and apnea induction requires general anesthesia, which relies on the availability of an anesthesiologist and the protocol of the center where the procedure is performed. Problems associated with general anesthesia include increased risk of atrial-esophageal fistula, although this is extremely rare [76]. Among the Heart Rhythm Society and European Heart Rhythm Association expert consensus, approximately 70% routinely employ general anesthesia (and apnea induction) for AF cases, and only 8% reported the use of HFJV [1].

As RF catheter ablation extends to more and less experienced operators, clinical success will continue to vary centre-to-centre. This is further exacerbated by the variety of tools and technologies at the electrophysiologist's disposal. With limited methods to mitigate the effect of excessive cardiorespiratory or patient motion, it is virtually impossible for EPs to reliably meet any CF guidelines outlined by these reported clinical studies. It is evident that there is a clear need for new technology to control catheter-tissue CF to optimize point-by-point RF ablation technique. Controlling for catheter-tissue CF and its effect in lesion production is a principal component of this thesis.

1.3 State-of-the-Art Commercial Technology

This section presents tools and technologies routinely employed for AF ablation procedures. Emerging technologies, tools, and approaches such as cryoablation, laser and

ultrasound ablation, balloon-based single-shot catheters, and electroporation are not addressed. This section is limited to existing commercial technologies – relevant to the context of this thesis – utilized in point-by-point RF catheter ablation strategies.

1.3.1   Electro-Anatomical Mapping Systems

Modern EP labs incorporate an EAM system, which is used to track the position of an ablation catheter tip in relationship to an electro-anatomical map of the patient's cardiac chamber. EAM systems record and display electrical activation related to the anatomical location of the recorded sites, which help diagnose and guide ablation procedures. Innovative catheter technologies, specifically robotic technologies, are typically incorporated with EAM systems. For this reason, it is essential that a basic comprehension of EAM systems is acquired. To this end, three commercially available EAM systems routinely used in the clinic are described in this section.

1.3.1.1   CARTO® 3 Catheter Mapping System

The CARTO® 3 System (Biosense Webster, Irvine, CA) [77] is an advanced mapping technology that utilizes electromagnetic tracking to create real-time 3D maps of a patient's cardiac structures. The system is designed to help electrophysiologists navigate the heart by generating an accurate 3D map, as well as track the location and orientation of catheters in the heart during ablation therapy.

CARTO® is based on three foundations: ECG, location, and mapping. The ECG subsystem receives body surface and intracardiac ECG, which are filtered, presented and recorded with CARTO®. To ensure that catheter tracking is not influenced by human conductivity, CARTO® uses an electromagnetic field generator, consisting of three magnetic coils, to track the electromagnetic sensors on the tip of the catheter (**Figure 1.9**), as well as locations from six patches attached to the patient (three on the back and three on the chest). Lastly,

CARTO® mapping technology is used to build maps of the heart chambers by combining the precise location and ECG data.

The base CARTO® system can be equipped with optional software modules for differing clinical needs. Some of these modules include force-sensing ablation catheter (SMARTTOUCH™ Module); computed tomography (CT) and magnetic resonance imaging (MRI) image integration and registration (CARTOMERGE®); and remote catheter magnetic navigation (RMT Module) [77].
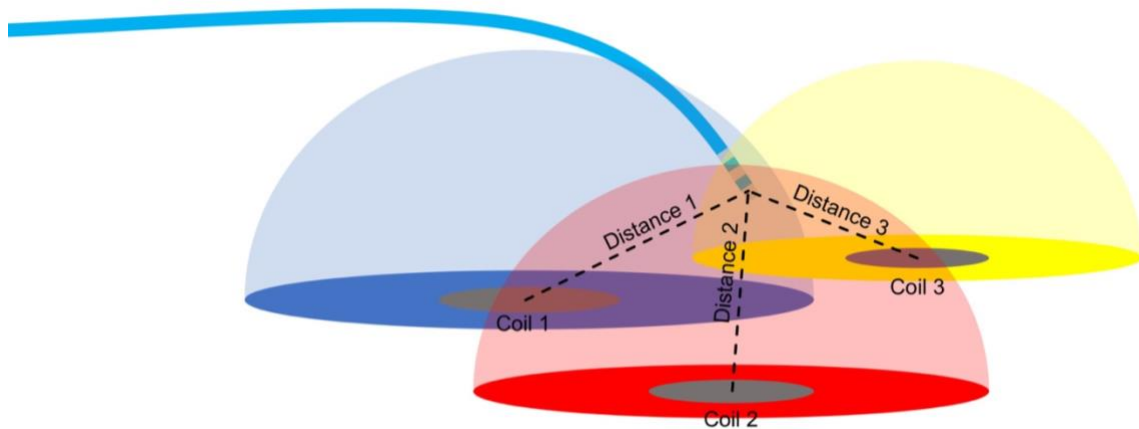
Figure 1.9 Illustration demonstrating electromagnetic tracking of the catheter tip. Three coils, suspended under the patient's chests beneath the EP table, emit a low-level magnetic field represented by colour-coded hemispheres. A 6 degree-of-freedom electromagnetic sensor within the tap of the mapping or ablation catheter, measures the field strength from each coil. The relative position to each coil is then triangulated to determine the relative position and orientation of the catheter tip. Illustration adapted from Bhakta *et al*. [78].

1.3.1.2   EnSite Precision™ Cardiac Mapping System

The EnSite Precision™ Cardiac Mapping System (Abbott Laboratories, Minneapolis, MN) [79] is a 3D cardiac mapping system with features similar to that of CARTO® such as catheter tracking, mapping and recording ECG with expanded optional software modules.

The distinguishing technical difference between the two systems is that the EnSite Precision™ system combines impedance-based and electromagnetic-based tracking

technologies to enable navigation and accurate tracking of both conventional catheters (open to 3rd-party manufacturers) and sensor-enabled catheters. EnSite Precision™ is an open-platform system that compliments both tracking technologies.

Over the past two decades, the CARTO® and EnSite Precision™ have dominated this market and have been used in thousands of clinical studies worldwide, demonstrating its efficacy in treating several forms of cardiac arrhythmia. PVI procedures guided by either of these systems have been shown to yield similar clinical outcome [80]. The widespread use of these systems is associated with higher success rates, shorter fluoroscopy and procedure times, and accurate visualization of the cardiac chambers.

1.3.1.3   RHYTHMIA HDx™ Mapping System

A third system – the RHYTHMIA HDx™ Mapping System (Boston Scientific, Marlborough, MA) [81] – is similar to the EnSite Precision™ system whereby it utilizes both electromagnetic-based and impedance-based catheter tracking technology. Although this system holds a smaller percentage of the market, in comparison to CARTO® and EnSite Precision™, it does stand out by providing a unique mapping catheter. The INTELLAMAP ORION™ mapping catheter is capable of generating a rapid ultra-high-density ECG map of the patient's cardiac chamber [81]. This unique catheter has been shown to improve long-term success in comparison to procedures guided by CARTO® or EnSite Precision™ [82]. The RHYTHMIA HDx™ and INTELLAMAP ORION™ are effective for treating various forms of cardiac arrhythmia, as demonstrated in several pre-clinical and clinical studies [83-92].

Unfortunately, unlike their competitors, to date, Boston Scientific does not provide an ablation catheter capable of detecting real-time contact force measurements. Several patents granted to Boston Scientific in 2017 describe a catheter capable of detecting catheter-tissue CF [93-96], suggesting that such a catheter will soon be available.

1.3.2   Force-Sensing Ablation Catheters

1.3.2.1   THERMOCOOL® SMARTTOUCH™ Catheter

The THERMOCOOL® SMARTTOUCH™ Catheter (Biosense Webster, Irvine, CA) [77] is an ablation catheter that measures the CF between the catheter tip and moving tissue. A precision spring located just proximal to the ablation tip electrode is affixed to an electromagnetic transmitter coil (distal to the spring), which emits a magnetic field. Three additional electromagnetic coils (positioned circumferential proximal to the spring) generate an electrical current proportional to the micro-deflection caused by an applied force to the catheter tip (**Figure 1.10**). A proprietary algorithm computes a 3D force vector at approximately 20 Hz and displays both magnitude and direction continuously on the CARTO® 3 System [97].
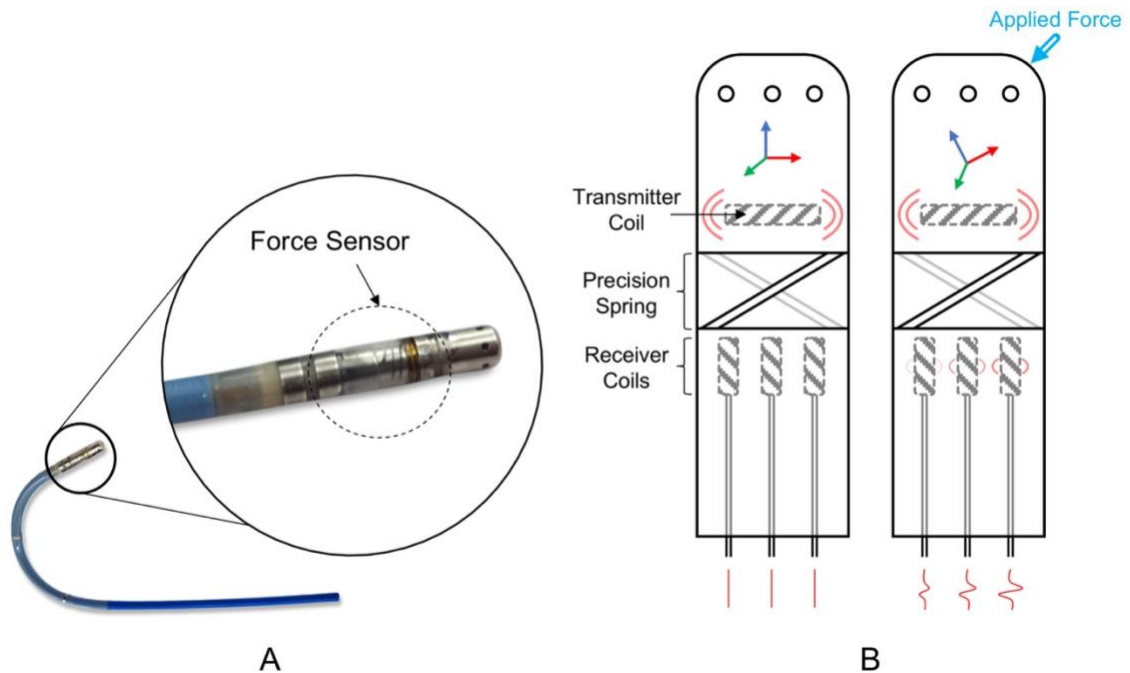
Figure 1.10. Photograph of THERMOCOOL® SMARTTOUCH™ force-sensing ablation catheter tip **A**. A precision spring is affixed to a transmitter coil emits a magnetic field. Three electromagnetic receiver coils generate an electrical current proportional to the deflection caused by force applied to the tip (blue arrow) **B**.

The THERMOCOOL® SMARTTOUCH™ catheter also comprises standard electrophysiology catheter features, such as an RF electrode tip, location sensors, ECG mapping and pacing as well as a saline irrigation port. The THERMOCOOL® SMARTTOUCH™ catheter was the first catheter with force-sensing technology to be approved by the U.S Food and Drug Administration (FDA) for use in cardiac ablation therapy.

1.3.2.2   QDOT MICRO™ Catheter

The QDOT MICRO™ Catheter (Biosense Webster, Irvine, CA) [77] is the next generation force-sensing ablation catheter developed by Biosense Webster (**Figure 1.11**). In addition to force-sensing technology, the new catheter incorporates three micro-electrodes embedded at the distal circumference within the standard distal RF electrode. Each acquired point within CARTO® records four intracardiac electrograms: one from the standard electrodes and three from the micro-electrodes. This design allows for recording an ECG from a small tissue area, which has been shown to improve mapping resolution and diagnosis of electrograms while limiting the need for and cost associated with the use of separate mapping catheters [98]. The QDOT MICRO™ also incorporates six thermocouple temperature sensors (three proximal and three distal) embedded 75 micrometres underneath the surface of the RF electrode's metal shell. The symmetrical distribution of thermocouples is optimized to monitor temperature at all orientations the catheter makes to the tissue (defined as catheter-tissue incidence angle), resulting in more accurate temperature readings from parts of the RF electrode in contact with the tissue. In contrast, conventional catheters average the tip temperature, which is diluted by the cooler parts of the tip that are not touching the tissue and the effects of blood and irrigation.

The incorporation of accurate local temperature monitoring allows for safe delivery of an emerging RF technique, which uses high-power RF ablation. The proposed benefit of this

approach is to reduce the effects of lesion-to-lesion variability that result in reconnection gaps. Several pre-clinical studies have shown to improve linear continuity, the delivery of transmural ablation lesions, shorter ablation time, feasibility and safety. [99-101]
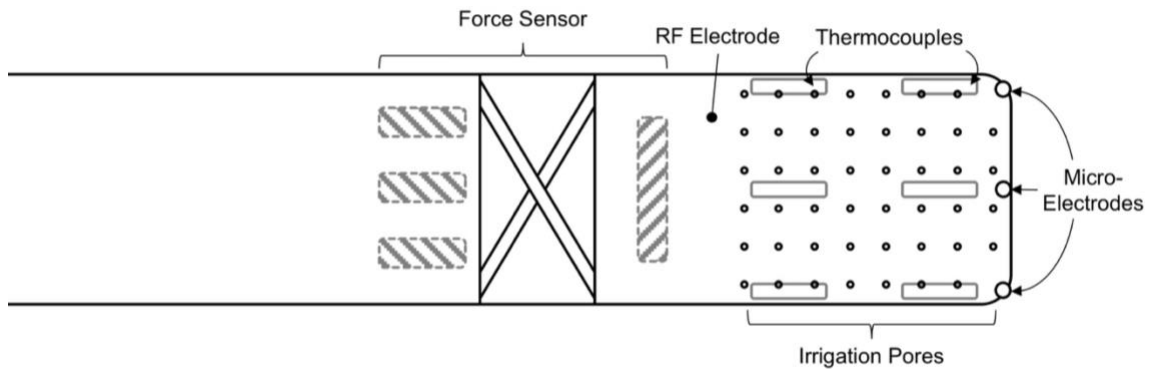
Figure 1.11. Line illustration of the tip of the QDOT MICRO™. The novel force-sensing ablation catheter incorporates (1) six thermocouple temperature sensors underneath the surface of the RF electrode for improved temperature monitoring of the tissue surface; (2) three micro-electrodes for high-resolution intracardiac EC mapping; and (3) an improved tip irrigation system.

1.3.2.3   TactiCath™ Quartz Contact Force Ablation Catheter

The TactiCath™ Quartz Contact Force Ablation Catheter (Abbott Laboratories, Minneapolis, MN) [79] contains a force sensor consisting of a deformable body and three optical fibres [102]. Infrared light (emitted through the proximal end of the optical fibres) travels through the catheter towards a cavity within the catheter tip (**Figure 1.12**). The incoming light is bounced back and forth between two parallel reflective mirrors within the cavity, resulting in reflected light with different wavelengths creating interference patterns. When force is applied, the cavity length changes (on the order of nanometers) resulting in a proportional change in the interference pattern. The reflected light is returned through to the proximal handle by three optical fibres symmetrically distributed around the cavity. A CF vector (magnitude and direction) is calculated and displayed on the EnSite Precision™ Cardiac Mapping System (Abbott Laboratories, Minneapolis, MN) [46].
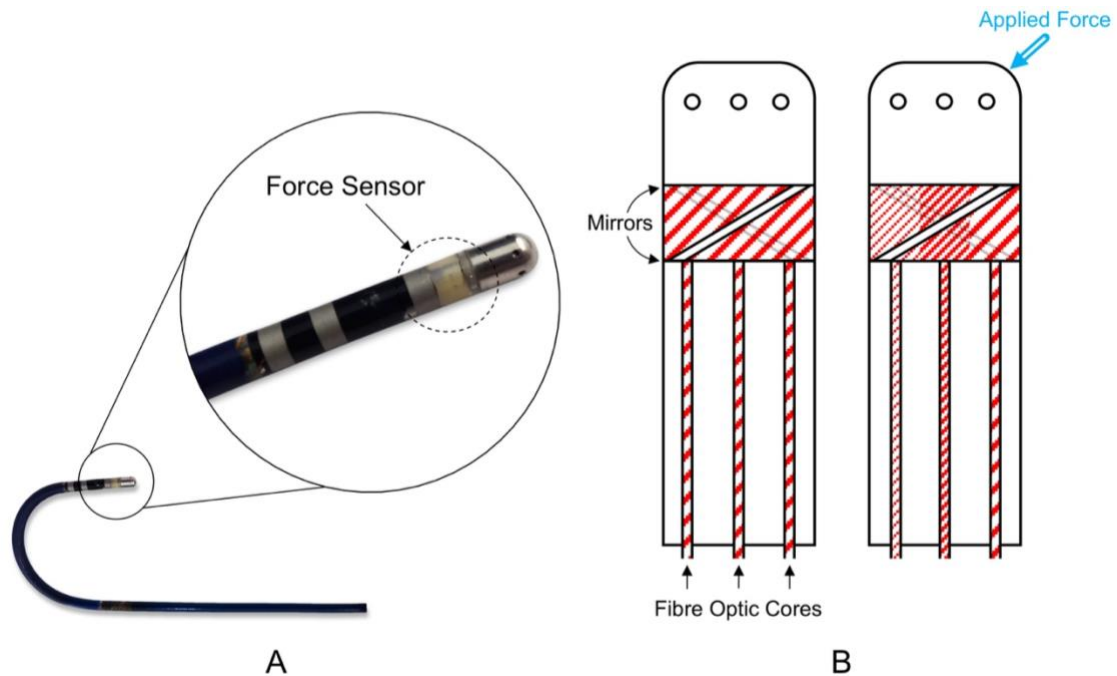
Figure 1.12. Photograph of TactiCath™ force-sensing ablation catheter tip **A**. The force sensor consists of a deformable body and three optical fibres. When force is applied to the tip (blue arrow), a cavity within the deformable body reflects infrared light (indicated in red) with an interference pattern proportional to the change in force **B**.

The accuracy and precision of TactiCath™, as well as its safety and effectiveness in ablation procedures, have been investigated in several studies [45, 46, 57, 103]. The TactiCath™ was shown to have improved accuracy over the THERMOCOOL® SMARTTOUCH™ catheter, specifically while the catheter is in an orientation parallel to the tissue (*i.e.* delivering "linear" lesions) [104].

1.3.3   Steerable Sheaths

A steerable guiding sheath is a widely used tool available to the EP during ablation procedures. Used in conjunction with ablation catheter, steerable sheaths have been shown to improve maneuverability and stability of the ablation catheter, as well as enhance contact between the catheter tip and cardiac tissue during lesion production [105-109]. Incorporating a steerable sheath has also been shown to increase first-procedure clinical success rates over its non-steerable counterpart [110].

The Agilis™ NxT Steerable Introducer (Abbott Laboratories, Minneapolis, MN) [79] is the world's most commonly used steerable sheath. The handle of the Agilis™ consists of a hemostatic seal and side-port irrigation line proximal to the handle. An ablation catheter can be inserted into the hemostatic seal and entirely fed through the hollow braided shaft of the sheath (**Figure 1.13**). The bi-directional deflection mechanism located on the handle allows the EP to deflect the distal tip of the sheath bi-directionally up to 180°.
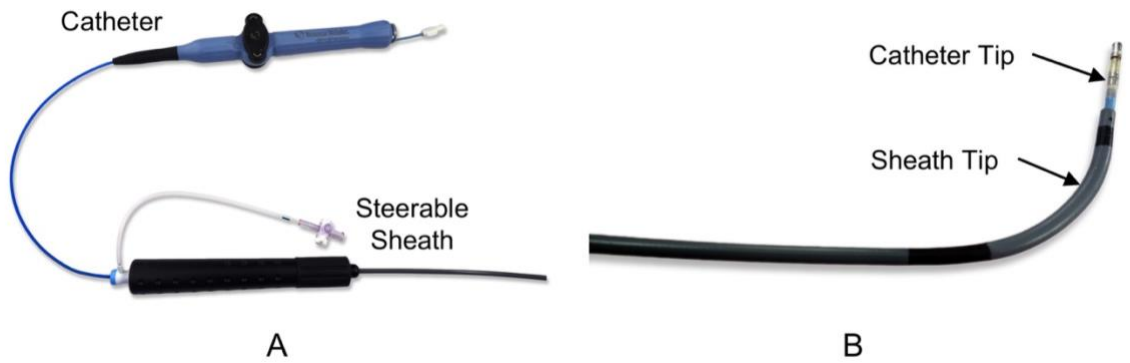
Figure 1.13. Photographs of a force-sensing ablation catheter in conjunction with the Agilis™ steerable sheath **A**, and their corresponding tips **B**. The operator now can insert, withdraw, rotate, and deflect both the catheter and sheath independently from one another.

The steerable sheath provides additional degrees-of-freedom associated with catheter manipulation. The EP now can insert, withdraw, rotate, and deflect both the catheter and sheath independently from one another, which allows the EP to reach extended targets and manage complex anatomy. In practice, however, catheter manipulation primarily involves manipulating the steerable sheath (insertion, withdrawal, rotation, and deflection) and only inserting or withdrawing the catheter to change the amount of CF the catheter tip applies to the cardiac tissue (**Figure 1.14**). This approach is popular among recently trained electrophysiologists and residents entering the field.
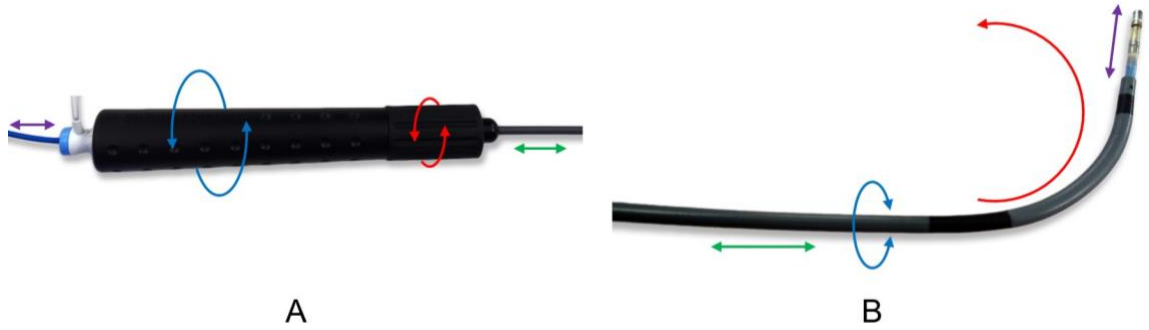
Figure 1.14. Photographs of the steerable sheath handle **A**, and the catheter and sheath tips **B**. Manipulation primarily involves in manipulating the steerable sheath includes rotation (blue), insertion and withdrawal (green) and deflection (red). By inserting and withdrawing the catheter through the sheath (purple), the operator can adjust the amount of applied force the electrode tip exerts on the tissue.

The MOBICATH® Sheath (Biosense Webster, Irvine, CA) and Vizigo™ Bi-Directional Guiding Sheath (Biosense Webster, Irvine, CA) are steerable sheaths developed by Biosense Webster, which have the similar operation as the Agilis™. Vizigo™ incorporates electromagnetic sensors incorporated at the distal tip, which allows the sheath tip to be visualized by CARTO® and display its position and orientation within the EAM systems. The Vizigo™ is the first commercially available steerable sheath that provides this capability.

1.3.4   Remote Catheter Navigation Systems

Ablation strategies to treat cardiac arrhythmia are complex, technically challenging, and require a high degree of skill and physical effort. To address these challenges, remote catheter navigation systems, utilizing both robotic and magnetic actuation technologies, have been developed and introduced clinically. Robotic and magnetic navigation systems (RNS and MNS, respectively) are appealing because they provide remote precise catheter navigation and have ancillary benefits, such as reducing fluoroscopic x-ray radiation exposure and the risk to the physician of developing orthopedic problems related to prolonged use of protective lead aprons. This section will describe four remote catheter navigation technologies developed for clinical use.

1.3.4.1   Amigo™ Remote Catheter System

The Amigo™ Remote Catheter System (Catheter Precision, Mount Olive, NJ) [111] comprises of a robotic arm attached to the rails of a standard electrophysiology table and is positioned above the patient's legs when in use. A conventional RF ablation catheter is inserted into the patient before being loaded into the Amigo™. The RNS is operated by a wired hand-held remote-control device that looks similar to the proximal handle of a conventional catheter. The remote control, which may be used up to 30 m away from the patient, provides full-range manipulation: inserting; withdrawing; rotating and deflecting the tip of the catheter. The Amigo™ does not incorporate separate workstations, monitors, or other hardware and introducing it into the catheter lab does not require additional room construction. The open platform approach of the system is designed to accommodate a range of commercially available catheters; however, the robotic system is only compatible with a few catheters manufactured by either Biosense Webster or Boston Scientific.

The Amigo™ underwent its first clinical trial to evaluate its performance and safety in mapping the right side of the heart [112]. In the following years, several clinical studies have demonstrated that the Amigo™ can perform safe and effective right atrial ablation, as well as left atrial mapping and pulmonary vein isolation comparable to the standard approach [113-116]. The Amigo™ has a short learning curve and significantly reduces fluoroscopic x-ray radiation exposure to the operator. A drawback of the system is the lack of a steerable sheath limiting the manoeuvrability and stability of the catheter tip.

1.3.4.2   Sensei® X Robotic System

The Sensei® X Robotic System (Hansen Medical, Mountain View, CA) [117] provides robotic steering of two concentric sheaths (14 Fr outer and 10.5 Fr inner), through which any conventional ablation catheter can be inserted. The assembly is manipulated within the heart by a robotic arm positioned over the patient's legs and fixed to the rails of a standard

electrophysiology table. The Sensei® is controlled within a separate console workstation positioned in the control room, which provides a 3D joystick and visual feedback to the EP. Manipulating the ball-like joystick changes the applied tension to the pull-wires embedded within the inner and outer steerable sheaths, resulting in a broad range of motion in any direction. If the EP uses the Artisan® X Control Catheter (Hansen Medical, Mountain View, CA), the incorporated force sensor within the catheter shaft detects real-time perpendicular contact-force between the catheter tip and moving tissue. This information is provided visually to the physician as well as through their IntelliSense® Fine Force (Hansen Medical, Mountain View, CA) haptic technology.

Although the Sensei® can be used with virtually all commercially available EAM systems, their CoHesion™ 3D Visualization Module (Hansen Medical, Mountain View, CA) specialized software was developed for robotic integration, 3D visualization, mapping and tracking with the EnSite™ Prevision Cardiac Mapping system (Abbott Laboratories, Minneapolis, MN).

In early clinical use, the initial concern regarding the Sensei® system was the increased risk of perforation [118, 119]. However, more recent reports have demonstrated the feasibility of performing PVI without major complications [120, 121]. Unfortunately, the huge trans-septal outer sheath limits access to critical cardiac structures such as the left ventricle and coronary sinus [122], which significantly limit the application of the Sensei® system to atrial ablation.

In 2016, Hansen Medical was acquired by Auris Health, a medical device company that develops a bronchoscopic robotic navigation system. Since the acquisition, Auris has terminated the Sensei® platform and incorporated the technology into its platform.

1.3.4.3   NIOBE™ Magnetic Navigation System

The NIOBE™ Magnetic Navigation System (Stereotaxis, St. Louis, MO) [123] is the most widely used remote navigation system with more than 100 active hospital installations, 300 physicians and 9,000 procedures performed annually. NIOBE™ consists of two neodymium-iron-boron permanent magnets positioned on both sides of a standard electrophysiology table, creating a uniform magnetic field (0.08 Tesla [T]) across the patient's chest [124-126]. A specialized ablation catheter, which incorporates three small magnets affixed to the distal tip, is navigated to target locations by first manipulating the magnetic field orientation. This is done by computer-aided mechanical movements of the external permanent magnets. The distal portion of the magnetic catheter becomes aligned with the new orientation of the magnetic field. The Cardiodrive® (Stereotaxis, St. Louis, MO) electromechanical unit is used to position the catheter along the magnetic field. Once the catheter is inserted into the patient's cardiac chamber and loaded into the Cardiodrive® unit, all further manipulation can be done remotely from a control room utilizing a joystick, keyboard, or mouse control. NIOBE™ also has functional automation software designed to allow for automatic movement of the catheter to specific points, along with defined paths, in a preprogrammed motion [123].

The weak magnetic field in conjunction with a soft and flexible catheter provides unique capabilities and benefits, as demonstrated in clinical use: (1) increased precision with catheter movement and control; (2) reduce the risk of intermittent contact; and (3) decreased risk of cardiac perforation due to the compliant nature of the catheter [127]. However, whether these benefits translate to improved clinical success remains to be determined, as clinical trials of patients undergoing PVI guided by NIOBE™ versus the manual approach has reported mixed results [118, 125, 126, 128, 129].

The NIOBE™ system also has several shortcomings, which include: (1) incredible costs associated with the system and room construction; (2) installation of the system in existing catheter laboratory requires special room shielding and additional regulation because of the additional permanent magnetic field; (3) since the magnetic fields are changed by mechanical movements, a large delay occurs between designation of magnetic field vector and catheter movement within the heart; (4) risk of interference with patients implanted with a cardiac defibrillation device; (5) the only EAM compatible with NIOBE™ is CARTO®; (6) the magnetic catheter cannot detect catheter-tissue CF; and importantly (7) due to the weak magnetic field strength the NIOBE™ system has been scrutinize by its users that it cannot reach adequate levels of catheter-tissue CF [122, 130, 131]. Described in detail in previous sections, insufficient CF results in ineffective lesion production correlates with reconnection gaps.

1.3.4.4   Catheter Guidance Control and Imaging

The Catheter Guidance Control and Imaging (CGCI, Magnetecs, Inglewood, CA) [132] is a non-commercial MNS that uses eight electromagnets affixed semi-spherically around the patient's chest generating a dynamic 15 cm^3 magnetic field within the heart [122]. The CGCI can navigate a specialized magnetic catheter by manipulating the field strength, orientation and gradient in near real-time. Similar to NIOBE™, the CGCI uses an electromechanical unit to advance and retract the catheter along the magnetic field vector. The CGCI has a maximum field strength of (0.16 T) resulting in a stronger field gradient (0.7 T/m). The stronger field gradient results in a maximum perpendicular force of 25 g; however, this has yet to be validated. The EP manipulates the catheter from a workstation manually, using a joystick to guide the catheter, or automatically, whereby the physician selects a target on display and the CGCI system plans the path and automatically moves the catheter accordingly.

The initial data collected from animal studies using the CGCI are promising [133]; however, clinical data are lacking. A 2010 clinical trial involving five patients was performed and published [134] and a second and third round of patients involving another 74 patients performed in 2011 [132]. In 2014, a third CGCI installation commenced a multi-site randomized study of paroxysmal AF ablation procedures with 100 patients. The results from this clinical trial will provide further validation and outline a path to FDA clearance [132].

1.4   Robotic Catheter Systems in Academia

Several robotic systems for remotely manipulating catheters during cardiovascular intervention have been developed in academia. These include systems for remotely positioning catheters guidance by different medical imaging modalities as well as improving lesion production. A brief overview of these projects is discussed in this section.

The robotic catheter system proposed in this thesis is inspired mainly by the design approach of earlier work in our group. Thakur *et al.* developed a 2 degrees-of-freedom (2-DOF) RNS designed for remote navigation during fluoroscopically guided catheterization [135-137]. The design of the system attempted to take advantage of the EP's already acquired dexterous skill of the catheter. The preliminary work defined velocities and accelerations of a catheter, manipulated by an EP, during catheter intervention [138]. The system was then further improved by Tavallaei *et al*. whereby the group developed a 3-DOF RNS designed to be compatible with MRI guidance [139-141]. The group developed and evaluated a novel RNS capable of remotely manipulating a catheter within the bore of an MRI scanner using non-ferromagnetic ultrasonic motors.

Cercenelli *et al*. [142] designed and developed a versatile RNS for remote navigation of a standard ablation catheter. Entitled CathROB, the RNS is impressively compact has built-in features including automatic catheter repositioning and a force-sensing mechanism

designed for haptic applications. The system has been evaluated *in vitro* and *in vivo* using an animal model.

Several other groups have developed robotic devices to address problems relating to various intracardiac interventions. Notably, Dr. R. Howe's group has developed a catheter RNS to assist with intracardiac mitral valve annuloplasty [143, 144]. This project included concepts of remote catheter manipulation and force control of a surgical instrument within a beating heart. The group also developed an open-source 3D-printed force sensor with an integrated RF electrode tip [145]. This custom force sensor, fixed to a catheter tip, was used to develop and evaluate a robotic system enabled with CF control of the electrode tip with moving tissue [146].

Khoshnam *et al*. undertook attempts to improve catheter-tissue CF using robotic platforms. The group developed a method to estimate CF of a catheter without an incorporated force sensor. The catheter tip was modelled as a large deflection beam to derive a load-displacement relationship of the curvature of the catheter tip caused by an applied external force [147, 148]. Based on this preliminary work, a robotic system was developed to enable CF control and tested on a lab-bench setup [149].

The projects discussed in this section have highlighted important aspects relating to remote catheter manipulation and CF control. The knowledge obtained from these projects contributed to the overall design, architecture, and engineering approach used to develop and test the robotic platforms proposed in this thesis.

1.5   Design Approach of Proposed Robotic System

In this thesis, a novel RNS is proposed, designed to enable remote catheter navigation and CF control between the catheter tip and moving tissue. An operator uses an interface to robotically navigate a remote catheter tip to a target location within a moving cardiac chamber. Before the RF application, the operator can employ force control mechanism that

would advance the catheter and automatically adjust its position in order to maintain catheter-tissue CF at the desired force set by the operator.

The proposed RNS will enable remote manipulation of conventional commercially available force-sensing ablation catheters permitting access to all cardiac chambers and preserving compatibility of existing EAM systems. The RNS will provide improved catheter tip stability and manoeuvrability in real-time, while at the same time reducing the learning curve by providing an intuitive method of controlling the robotic system. Lastly, but importantly, the proposed RNS will allow the EP to deliver reliably transmural RF ablation lesions by providing the capability to control CF between the catheter electrode tip and moving tissue.

The design of the proposed RNS was inspired by the observation of modern RF catheter intervention in the EP lab and independent interviews with electrophysiologists and clinical staff. A series of formative studies were performed to acquire basic comprehension of manual catheter manipulation techniques. Several EPs, with a variety of clinical experience, participated in an *in vitro* phantom-based formative study. Based on these data, it was observed that most EPs navigate a catheter tip to targets within the cardiac chamber primarily using a steerable sheath. Once preliminary contact is made, the EP then inserts or withdraws the catheter through the sheath until an acceptable CF is experienced on the electrode tip. Conventional catheter manipulation technique is illustrated in **Figure 1.14**. After observing that the CF is adequate and safe, an RF application would be initiated, and an ablation lesion would be delivered into the tissue. This process would be repeated contiguously encircling the PVs and other necessary cardiac structures.

The proposed RNS will reproduce the same manipulation technique described above, by providing remote control of a force-sensing ablation catheter in conjunction with a steerable sheath. The *Steerable Sheath and Catheter Robotic Navigation System (SSC-*

RNS) will allow for full-range manipulation of a conventional steerable sheath (insertion, withdrawal, rotation, and deflection) in 3-DOF and permit coaxial displacement of the catheter (insertion and withdrawal) within the sheath in 1-DOF. This design allows for CF control by autonomously displacing the catheter within the sheath to ensure that the CF of the catheter tip is always maintained at the set level. An overview of the proposed architecture is illustrated in **Figure 1.15**. Various microcontroller-based electronics within the SSC-RNS receive data wirelessly from an input device and process numerous control algorithms, based on linear control theory, to generate proportional control signals. The robotic systems' numerous motors actuate the steerable sheath and catheter (mounted within the SSC-RNS), replicating the motion of the input device. Furthermore, the SSC-RNS continuously receives wireless real-time CF measurements provided by an EAM system (connected to a corresponding force-sensing ablation catheter) and processes a predictive control algorithm and generate a control signal that positions the catheter within the sheath under closed-loop CF control.

The robotic system of the SSC-RNS uses an electromechanical mechanism for catheter-tissue CF control. This device was initially designed, developed and evaluated independently from the SSC-RNS. The compact device aptly named the *Catheter Contact-Force Controller (CFC)* was then incorporated into the SSC-RNS platform, further enabling remote navigation of the steerable sheath.

The SSC-RNS is controlled remotely by an intuitive input device that is designed to utilize the dextrous skills and hand-eye coordination of a trained EP. The input device is fitted with encoders and electronics to capture the motion (insertion, withdrawal, rotation, and deflection) of a repurposed steerable sheath handle and wirelessly transmit the data to the robotic system. Manipulation of the input device results in direct robotic manipulation of a remote steerable sheath and catheter in real-time. The input device also provides a user interface enabling the operator to select navigation and force control parameters.
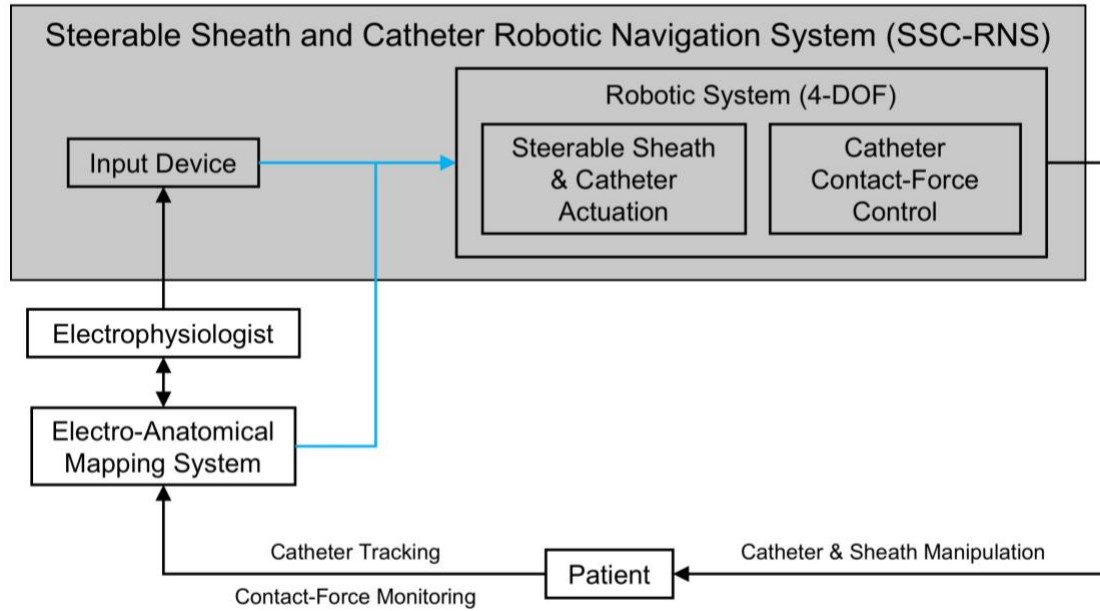
Figure 1.15. A block diagram describing the architecture of the proposed SSC-RNS. An EAM system tracks the location of the tip of a force-sensing ablation catheter within a patient's cardiac chamber and monitors its CF between the catheter tip and moving cardiac tissue. The EP then manipulates an input device, which captures the desired motion to be replicated a robotic system. The robotic system wirelessly receives position data from the input device and real-time CF measurements from the EAM (indicated in blue). The robotic system actuates a remote steerable sheath and force-sensing catheter (within the patient) according to the changes in the position of the input device. Furthermore, the robotic system can enable CF control between the catheter tip and moving cardiac tissue employed by the input device.

In a clinical setting, the distal tip of the catheter and sheath would be first manually introduced into the patient's cardiac chamber. The proximal handles of both the catheter and sheath would then be mounted into the SSC-RNS. The operator would then sit comfortably at the workstation of the EAM system with the input device, thereby decreasing fluoroscopic exposure and operator fatigue. Guided by the EAM system, the operator would use the SSC-RNS to navigate the catheter tip to the desired location and engage the catheter tip and the moving tissue. The force controller set to the desired level (typically between 10 g and 20 g), would be employed resulting in a CF profile with low variability. An RF application would then be delivered before continuing to the adjacent target. Point-by-point ablation would continue until the therapy is completed.

1.6   Thesis Overview

This introductory chapter provided a description of AF and modern catheter-based therapeutic techniques, along with a brief overview of state-of-the-art commercial tools and technology relating to RF catheter ablation. Because this thesis is presented in an "integrated article format" the remaining body chapters represent publications that are either published, accepted for publication, or in preparation for submission, and inevitably some duplication of the introductory material is present. Efforts have been made to link the independent papers as much as possible.

This introductory chapter provided a description of AF and modern catheter-based therapeutic techniques. A brief overview of the current state-of-the-art commercial tools and technology relating to RF catheter ablation was also described. This chapter also discussed the benefits and limitations of commercial remote navigation systems as well as novel technologies developed in academia. The outline of this thesis and the corresponding contributions in each chapter are as follows.

Chapter 2 describes the design, development, and lab-bench evaluation of a novel device, designed by me, enabling catheter-tissue CF control. A custom-built linear motion stage, capable of reproducing clinically relevant motion, was used to evaluate the force control performance of the CFC. CF profiles of a catheter engaging with tissue-mimicking material were recorded with and without the use of the CFC (representative of manual intervention). Manual and CFC-assisted CF profiles were compared with one another. A version of this chapter, entitled "*Design and Evaluation of a Catheter Contact-Force Controller for Cardiac Ablation Therapy,*" has been published in IEEE Transactions on Biomedical Engineering (vol. 63, no. 11, pp. 2301-2307, 2016).

Chapter 3 further evaluates the CFC *in vitro* to examines its impact on RF lesion production. CFC-assisted RF ablation lesions were delivered to moving tissue at different

clinically relevant force levels and were compared to lesions delivered in tissue in the absence of motion. CFC-assisted ablation lesions were also compared to lesions without force control representing manual catheter intervention. Furthermore, the CFC was also tested *in vivo* in a pig model to evaluate its force control performance in a beating heart. A version of this chapter, entitled "*Eliminating the effects of motion during radiofrequency lesion delivery using a novel contact-force controller,*" has been accepted for publication to the Journal of Cardiovascular Electrophysiology.

The work in Chapter 4 incorporates the CFC technology into a robotic platform that enables remote navigation of the steerable sheath and force-sensing ablation catheter. In a lab-bench study, an operator robotically navigated a remote catheter tip to stationary and moving targets within a contractile motion phantom. The operator employed the force controller on moving targets to a set amount of force. Catheter tip-target accuracy and force-controlled profiles were compared to a repeat experiment where the tasks were performed manually. A version of this chapter, entitled "*Remote catheter navigation and contact-force control: design and evaluation of a novel steerable sheath and catheter robotic navigation system,*" is in preparation for submission to IEEE Transaction on Biomedical Engineering.

Chapter 5 provides a summary of the accomplishments and contributions of the thesis, followed by suggestions for future work that uses the CFC to improve understanding of the effects of contact force on lesion production and translation of the device into clinical use.

1.7   References

[1]   H. Calkins *et al.*, "2017 HRS/EHRA/ECAS/APHRS/SOLAECE expert consensus statement on catheter and surgical ablation of atrial fibrillation," *Heart Rhythm,* vol. 14, no. 10, pp. e275-e444, 2017

[2]   H. Calkins *et al.*, "2012 HRS/EHRA/ECAS expert consensus statement on catheter and surgical ablation of atrial fibrillation: recommendations for patient selection, procedural techniques, patient management and follow-up, definitions, endpoints, and research trial design: a report of the Heart Rhythm Society (HRS) Task Force on Catheter and Surgical Ablation of Atrial Fibrillation. Developed in partnership with the European Heart Rhythm Association (EHRA), a registered branch of the European Society of Cardiology (ESC) and the European Cardiac Arrhythmia Society (ECAS); and in collaboration with the American College of Cardiology (ACC), American Heart Association (AHA), the Asia Pacific Heart Rhythm Society (APHRS), and the Society of Thoracic Surgeons (STS). Endorsed by the governing bodies of the American College of Cardiology Foundation, the American Heart Association, the European Cardiac Arrhythmia Society, the European Heart Rhythm Association, the Society of Thoracic Surgeons, the Asia Pacific Heart Rhythm Society, and the Heart Rhythm Society," *Heart Rhythm,* vol. 9, no. 4, pp. 632-96 e21, 2012

[3]   A. J. Camm *et al.*, "Guidelines for the management of atrial fibrillation: the Task Force for the Management of Atrial Fibrillation of the European Society of Cardiology (ESC)," *Europace,* vol. 12, no. 10, pp. 1360-420, 2010

[4]   C. T. January *et al.*, "2014 AHA/ACC/HRS guideline for the management of patients with atrial fibrillation: a report of the American College of Cardiology/American Heart Association Task Force on Practice Guidelines and the Heart Rhythm Society," *J Am Coll Cardiol,* vol. 64, no. 21, pp. e1-76, 2014

[5]   H. Zulkifly, G. Y. H. Lip, and D. A. Lane, "Epidemiology of atrial fibrillation," *Int J Clin Pract,* vol. 72, no. 3, p. e13070, 2018

[6]   G. Y. H. Lip, C. M. Brechin, and D. A. Lane, "The global burden of atrial fibrillation and stroke: a systematic review of the epidemiology of atrial fibrillation in regions outside North America and Europe," *Chest,* vol. 142, no. 6, pp. 1489-98, 2012

[7]   A. S. Go *et al.*, "Prevalence of diagnosed atrial fibrillation in adults: national implications for rhythm management and stroke prevention: the AnTicoagulation and Risk Factors in Atrial Fibrillation (ATRIA) Study," *Jama,* vol. 285, no. 18, pp. 2370-5, 2001

[8]   A. Alonso *et al.*, "Simple risk model predicts incidence of atrial fibrillation in a racially and geographically diverse population: the CHARGE-AF consortium," *J Am Heart Assoc,* vol. 2, no. 2, p. e000102, 2013

[9] S. A. Lubitz *et al.*, "Association between familial atrial fibrillation and risk of new-onset atrial fibrillation," *Jama,* vol. 304, no. 20, pp. 2263-2269, 2010

[10] S. S. Chugh *et al.*, "Worldwide epidemiology of atrial fibrillation: a Global Burden of Disease 2010 Study," *Circulation,* vol. 129, no. 8, pp. 837-47, 2014

[11] S. Colilla, A. Crow, W. Petkun, D. E. Singer, T. Simon, and X. Liu, "Estimates of current and future incidence and prevalence of atrial fibrillation in the U.S. adult population," *Am J Cardiol,* vol. 112, no. 8, pp. 1142-7, 2013

[12] P. P. Kneeland and M. C. Fang, "Trends in catheter ablation for atrial fibrillation in the United States," *J Hosp Med,* vol. 4, no. 7, pp. E1-5, 2009

[13] M. Writing Group *et al.*, "Executive Summary: Heart Disease and Stroke Statistics--2016 Update: A Report From the American Heart Association," *Circulation,* vol. 133, no. 4, pp. 447-54, 2016

[14] M. H. Kim, S. S. Johnston, B. C. Chu, M. R. Dalal, and K. L. Schulman, "Estimation of total incremental health care costs in patients with atrial fibrillation in the United States," *Circ Cardiovasc Qual Outcomes,* vol. 4, no. 3, pp. 313-20, 2011

[15] D. J. O'Reilly *et al.*, "The burden of atrial fibrillation on the hospital sector in Canada," *Can J Cardiol,* vol. 29, no. 2, pp. 229-35, 2013

[16] N. J. Patel, V. Atti, R. D. Mitrani, J. F. Viles-Gonzalez, and J. J. Goldberger, "Global rising trends of atrial fibrillation: a major public health concern," *Heart,* vol. 104, no. 24, pp. 1989-90, 2018

[17] A. Verma, L. Macle, J. Cox, A. C. Skanes, and C. C. S. A. F. G. Committee, "Canadian Cardiovascular Society atrial fibrillation guidelines 2010: catheter ablation for atrial fibrillation/atrial flutter," *Can J Cardiol,* vol. 27, no. 1, pp. 60-6, 2011

[18] P. A. Wolf, R. D. Abbott, and W. B. Kannel, "Atrial fibrillation as an independent risk factor for stroke: the Framingham Study," *Stroke,* vol. 22, no. 8, pp. 983-8, 1991

[19] E. J. Benjamin, P. A. Wolf, R. B. D'Agostino, H. Silbershatz, W. B. Kannel, and D. Levy, "Impact of atrial fibrillation on the risk of death: the Framingham Heart Study," *Circulation,* vol. 98, no. 10, pp. 946-52, 1998

[20] W. B. Kannel, P. A. Wolf, E. J. Benjamin, and D. Levy, "Prevalence, incidence, prognosis, and predisposing conditions for atrial fibrillation: population-based estimates," *Am J Cardiol,* vol. 82, no. 8A, pp. 2N-9N, 1998

[21]   P. S. Miller, F. L. Andersson, and L. Kalra, "Are cost benefits of anticoagulation for stroke prevention in atrial fibrillation underestimated?," *Stroke,* vol. 36, no. 2, pp. 360-6, 2005

[22]   T. J. Wang *et al.*, "A risk score for predicting stroke or death in individuals with new-onset atrial fibrillation in the community: the Framingham Heart Study," *Jama,* vol. 290, no. 8, pp. 1049-56, 2003

[23]   M. W. Rich and R. B. Fohtung, "Identification of Patients at Risk of Stroke From Atrial Fibrillation," *US Cardiology Review,* vol. 10, no. 2, pp. 60-4, 2016

[24]   R. Wakili, N. Voigt, S. Kaab, D. Dobrev, and S. Nattel, "Recent advances in the molecular pathophysiology of atrial fibrillation," *J Clin Invest,* vol. 121, no. 8, pp. 2955-68, 2011

[25]   J. Heijman, N. Voigt, S. Nattel, and D. Dobrev, "Cellular and molecular electrophysiology of atrial fibrillation initiation, maintenance, and progression," *Circ Res,* vol. 114, no. 9, pp. 1483-99, 2014

[26]   S. Nattel, B. Burstein, and D. Dobrev, "Atrial remodeling and atrial fibrillation: mechanisms and implications," *Circ Arrhythm Electrophysiol,* vol. 1, no. 1, pp. 62-73, 2008

[27]   M. Haissaguerre *et al.*, "Spontaneous initiation of atrial fibrillation by ectopic beats originating in the pulmonary veins," *N Engl J Med,* vol. 339, no. 10, pp. 659-66, 1998

[28]   L. Gepstein and S. J. Evans, "Electroanatomical mapping of the heart: basic concepts and implications for the treatment of cardiac arrhythmias," *Pacing Clin Electrophysiol,* vol. 21, no. 6, pp. 1268-78, 1998

[29]   C. Pappone, C. Garzillo, S. Crisà, and V. Santinelli, "Electroanatomical Mapping Systems. An Epochal Change in Cardiac Electrophysiology," in *Medical Imaging in Clinical Applications*: Springer, 2016, pp. 237-55.

[30]   H. Oral *et al.*, "Clinical significance of early recurrences of atrial fibrillation after pulmonary vein isolation," *J Am Coll Cardiol,* vol. 40, no. 1, pp. 100-4, 2002

[31]   H. Oral *et al.*, "Segmental ostial ablation to isolate the pulmonary veins during atrial fibrillation: feasibility and mechanistic insights," *Circulation,* vol. 106, no. 10, pp. 1256-62, 2002

[32]   A. Arya *et al.*, "Long-term results and the predictors of outcome of catheter ablation of atrial fibrillation using steerable sheath catheter navigation after single procedure in 674 patients," *Europace,* vol. 12, no. 2, pp. 173-80, 2010

[33]   A. N. Ganesan *et al.*, "Long-term outcomes of catheter ablation of atrial fibrillation: a systematic review and meta-analysis," *J Am Heart Assoc,* vol. 2, no. 2, p. e004549, 2013

[34]   O. M. Wazni *et al.*, "Radiofrequency ablation vs antiarrhythmic drugs as first-line treatment of symptomatic atrial fibrillation: a randomized trial," *Jama,* vol. 293, no. 21, pp. 2634-40, 2005

[35]   J. Cosedis Nielsen *et al.*, "Radiofrequency ablation as initial therapy in paroxysmal atrial fibrillation," *N Engl J Med,* vol. 367, no. 17, pp. 1587-95, 2012

[36]   C. A. Morillo *et al.*, "Radiofrequency ablation vs antiarrhythmic drugs as first-line treatment of paroxysmal atrial fibrillation (RAAFT-2): a randomized trial," *Jama,* vol. 311, no. 7, pp. 692-700, 2014

[37]   A. Hakalahti, F. Biancari, J. C. Nielsen, and M. J. Raatikainen, "Radiofrequency ablation vs. antiarrhythmic drug therapy as first line treatment of symptomatic atrial fibrillation: systematic review and meta-analysis," *Europace,* vol. 17, no. 3, pp. 370-8, 2015

[38]   D. L. Packer *et al.*, "Effect of Catheter Ablation vs Antiarrhythmic Drug Therapy on Mortality, Stroke, Bleeding, and Cardiac Arrest Among Patients With Atrial Fibrillation: The CABANA Randomized Clinical Trial," *Jama,* 2019

[39]   S. K. S. Huang and J. M. Miller, *Catheter Ablation of Cardiac Arrhythmias*, 4th ed. Elsevier, 2019.

[40]   C. Herrera Siklody *et al.*, "Incidence of asymptomatic intracranial embolic events after pulmonary vein isolation: comparison of different atrial fibrillation ablation technologies in a multicenter study," *J Am Coll Cardiol,* vol. 58, no. 7, pp. 681-8, 2011

[41]   F. Gaita *et al.*, "Radiofrequency catheter ablation of atrial fibrillation: a cause of silent thromboembolism? Magnetic resonance imaging assessment of cerebral thromboembolism in patients undergoing ablation of atrial fibrillation," *Circulation,* vol. 122, no. 17, pp. 1667-73, 2010

[42]   F. Kilicaslan *et al.*, "Transcranial Doppler detection of microembolic signals during pulmonary vein antrum isolation: implications for titration of radiofrequency energy," *J Cardiovasc Electrophysiol,* vol. 17, no. 5, pp. 495-501, 2006

[43]   J. M. Kalman *et al.*, "Biophysical characteristics of radiofrequency lesion formation in vivo: dynamics of catheter tip-tissue contact evaluated by intracardiac echocardiography," *Am Heart J,* vol. 133, no. 1, pp. 8-18, 1997

[44]   D. C. Shah, H. Lambert, H. Nakagawa, A. Langenkamp, N. Aeby, and G. Leo, "Area under the real-time contact force curve (force-time integral) predicts

radiofrequency lesion size in an in vitro contractile model," *J Cardiovasc Electrophysiol,* vol. 21, no. 9, pp. 1038-43, 2010

[45]   P. Neuzil *et al.*, "Electrical reconnection after pulmonary vein isolation is contingent on contact force during initial treatment: results from the EFFICAS I study," *Circ Arrhythm Electrophysiol,* vol. 6, no. 2, pp. 327-33, 2013

[46]   V. Reddy *et al.*, "The relationship between contact force and clinical outcome during radiofrequency catheter ablation of atrial fibrillation in the TOCCATA study," *Heart Rhythm,* vol. 9, no. 11, pp. 1789-1795, 2012

[47]   K. H. Kuck *et al.*, "A novel radiofrequency ablation catheter using contact force sensing: Toccata study," *Heart Rhythm,* vol. 9, no. 1, pp. 18-23, 2012

[48]   S. Haldar *et al.*, "Contact force sensing technology identifies sites of inadequate contact and reduces acute pulmonary vein reconnection: a prospective case control study," *Int J Cardiol,* vol. 168, no. 2, pp. 1160-6, 2013

[49]   B. J. Tofig *et al.*, "Recurrence after pulmonary vein isolation is associated with low contact force," *Scand Cardiovasc J,* vol. 52, no. 1, pp. 28-33, 2018

[50]   W. Ullah, R. J. Schilling, and T. Wong, "Contact Force and Atrial Fibrillation Ablation," *J Atr Fibrillation,* vol. 8, no. 5, p. 1282, 2016

[51]   B. Avitall, K. Mughal, J. Hare, R. Helms, and D. Krum, "The effects of electrode-tissue contact on radiofrequency lesion generation," *Pacing Clin Electrophysiol,* vol. 20, no. 12 Pt 1, pp. 2899-910, 1997

[52]   A. Thiagalingam *et al.*, "Importance of catheter contact force during irrigated radiofrequency ablation: evaluation in a porcine ex vivo model using a force-sensing catheter," *J Cardiovasc Electrophysiol,* vol. 21, no. 7, pp. 806-11, 2010

[53]   K. Yokoyama *et al.*, "Novel contact force sensor incorporated in irrigated radiofrequency ablation catheter predicts lesion size and incidence of steam pop and thrombus," *Circ Arrhythm Electrophysiol,* vol. 1, no. 5, pp. 354-362, 2008

[54]   C. Pappone *et al.*, "Atrio-esophageal fistula as a complication of percutaneous transcatheter ablation of atrial fibrillation," *Circulation,* vol. 109, no. 22, pp. 2724-6, 2004

[55]   D. C. Shah and M. Namdar, "Real-time contact force measurement: a key parameter for controlling lesion creation with radiofrequency energy," *Circ Arrhythm Electrophysiol,* vol. 8, no. 3, pp. 713-21, 2015

[56]   A. Ikeda *et al.*, "Relationship between catheter contact force and radiofrequency lesion size and incidence of steam pop in the beating canine heart: electrogram amplitude, impedance, and electrode temperature are poor predictors of electrode-

tissue contact force and lesion size," *Circ Arrhythm Electrophysiol,* vol. 7, no. 6, pp. 1174-80, 2014

[57]   J. Kautzner *et al.*, "EFFICAS II: optimization of catheter contact force improves outcome of pulmonary vein isolation for paroxysmal atrial fibrillation," *Europace,* vol. 17, no. 8, pp. 1229-35, 2015

[58]   A. Natale *et al.*, "Paroxysmal AF catheter ablation with a contact force sensing catheter: results of the prospective, multicenter SMART-AF trial," *J Am Coll Cardiol,* vol. 64, no. 7, pp. 647-56, 2014

[59]   V. Y. Reddy *et al.*, "The relationship between contact force and clinical outcome during radiofrequency catheter ablation of atrial fibrillation in the TOCCATA study," *Heart Rhythm,* vol. 9, no. 11, pp. 1789-95, 2012

[60]   V. Y. Reddy *et al.*, "Randomized, Controlled Trial of the Safety and Effectiveness of a Contact Force-Sensing Irrigated Catheter for Ablation of Paroxysmal Atrial Fibrillation: Results of the TactiCath Contact Force Ablation Catheter Study for Atrial Fibrillation (TOCCASTAR) Study," *Circulation,* vol. 132, no. 10, pp. 907-15, 2015

[61]   N. Ariyarathna, S. Kumar, S. P. Thomas, W. G. Stevenson, and G. F. Michaud, "Role of Contact Force Sensing in Catheter Ablation of Cardiac Arrhythmias: Evolution or History Repeating Itself?," *JACC Clin Electrophysiol,* vol. 4, no. 6, pp. 707-723, 2018

[62]   W. Ullah *et al.*, "Factors affecting catheter contact in the human left atrium and their impact on ablation efficacy," *J Cardiovasc Electrophysiol,* vol. 26, no. 2, pp. 129-36, 2015

[63]   H. Makimoto *et al.*, "Incidence and anatomical locations of catheter instability during circumferential pulmonary vein isolation using contact force," *Int Heart J,* vol. 55, no. 3, pp. 249-55, 2014

[64]   K. Rajappan *et al.*, "Acute and chronic pulmonary vein reconnection after atrial fibrillation ablation: a prospective characterization of anatomical sites," *Pacing Clin Electrophysiol,* vol. 31, no. 12, pp. 1598-605, 2008

[65]   A. Furnkranz *et al.*, "Ipsilateral pulmonary vein isolation performed by a single continuous circular lesion: role of pulmonary vein mapping during ablation," *Europace,* vol. 13, no. 7, pp. 935-41, 2011

[66]   S. Kumar *et al.*, "Effect of respiration on catheter-tissue contact force during ablation of atrial arrhythmias," *Heart Rhythm,* vol. 9, no. 7, pp. 1041-1047.e1, 2012

[67]   S. Kumar *et al.*, "Prospective characterization of catheter-tissue contact force at different anatomic sites during antral pulmonary vein isolation," *Circ Arrhythm Electrophysiol,* vol. 5, no. 6, pp. 1124-9, 2012

[68] R. De Ponti, R. Marazzi, L. A. Doni, J. Marazzato, C. Baratto, and J. A. Salerno-Uriarte, "Optimization of catheter/tissue contact during pulmonary vein isolation: the impact of atrial rhythm," *Europace,* vol. 20, no. 2, pp. 288-94, 2018

[69] A. Sarkozy *et al.*, "Contact force variability during catheter ablation of atrial fibrillation: the role of atrial rhythm and ventricular contractions: co-force AF Study," *Circ Arrhythm Electrophysiol,* vol. 8, no. 6, pp. 1342-50, 2015

[70] H. Matsuda *et al.*, "Atrial rhythm influences catheter tissue contact during radiofrequency catheter ablation of atrial fibrillation: comparison of contact force between sinus rhythm and atrial fibrillation," *Heart Vessels,* vol. 31, no. 9, pp. 1544-52, 2016

[71] A. Aizer *et al.*, "Pacing Mediated Heart Rate Acceleration Improves Catheter Stability and Enhances Markers for Lesion Delivery in Human Atria During Atrial Fibrillation Ablation," *JACC Clin Electrophysiol,* vol. 4, no. 4, pp. 483-90, 2018

[72] J. S. Goode, Jr., R. L. Taylor, C. W. Buffington, M. M. Klain, and D. Schwartzman, "High-frequency jet ventilation: utility in posterior left atrial catheter ablation," *Heart Rhythm,* vol. 3, no. 1, pp. 13-9, 2006

[73] N. Elkassabany *et al.*, "Anesthetic management of patients undergoing pulmonary vein isolation for treatment of atrial fibrillation using high-frequency jet ventilation," *J Cardiothorac Vasc Anesth,* vol. 26, no. 3, pp. 433-8, 2012

[74] L. Di Biase *et al.*, "General anesthesia reduces the prevalence of pulmonary vein reconnection during repeat ablation when compared with conscious sedation: results from a randomized study," *Heart Rhythm,* vol. 8, no. 3, pp. 368-72, 2011

[75] W. C. Beamer, D. S. Prough, R. L. Royster, W. E. Johnston, and J. C. Johnson, "High-frequency jet ventilation produces auto-PEEP," *Crit Care Med,* vol. 12, no. 9, pp. 734-7, 1984

[76] L. Di Biase *et al.*, "Esophageal capsule endoscopy after radiofrequency catheter ablation for atrial fibrillation: documented higher risk of luminal esophageal damage with general anesthesia as compared with conscious sedation," *Circ Arrhythm Electrophysiol,* vol. 2, no. 2, pp. 108-12, 2009

[77] "Biosense Webster, Inc." [Online]. Available: www.biosensewebster.com.

[78] D. Bhakta and J. M. Miller, "Principles of electroanatomic mapping," *Indian Pacing Electrophysiol J,* vol. 8, no. 1, pp. 32-50, 2008

[79] "Abbott Laboratories, Ltd." [Online]. Available: www.abbott.com.

[80] X. Liu, X.-h. Wang, J.-N. Gu, L. Zhou, and J.-h. Qiu, "Electroanatomical systems to guided circumferential pulmonary veins ablation for atrial fibrillation: initial

experience from comparison between the Ensite/NavX and CARTO system," *Chin Med J,* vol. 118, no. 14, pp. 1156-60, 2005

[81]   "Boston Scientific, Inc." [Online]. Available: www.bostonscientific.com.

[82]   P. Maury *et al.*, "Comparison between novel and standard high-density 3D electro-anatomical mapping systems for ablation of atrial tachycardia," *Heart Vessels,* vol. 34, no. 5, pp. 801-808, 2018

[83]   A. Thajudeen *et al.*, "Correlation of scar in cardiac MRI and high-resolution contact mapping of left ventricle in a chronic infarct model," *Pacing Clin Electrophysiol,* vol. 38, no. 6, pp. 663-74, 2015

[84]   Y. Tanaka, M. Genet, L. Chuan Lee, A. J. Martin, R. Sievers, and E. P. Gerstenfeld, "Utility of high-resolution electroanatomic mapping of the left ventricle using a multispline basket catheter in a swine model of chronic myocardial infarction," *Heart Rhythm,* vol. 12, no. 1, pp. 144-54, 2015

[85]   L. Rottner *et al.*, "Direct Comparison of Point-by-Point and Rapid Ultra-High-Resolution Electroanatomical Mapping in Patients Scheduled for Ablation of Atrial Fibrillation," *J Cardiovasc Electrophysiol,* vol. 28, no. 3, pp. 289-97, 2017

[86]   L. M. Ptaszek *et al.*, "Rapid acquisition of high-resolution electroanatomical maps using a novel multielectrode mapping system," *J Interv Card Electrophysiol,* vol. 36, no. 3, pp. 233-42, 2013

[87]   B. Pathik and J. M. Kalman, "Perceiving the Imperceptible in Atrial Macro-Reentry: Ultrahigh Resolution Mapping to Characterize the Critical Isthmus," *Circ Arrhythm Electrophysiol,* vol. 10, no. 1, p. e004850, 2017

[88]   H. Nakagawa, A. Ikeda, T. Sharma, R. Lazzara, and W. M. Jackman, "Rapid high resolution electroanatomical mapping: evaluation of a new system in a canine atrial linear lesion model," *Circ Arrhythm Electrophysiol,* vol. 5, no. 2, pp. 417-24, 2012

[89]   D. G. Latcu *et al.*, "Selection of Critical Isthmus in Scar-Related Atrial Tachycardia Using a New Automated Ultrahigh Resolution Mapping System," *Circ Arrhythm Electrophysiol,* vol. 10, no. 1, 2017

[90]   A. Bollmann, S. Hilbert, S. John, J. Kosiuk, and G. Hindricks, "Initial Experience With Ultra High-Density Mapping of Human Right Atria," *J Cardiovasc Electrophysiol,* vol. 27, no. 2, pp. 154-60, 2016

[91]   E. Anter, C. M. Tschabrunn, F. M. Contreras-Valdes, J. Li, and M. E. Josephson, "Pulmonary vein isolation using the Rhythmia mapping system: Verification of intracardiac signals using the Orion mini-basket catheter," *Heart Rhythm,* vol. 12, no. 9, pp. 1927-34, 2015

[92]   E. Anter *et al.*, "Evaluation of a novel high-resolution mapping technology for ablation of recurrent scar-related atrial tachycardias," *Heart Rhythm,* vol. 13, no. 10, pp. 2048-55, 2016

[93]   D. L. Rankin and J. C. Potosky, "Force sensing catheter with a magnet and an inductive sensor," Patent Appl. US20170290617A1, 2017.

[94]   I. Guler, D. L. Rankin, and J. C. Potosky, "Force sensing catheter with a slotted tube element," Patent Appl. US20170143416A1, 2017.

[95]   D. L. Rankin and J. C. Potosky, "Catheter with inductive force sensing elements," United States Patent Appl. US20170035357A1, 2017.

[96]   M. M. Byron, J. I. Laughner, and S. Shome, "Force sensing catheter with impedance-guided orientation," Patent Appl. US20170215802A1, 2017.

[97]   H. Nakagawa *et al.*, "Locations of high contact force during left atrial mapping in atrial fibrillation patients: electrogram amplitude and impedance are poor predictors of electrode-tissue contact force for ablation of atrial fibrillation," *Circ Arrhythm Electrophysiol,* vol. 6, no. 4, pp. 746-53, 2013

[98]   E. Leshem *et al.*, "High-Resolution Mapping of Ventricular Scar: Evaluation of a Novel Integrated Multielectrode Mapping and Ablation Catheter," *JACC Clin Electrophysiol,* vol. 3, no. 3, pp. 220-31, 2017

[99]   G. Rozen *et al.*, "Safety and efficacy of delivering high-power short-duration radiofrequency ablation lesions utilizing a novel temperature sensing technology," *Europace,* vol. 20, no. Fi_3, pp. f444-f450, 2018

[100] E. Leshem *et al.*, "High-Power and Short-Duration Ablation for Pulmonary Vein Isolation: Biophysical Characterization," *JACC Clin Electrophysiol,* vol. 4, no. 4, pp. 467-79, 2018

[101] M. Barkagan, F. M. Contreras-Valdes, E. Leshem, A. E. Buxton, H. Nakagawa, and E. Anter, "High-power and short-duration ablation for pulmonary vein isolation: Safety, efficacy, and long-term durability," *J Cardiovasc Electrophysiol,* vol. 29, no. 9, pp. 1287-96, 2018

[102] K. Yokoyama *et al.*, "Novel contact force sensor incorporated in irrigated radiofrequency ablation catheter predicts lesion size and incidence of steam pop and thrombus," *Circ Arrhythm Electrophysiol,* vol. 1, no. 5, pp. 354-362, 2008

[103] F. Bourier *et al.*, "Fiberoptic Contact-Force Sensing Electrophysiological Catheters: How Precise Is the Technology?," *J Cardiovasc Electrophysiol,* vol. 28, no. 1, pp. 109-14, 2017

[104] F. Bourier *et al.*, "Electromagnetic Contact-Force Sensing Electrophysiological Catheters: How Accurate Is the Technology?," *J Cardiovasc Electrophysiol,* vol. 27, no. 3, pp. 347-50, 2016

[105] M. W. Deyell *et al.*, "The impact of steerable sheaths on unblinded contact force during catheter ablation for atrial fibrillation," *J Interv Card Electrophysiol,* 2019

[106] C. Piorkowski *et al.*, "Steerable versus nonsteerable sheath technology in atrial fibrillation ablation a prospective, randomized study," *Circ Arrhythm Electrophysiol,* vol. 4, no. 2, pp. 157-165, 2011

[107] W. Ullah *et al.*, "Impact of steerable sheaths on contact forces and reconnection sites in ablation for persistent atrial fibrillation," *J Cardiovasc Electrophysiol,* vol. 26, no. 3, pp. 266-73, 2015

[108] T. Kimura *et al.*, "Operator-blinded contact force monitoring during pulmonary vein isolation using conventional and steerable sheaths," *Int J Cardiol,* vol. 177, no. 3, pp. 970-6, 2014

[109] M. Masuda *et al.*, "Steerable versus non-steerable sheaths during pulmonary vein isolation: impact of left atrial enlargement on the catheter-tissue contact force," *J Interv Card Electrophysiol,* vol. 47, no. 1, pp. 99-107, 2016

[110] C. Piorkowski *et al.*, "Steerable sheath catheter navigation for ablation of atrial fibrillation: a case-control study," *Pacing Clin Electrophysiol,* vol. 31, no. 7, pp. 863-73, 2008

[111] "Catheter Precision, Inc." [Online]. Available: www.catheterprecision.com.

[112] E. M. Khan *et al.*, "First experience with a novel robotic remote catheter system: Amigo mapping trial," *J Interv Card Electrophysiol,* vol. 37, no. 2, pp. 121-9, 2013

[113] T. Datino *et al.*, "Arrhythmia ablation using the Amigo Robotic Remote Catheter System versus manual ablation: One year follow-up results," *Int J Cardiol,* vol. 202, pp. 877-8, 2016

[114] A. Wutzler *et al.*, "Robotic ablation of atrial fibrillation with a new remote catheter system," *J Interv Card Electrophysiol,* vol. 40, no. 3, pp. 215-9, 2014

[115] A. Wutzler, T. Wolber, W. Haverkamp, and L. H. Boldt, "Robotic ablation of atrial fibrillation," *J Vis Exp,* no. 99, p. e52560, 2015

[116] M. Lopez-Gil *et al.*, "Cavo-tricuspid isthmus radiofrequency ablation using a novel remote navigation catheter system in patients with typical atrial flutter," *Europace,* vol. 16, no. 4, pp. 558-62, 2014

[117] "Hansen Medical, Inc." [Online]. Available: www.aurishealth.com/hansen-medical.

[118] L. Di Biase *et al.*, "Remote magnetic navigation: human experience in pulmonary vein ablation," *J Am Coll Cardiol,* vol. 50, no. 9, pp. 868-74, 2007

[119] A. Al-Ahmad, J. D. Grossman, and P. J. Wang, "Early experience with a computerized robotically controlled catheter system," *J Interv Card Electrophysiol,* vol. 12, no. 3, pp. 199-202, 2005

[120] V. Y. Reddy *et al.*, "View-synchronized robotic image-guided therapy for atrial fibrillation ablation: experimental validation and clinical feasibility," *Circulation,* vol. 115, no. 21, pp. 2705-14, 2007

[121] A. Dello Russo *et al.*, "Analysis of catheter contact force during atrial fibrillation ablation using the robotic navigation system: results from a randomized study," *J Interv Card Electrophysiol,* vol. 46, no. 2, pp. 97-103, 2016

[122] B. L. Nguyen, J. L. Merino, and E. Gang, "Remote Navigation For Ablation Procedures - A New Step Forward In The Treatment Of Cardiac Arrhythmias," *European Cardiology Review,* vol. 13, no. 2, pp. 50-6, 2010

[123] "Stereotaxis, Inc." [Online]. Available: www.stereotaxis.com.

[124] M. N. Faddis *et al.*, "Novel, magnetically guided catheter for endocardial mapping and radiofrequency catheter ablation," *Circulation,* vol. 106, no. 23, pp. 2980-5, 2002

[125] S. Ernst *et al.*, "Initial experience with remote catheter ablation using a novel magnetic navigation system: magnetic remote catheter ablation," *Circulation,* vol. 109, no. 12, pp. 1472-5, 2004

[126] C. Pappone *et al.*, "Robotic magnetic navigation for atrial fibrillation ablation," *J Am Coll Cardiol,* vol. 47, no. 7, pp. 1390-400, 2006

[127] J. Bradfield, R. Tung, R. Mandapati, N. G. Boyle, and K. Shivkumar, "Catheter ablation utilizing remote magnetic navigation: a review of applications and outcomes," *Pacing Clin Electrophysiol,* vol. 35, no. 8, pp. 1021-34, 2012

[128] K. R. Chun *et al.*, "Remote-controlled magnetic pulmonary vein isolation using a new irrigated-tip catheter in patients with atrial fibrillation," *Circ Arrhythm Electrophysiol,* vol. 3, no. 5, pp. 458-64, 2010

[129] R. Proietti *et al.*, "Remote magnetic with open-irrigated catheter vs. manual navigation for ablation of atrial fibrillation: a systematic review and meta-analysis," *Europace,* vol. 15, no. 9, pp. 1241-8, 2013

[130] S. Miyazaki *et al.*, "Remote magnetic navigation with irrigated tip catheter for ablation of paroxysmal atrial fibrillation," *Circ Arrhythm Electrophysiol,* vol. 3, no. 6, pp. 585-9, 2010

[131] C. Jilek *et al.*, "Safety of implantable pacemakers and cardioverter defibrillators in the magnetic field of a novel remote magnetic navigation system," *J Cardiovasc Electrophysiol,* vol. 21, no. 10, pp. 1136-41, 2010

[132] "Magnetecs, Corp." [Online]. Available: www.magnetecs.com.

[133] E. S. Gang *et al.*, "Dynamically shaped magnetic fields: initial animal validation of a new remote electrophysiology catheter guidance and control system," *Circ Arrhythm Electrophysiol,* vol. 4, no. 5, pp. 770-7, 2011

[134] D. Filgueiras-Rama *et al.*, "Remote magnetic navigation for accurate, real-time catheter positioning and ablation in cardiac electrophysiology procedures," *J Vis Exp,* no. 74, 2013

[135] Y. Thakur, J. S. Bax, D. W. Holdsworth, and M. Drangova, "Design and performance evaluation of a remote catheter navigation system," *IEEE Trans Biomed Eng,* vol. 56, no. 7, pp. 1901-8, 2009

[136] Y. Thakur, D. L. Jones, A. Skanes, R. Yee, and M. Drangova, "Right-side RF ablation using remote catheter navigation: experimental results in vivo," *J Cardiovasc Electrophysiol,* vol. 23, no. 1, pp. 81-7, 2012

[137] Y. Thakur, J. H. Cakiroglu, D. W. Holdsworth, and M. Drangova, "A device for real-time measurement of catheter-motion and input to a catheter navigation system," in *SPIE*, 2007, vol. 6509, pp. 65090G-65090G-8.

[138] Y. Thakur, D. W. Holdsworth, and M. Drangova, "Characterization of catheter dynamics during percutaneous transluminal catheter procedures," *IEEE Trans Biomed Eng,* vol. 56, no. 8, pp. 2140-3, 2009

[139] M. A. Tavallaei, Y. Thakur, S. Haider, and M. Drangova, "A magnetic-resonance-imaging-compatible remote catheter navigation system," *IEEE Trans Biomed Eng,* vol. 60, no. 4, pp. 899-905, 2013

[140] M. A. Tavallaei, M. K. Lavdas, D. Gelman, and M. Drangova, "Magnetic resonance imaging compatible remote catheter navigation system with 3 degrees of freedom," *Int J Comput Assist Radiol Surg,* vol. 11, no. 8, pp. 1537-45, 2016

[141] M. A. Tavallaei *et al.*, "Design, development and evaluation of a compact telerobotic catheter navigation system," *Int J Med Robot,* vol. 12, no. 3, pp. 442-52, 2016

[142] L. Cercenelli, B. Bortolani, and E. Marcelli, "CathROB: A Highly Compact and Versatile Remote Catheter Navigation System," *Appl Bionics Biomech,* vol. 2017, no. 2712453, 2017

[143] S. B. Kesner and R. D. Howe, "Position Control of Motion Compensation Cardiac Catheters," *IEEE Trans Robot,* vol. PP, no. 99, pp. 1-11, 2011

[144] S. B. Kesner and R. D. Howe, "Design and Control of Motion Compensation Cardiac Catheters," in *IEEE Int Conf Robot Autom*, 2010, pp. 1059-65.

[145] S. B. Kesner and R. D. Howe, "Design Principles for Rapid Prototyping Forces Sensors using 3D Printing," *IEEE ASME Trans Mechatron,* vol. PP, no. 99, pp. 1-5, 2011

[146] S. B. Kesner and R. D. Howe, "Force Control of Flexible Catheter Robots for Beating Heart Surgery," in *IEEE Int Conf Robot Autom*, 2011, pp. 1589-94.

[147] M. Khoshnam, M. Azizian, and R. V. Patel, "Modeling of a steerable catheter based on beam theory," in *Int Conf Robot Autom*, IEEE, 2012, pp. 4681-6.

[148] M. Khoshnam, A. C. Skanes, and R. V. Patel, "Modeling and estimation of tip contact force for steerable ablation catheters," *IEEE Trans Biomed Eng,* vol. 62, no. 5, pp. 1404-15, 2015

[149] M. Khoshnam and R. V. Patel, "Robotics-assisted catheter manipulation for improving cardiac ablation efficiency," in *International Conference on Biomedical Robotics and Biomechatronics*, 2014: IEEE, pp. 308-13.

2 Design and Evaluation of a Catheter Contact-Force Controller

This chapter is adapted from *"Design and Evaluation of a Catheter Contact-Force Controller for Cardiac Ablation Therapy."*[1]

My contribution to this chapter involved (i) designing and developing the catheter contact-force controller, (ii) designing and developing phantoms, (iii) conducting experiments, (iv) collecting and analyzing data, and (v) writing manuscripts.

2.1 Introduction

Percutaneous radiofrequency (RF) catheter ablation is becoming the standard of care for a variety of cardiac arrhythmias. Cardiac electrophysiologists (EP) introduce ablation catheters into the heart and manipulate them until the distal tip contacts the targeted myocardium. Once reached, RF power is delivered to form ablation lesions that interrupt the electrical pathways responsible for the arrhythmia. For successful treatment, it is vital

---

[1]Gelman D, Tavallaei MA, Skanes AC, Drangova M. "Design and Evaluation of a Catheter Contact-Force Controller," *IEEE Transactions on Biomedical Engineering* (vol. 63, no. 11, pp. 2301-2307). Permission for reproduction provided in Appendix A.

that these lesions are transmural, as superficial lesions leave areas of healthy cardiac tissue that may result in conduction recurrence and ablation failure.

Catheter tip-to-tissue contact force (CF) is an indicator for assessing lesion development [1-5], and CF guidelines have been established to label a delivered lesion as effective [6-8]. Additional studies have shown that monitoring both the duration of the delivery and CF at a specific RF power can predict lesion volume [3, 6-11]. Conventionally described as the Force-Time Integral (FTI), the model may be used as a prospective quantitative tool to determine lesion volume under defined parameters. Unfortunately, this model is dependent on catheter stability, and while used in the clinic as a guide, it has not been used as a quantitative metric that can predict lesion volume or transmurality. Finally, lesions delivered with excessive CF present a risk of deep tissue overheating, which may result in "steam pop," perforation and injury outside the heart, including esophageal, pulmonary and phrenic nerve damage [2]. These potential risks often inhibit the EP and cause them to deliver the lesion tentatively, with a lower level of CF to lessen the risk of injury. Clinically, CF information is often used as a guide to ensure catheter tip contact and confine the CF within acceptable ranges, but is ultimately limited by tissue motion, as seen in the CF profile in the lower right-hand corner of **Figure 2.1**.

While ideally, the CF should be regulated within a prescribed range, EP cannot respond fast enough to compensate for cardiorespiratory motion [12]. Approaches to minimize cardiac motion during ablation, have been proposed, including high-frequency-jet ventilation [13]. None have successfully provided a motionless environment in all patients [14]. Kesner *et al.* [15] demonstrated CF control of catheters and instruments used for mitral valve repair; however, the implementation does not address problems associated with catheter ablation.
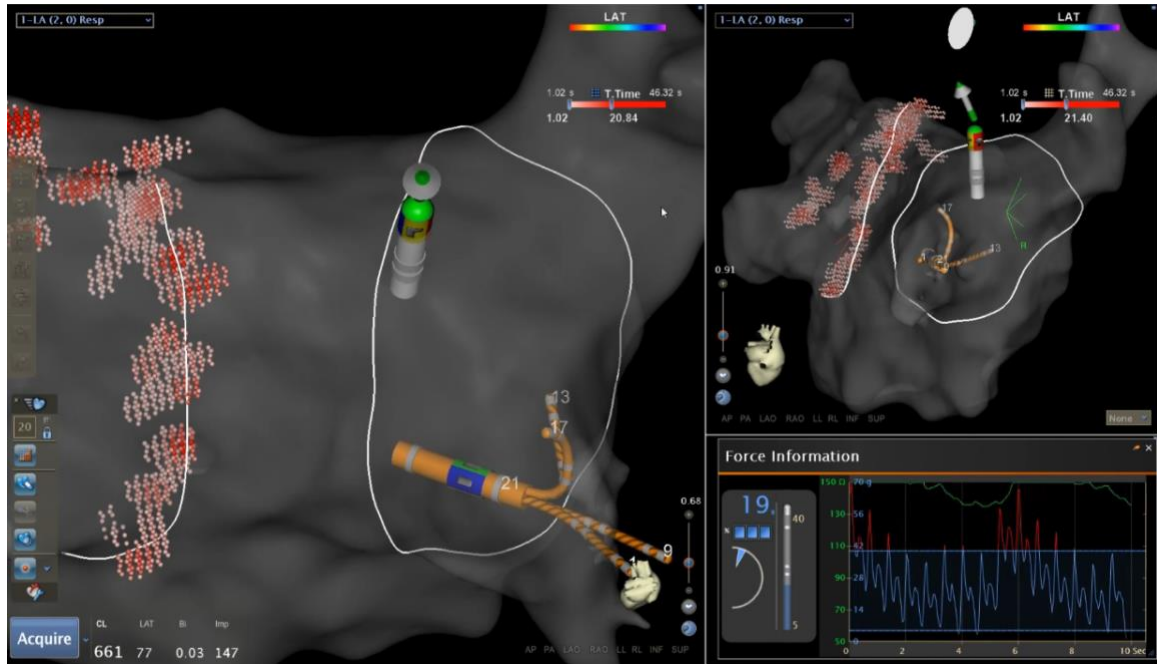
Figure 2.1. Modern electromagnetic catheter tracking systems (CARTO® 3, Biosense Webster, Irvine, CA) enable visual feedback of the real-time CF experienced on the tip of the catheter (THERMOCOOL® SMARTTOUCH™, Biosense Webster, Irvine, CA). The figure is a snapshot demonstrating catheter location in the rendered LA (white with green tip) and the CF as a function of time in the lower right-hand corner. Note the variation in CF with cardiorespiratory motion. Image courtesy of London Health Science Center.

Commercial force-sensing ablation catheters enable the EP to simultaneously monitor the CF in real-time while delivering the lesion, as illustrated in **Figure 2.1**. Often these catheters are used together with steerable sheaths, whose added level of versatility and stability has increased clinical success [13, 16, 17]. The EP typically manipulates the steerable sheath until the catheter is pointing at the target region, and then advances the catheter forward through the sheath until the desired level of CF is imparted onto the tissue.

In this chapter, we introduce a tool that enables the delivery of effective RF lesions by autonomously regulating the CF of a force-sensing ablation catheter, based only on the real-time CF measurements. The Catheter Contact-Force Controller (CFC) is a hand-held, modular device that enables robotic control of the catheter within the sheath, which

otherwise would be done manually by the interventionalist. The CFC is an add-on tool compatible with commercially available, pre-existing force-sensing ablation catheters and sheaths.

2.2   System Description

Incorporation of the CFC replaces the manual manipulation of the catheter through the sheath. Rather than advancing the catheter forward until a sufficient CF level is reached, the interventionalist would engage the CFC, which monitors the CF in real-time and updates the position of the catheter to maintain the CF experienced at the tip of the catheter at the desired level, despite the motion of the target tissue. The CFC system comprises a hand-held, compact, electromechanical device and an embedded system.

2.2.1   Hand-Held Device

The hand-held CFC device, **Figure 2.2**, is mechanically clamped to the distal end of the sheath handle (*i.e.*, at the hemostatic seal and insertion point of the catheter). A catheter-locking adapter rigidly clamps the catheter shaft onto a precision linear actuator (LM 2070, MICROMO, Clearwater, FL) travelling along a 12 mm diameter 134 mm long precision magnetic shaft. Movement of the actuator directly translates to movement of the catheter through the sheath. The specific linear actuator selected in the design was selected based on velocity, acceleration and torque requirements described in Appendix B.

The adapter and actuator are mounted within an enclosure, which is designed to securely lock onto the sheath handle while keeping the catheter concentrically mounted within the hemostatic seal. A set of hinges and latches enables easy clamping and removal of the CFC. Both the adapter and enclosure were fabricated in polypropylene using additive manufacturing (Objet3D Pro, Stratasys, Eden Prairie, MN).
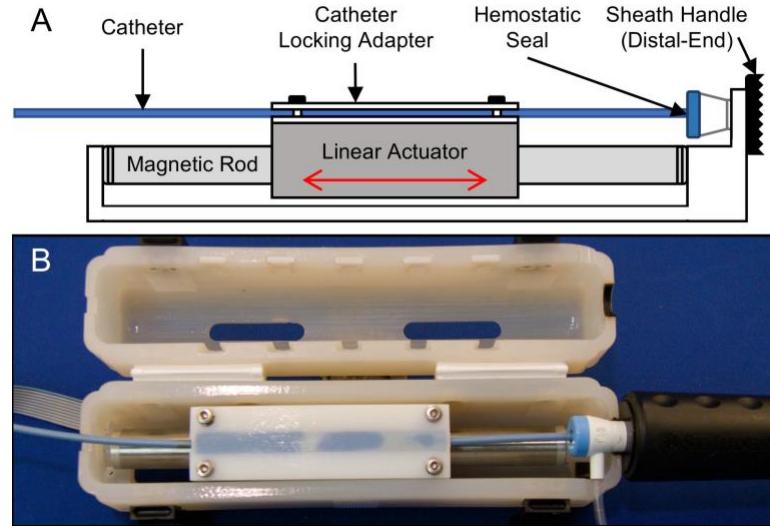
Figure 2.2. Schematic side-view, **A**, and photograph top-view, **B**, of the electromechanical hand-held CFC attached to a steerable sheath and force-sensing ablation catheter. Movement of the linear actuator along the fixed magnetic rod moves the catheter through the hemostatic seal of the sheath handle.

2.2.2   Hybrid Control System

To maintain a prescribed CF between the tip of the catheter and a moving target, we implemented a hybrid control system. Traditional closed-loop proportional-integral-derivative (PID) control algorithms are based on minimizing the error between the desired and actual inputs and are a viable solution in robotic catheter control systems [18-21]. The CFC uses a hybrid PID controller, a slight variation of a standard PID controller, whose control parameters change based on the error argument. The control signal *u(t)* is calculated as:

$$
u(t) = \begin{cases} K_{P_A}e(t) + K_{I_A}\displaystyle\int_0^t e(\tau)d\tau + K_{D_A}\dfrac{de(t)}{dt} & e(t) > F_T \\[2em] K_{P_C}e(t) + K_{I_C}\displaystyle\int_0^t e(\tau)d\tau + K_{D_C}\dfrac{de(t)}{dt} & 0 < e(t) \le F_T \end{cases}
$$

where the error *e(t)* is the difference between the desired and current contact forces, F_D and $F_C(t)$ respectively. The control parameters K_P, K_I and K_D generate a different control signal depending on the error measured in real-time. If the error is larger than a predefined CF threshold, F_T, the control system is in an "aggressive" state indicated by K_{PA}, K_{IA}, K_{DA}. When the error is lower than F_T, the control system operates in a "conservative" state indicated by K_{PC}, K_{IC}, K_{DC}. The CF threshold was empirically assigned to be 5 g – a level that was observed to retain steady-state accuracy.

Tuning of the aggressive control parameters was achieved using the Tyrues-Luyben tuning method, as implemented by [22]. The conservative control parameters were manually tuned for a desired steady-state response; in the current implementation, the conservative control parameters were at least a factor of 4 smaller than the aggressive ones.

2.2.3   Electronic Hardware Design

The hybrid control system was implemented within an embedded electronic system, enabling real-time control of the linear actuator. A microcontroller development platform based on a Atmel SAM3X8E 84 MHz 32-bit ARM architecture (Arduino Due, Arduino, Turin, Italy) generates a pulse-width modulated (PWM) control signal, based on the measured and desired CF, which acts as input to the linear actuator controller and driver circuitry (MCLM 3003, MICROMO, Clearwater, FL). This daughter-board is programmed with a native velocity proportional-integral (PI) controller that controls the speed of the motor based on the input PWM signal. Tuning of the PI controller was performed using the manufacturer's tuning software, before tuning the hybrid PID system. The update rate of the hybrid PID system was set to 1 kHz, which was the maximum rate of the linear actuator controller. A sampling rate exceeding 300 Hz will meet all requirements. This figure is based on "best practice," which is to sample the force data at a rate ten times faster

than the time constant associated with the open-loop response of the system. **Figure 2.3** is a block diagram of the designed embedded system.
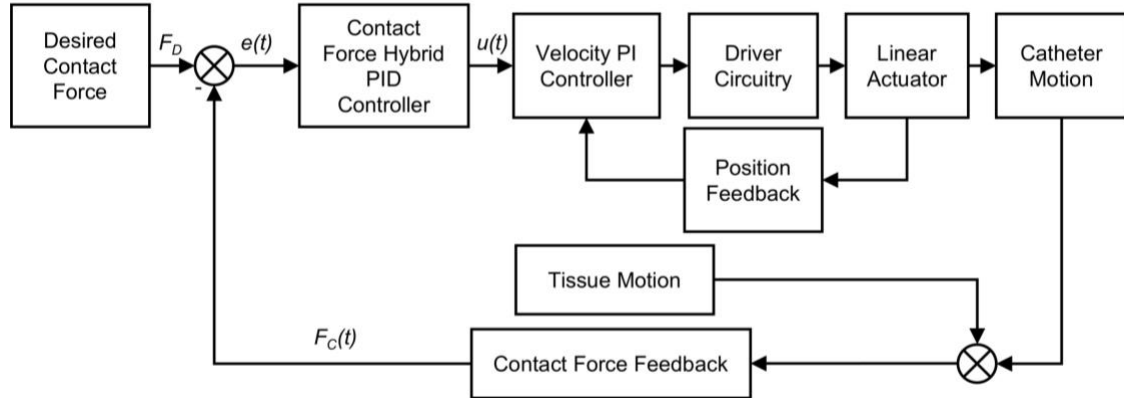
Figure 2.3. Block diagram of the CFC control system.

2.2.4   Linear Motion Phantom

To evaluate the CFC's ability to regulate CF on a moving target *in vitro*, a custom-built linear motion phantom was developed (**Figure 2.4**). The motion phantom was built to provide sinusoidal and physiologic motion profiles. A gear motor with a Hall effect encoder (37D Gearmotor, Pololu, Las Vegas, NV) drives a lead screw mechanism providing linear motion to a carriage. A second PID control system within an embedded electronic system controls the motion stage: the circuit board assembly includes a microcontroller development platform (Arduino Due, Arduino, Turin, Italy) and a DC motor driver daughter-board (VNH5019 Motor Driver Carrier, Pololu, Las Vegas, NV). A strain gauge capable of detecting the force with 200-milligram resolution (S100, Strain Measurement Devices, Wallingford, CT), coupled to a linear amplifier (CSG110, FUTEK, Irvine, CA), is mounted on the carriage and used to measure the CF of the tip of the catheter. The force signal provided by the strain gauge is a surrogate to the real-time force signal provided by the catheter tip. A silicone membrane (Dragon Skin 30, Smooth-On, Macungie, PA) is positioned between the strain gauge and the tip of the catheter to mimic soft tissue compliance. A setscrew fixes the sheath firmly in place without hindering the

movement of the catheter housed within the sheath. Linear calibration, according to Hooke's law, was first performed to determine the relationship between the displacement of the tissue and the force measured by the strain gauge.
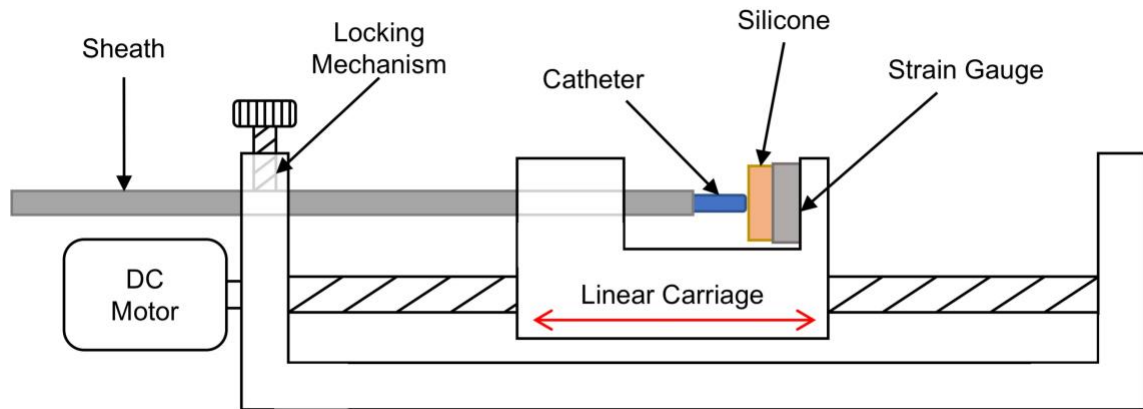
Figure 2.4. Linear motion phantom with the catheter and sheath loaded, used to evaluate the CFC. The linear motion imposed on the tip of the catheter simulates myocardial tissue motion.

The phantom was programmed to execute arbitrary sinusoidal and sine-sweep motion profiles and to replicate physiological motion. CF profiles were recorded by force-sensing ablation catheters during typical ablation procedures, similar to the profile illustrated in **Figure 2.1**. These profiles, containing both high-frequency low-amplitude cardiac and low-frequency high-amplitude respiratory motion, were programmed into the motion phantom as position trajectories, using the linear calibration parameters.

The signal from the strain gauge, measured in real-time, was used as the CF feedback signal of the CFC control system (**Figure 2.3**) and represented the CF signal that would be provided by a commercial force-sensing ablation catheter. Real-time CF data from proprietary catheters is not available routinely and could not be integrated with the CFC at the time of these experiments.

2.3   System Evaluation

2.3.1   Linear Motion Phantom Evaluation

The linear motion phantom was first evaluated to ensure that the executed motion profiles mimic the physiological motion that results in CF profiles similar to those measured clinically. The catheter was held fixed while the linear motion phantom imposed 16 different patient-specific motion profiles. The sheath was locked in place for half of the experiments. The real-time CF measurements provided by the strain gauge were recorded and compared to the corresponding CF profiles. No attempt was made to perfectly match the executed CF profiles to the corresponding patient profiles, and the measured CF profiles were only inspected visually, ensuring the range of amplitudes and frequencies were within the physiologic range.

2.3.2   Catheter Contact-Force Controller Evaluation

Experiments were performed to evaluate the overall accuracy and dynamic performance of the CFC. For these experiments, the CFC was attached to the rear end of a commonly used steerable sheath (Agilis™ NxT, St. Jude Medical, St. Paul, MN) and force-sensing ablation catheter (THERMOCOOL® SMARTTOUCH™, Biosense Webster, Irvine, CA) combination. Water was introduced via the sheath's side port to mimic the clinical setting and reduce the friction between the sheath and catheter. The distal portions of the sheath and catheter were inserted into the linear motion phantom, as illustrated in **Figure 2.5**.
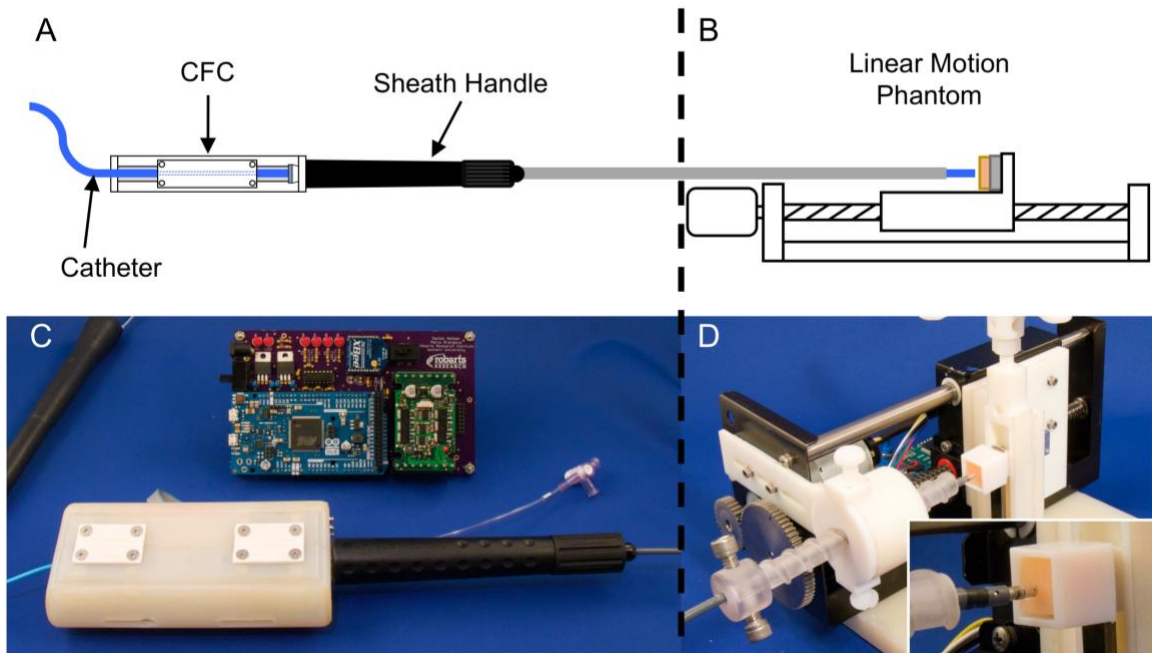
Figure 2.5. The experimental setup used to evaluate the performance of the CFC. **A** is a line drawing (not to scale) showing the CFC, **B** sheath and catheter mounted with the linear motion phantom; photographs of the CFC **C**, and motion phantom **D** are also shown.

2.3.2.1   Step Response

The response of the CFC control system to a step input (of 25 g) was first evaluated. The step response was then measured during 25 repeats and the rise time, overshoot, and peak level were characterized. During these experiments, the linear motion phantom was kept fixed.

2.3.2.2   Safety

It is vital to ensure that the CFC can respond to excessive, fast and sudden motions that may result in tissue perforation. The linear motion phantom was programmed to impose a bi-directional continuous sine sweep motion profile, sweeping from 0.1 Hz to 2.5 Hz with an amplitude of 70 g peak-to-peak. This unlikely clinical scenario was selected following Fourier analysis of over 40 patient-specific CF profiles and determining that the maximum frequency component observed was 2.5 Hz. While the phantom executed the prescribed

motion, the CFC was engaged and attempted to regulate the CF to the desired reference of 25 g. The maximum error between the desired and actual CF was measured. This experiment was repeated 10 times.

2.3.2.3   Patient-Specific Dynamic Response

To evaluate the overall performance of the CFC versus manual intervention, the linear motion phantom was programmed to execute 16 different patient motion profiles. Prior to any evaluation of the CFC, a control experiment was performed whereby the phantom replicated each profile with the CFC's disabled. This is representative of manual intervention, where the EP contacts the catheter to moving cardiac tissue and holds the catheter still to deliver a lesion. The experiment was then repeated with the CFC programmed to deliver 15 g, 25 g, and 40 g for the duration of the motion profile. Statistical analysis of the regulated CF profiles was performed to calculate mean, confidence interval, and root-mean-square error (RMSE). Histograms of CF were also plotted for the "manual" and CFC interventions. Note that for this study, we use the term "manual" to refer to the CF profile representative of CF profiles recorded during clinical ablation procedures.

2.3.2.4   Force-Time Integral

This experiment was designed to demonstrate that the CFC could be used not only to regulate the delivered force but also to deliver lesions with prescribed FTI. The CFC was programmed to deliver a prescribed FTI at the desired CF while the linear motion phantom imposed a patient motion profile. For each combination of set CF and FTI levels, an expected duration can be calculated. The CFC was programmed to monitor the FTI, and automatically retract the tip of the catheter back into the sheath once the desired FTI was reached. The generated CF profile and duration of catheter engagement was recorded and compared with expected values. This experiment was then repeated for various configurations of FTI and CF, which may be user-defined in a clinical setting. The tested

FTI values were 500, 1000, and 1500 gs, where each was repeated with 25 g and 40 g of CF. Each configuration was repeated 3 times.

2.4   Results

2.4.1   Linear Motion Phantom
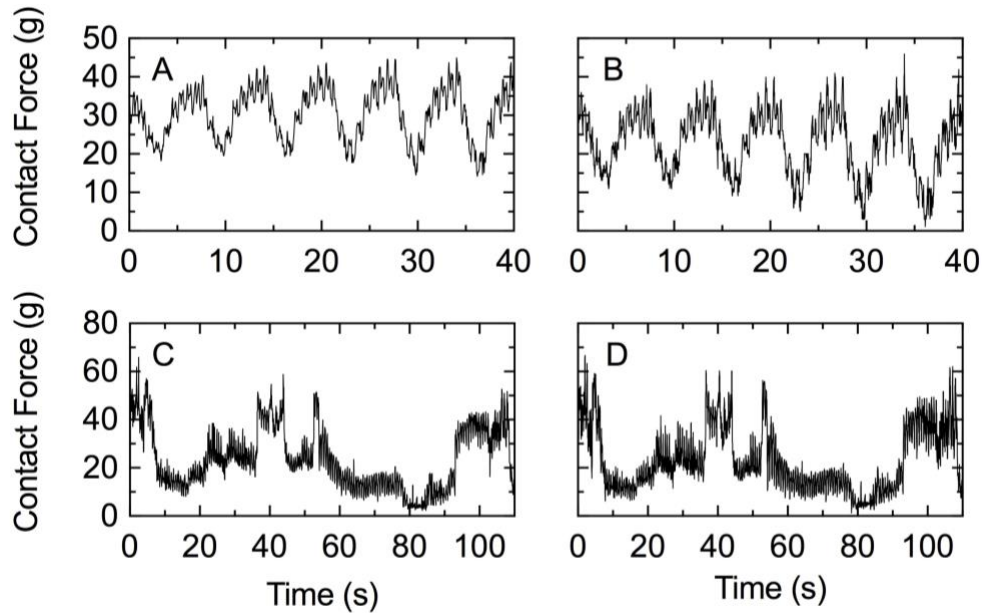
Figure 2.6. Two representative patient CF profiles (**A** and **C**) and the corresponding CF profiles (**B** and **D**, respectively) imposed on a fixed catheter tip by the linear motion phantom, executing the same patient profile. The motion profiles depicted in **B** and **D** are profile #13 and #3 in **Figure 2.8D**, respectively.

The linear motion phantom was able to replicate a range of patient-specific CF profiles. The profiles chosen to evaluate the CFC are characteristic of typical cardiorespiratory patterns depicted in **Figure 2.6A** as well as irregular profiles associated with patient motion or catheter instability depicted in **Figure 2.6C**. The generated CF curves, shown in **Figure 2.6B** and **Figure 2.6D**, visually demonstrate a high level of similarity to the corresponding clinically acquired profiles (**Figure 2.6A** and **Figure 2.6C**). These results demonstrate that the linear motion phantom can replicate cardiorespiratory forces that are typically

encountered during catheter RF delivery and is appropriate to be used as a phantom for the

CFC's evaluation. Locking the sheath in place did not affect the results.

2.4.2   CFC Performance

2.4.2.1   Step Response

The response of the CFC's control system to a 25 g step input is shown in **Figure 2.7**. The

following step response characteristics were calculated from the measurements: 38 ± 3 ms

rise time, 3 ± 2 g overshoot, and a peak of 29 ± 2 g; means and standard deviations of 25

repeats of the step response are reported. The negligible overshoot and oscillation indicate

that the tuning method used to determine the control parameters has resulted in a desired

transient and steady-state response.
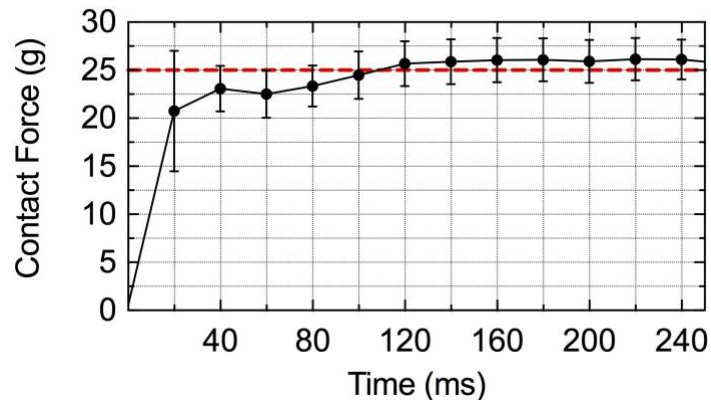
Figure 2.7. Step response of the CFC for a set force level of 25 g. At
every time point, the mean and standard deviation are plotted.

2.4.2.2   Safety

During the control of a 70 g peak-to-peak sine sweep from 0.1 Hz to 2.5 Hz, the maximum

difference between the prescribed and measured CF was 15 ± 2 g, with all measured CF

values being below 42 g. These results demonstrate that the CFC is capable of reacting to

sudden changes in tissue displacement that would otherwise result in large spikes of CF and potentially cause tissue damage.

2.4.2.3   Patient-Specific Dynamic Response
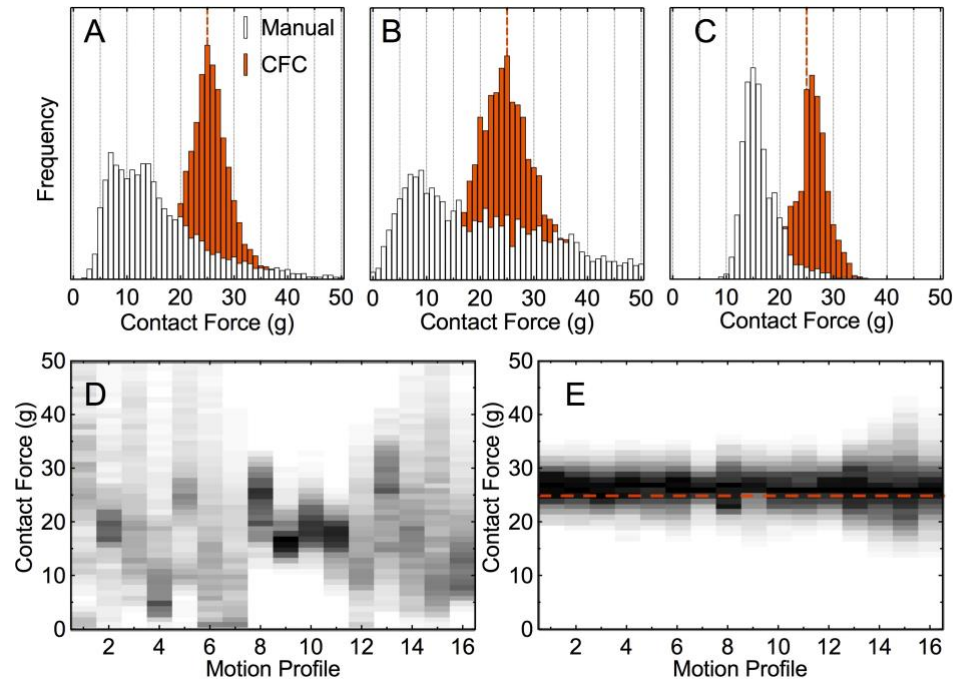
Figure 2.8. Histograms **A**-**C** show the distribution of manual and CFC-controlled CF for three unique motion profiles (16,15, and 9 from panel **D**, respectively). The manual intervention histograms indicate that: **A** majority of time was spent while CF was low (less than 20 g), **B** significant myocardial motion resulting in greatly fluctuation CF, and **C** a precise lesion was delivered but the force was not centred at the 25 g target. In each case, CFC-control brings the mean CF to the target. Histograms of manual **D** and CFC-controlled **E** interventions, represented as grey scale values, show a significant difference in CF distribution for all 16 motion profiles.

The CFC was able to significantly improve the CF profile in comparison to manual intervention ($p < 0.001$). **Figure 2.8A** through **Figure 2.8C** depicts the distribution of measured CF for three motion profiles, representative of CFs measured during the delivery of different lesions; histograms are plotted for both manual and CFC-controlled interventions, with a prescribed CF level of 25 g. The images in **Figure 2.8D** (manual) and **Figure 2.8E** (CFC-controlled) are grey-scale representations of the CF histograms for all

16 motion profiles; they clearly demonstrate that when the CFC is engaged the prescribed mean force is achieved for all motion profiles.

Similar performance was achieved regardless of the magnitude of the prescribed CF. Illustrated in **Figure 2.9**, are the results for one representative experiment where the CFC was programmed to deliver a CF of three clinically relevant levels – 15 g, 25 g, and 40 g. Consistently similar force distributions were achieved regardless of the prescribed CF value. Detailed performance metrics – averaged over all tested motion profiles – are shown in **Table 2.1** for the three prescribed CF levels.
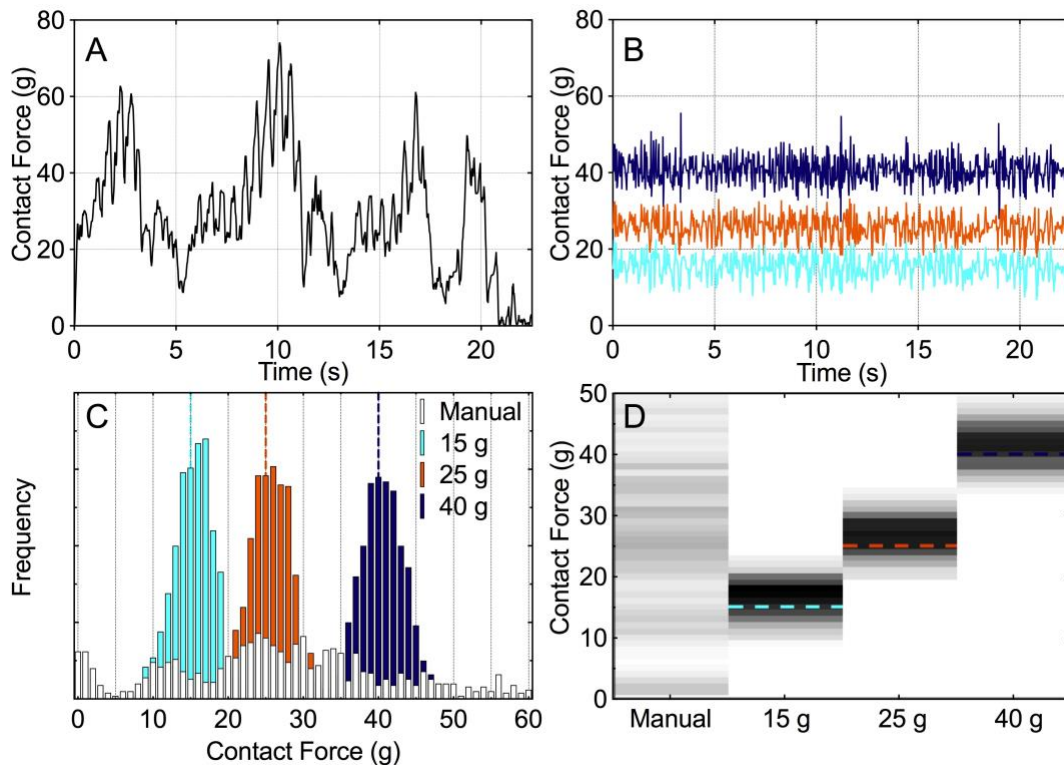
Figure 2.9. A original CF profile (green), while the CFC was disabled. **B** illustrates the generated CF profile while the CFC was engaged to deliver 15 g (cyan), 25 g (orange) and 40 g (navy). Histogram **C** and grey-scale representation **D** illustrate the CF distribution between manual and CFC intervention at various desired CF levels. The motion profile depicted here is profile #1 from **Figure 2.8D**.

Prescribed CF (g)	**15**	**25**	**40**
5% Percentile	10.1 ± 1.2	19.7 ± 1.2	34.3 ± 1.2
95% Percentile	20.6 ± 1.3	31.1 ± 1.5	46.9 ± 1.7
Mean	15.3 ± 0.1	25.4 ± 0.1	40.4 ± 0.1
RMSE	3.2 ± 0.6	3.4 ± 0.7	3.9 ± 0.8

Table 2.1. All measurements are presented in grams (g) of force. Mean and standard deviation of all 16 profiles are reported.

2.4.2.4   Force-Time Integral

For all experiments performed to demonstrate that the CFC could achieve a target FTI, the CFC successfully engaged the catheter with the desired CF until a target FTI was reached. The results obtained with each configuration of FTI and CF are presented in **Table 2.2**.

Desired		**Expected**	**Measured**		
FTI (gs)	**CF (g)**	**Duration (s)**	**FTI (gs)**	**CF (g)**	**Duration (s)**
500	25	20	500	25.7 ± 3.0	19.49 ± 0.01
	40	12.5	500	40.7 ± 3.5	12.29 ± 0.01
1000	25	40	1000	25.4 ± 3.1	39.36 ± 0.04
	40	25	999	40.4 ± 3.4	24.71 ± 0.01
1500	25	60	1500	25.3 ± 3.0	59.27 ± 0.06
	40	37.5	1499	40.4 ± 3.4	36.99 ± 0.22

Table 2.2. Results obtained with each configuration of FTI and CF tested. The measure CF and duration are comparable to the expected outcome.

A representative experiment is illustrated in **Figure 2.10**. The lesion delivery time was within 480 ± 199 ms of the expected duration. This is indicative of a regulated CF profile throughout the delivery, as excessive CF would result in short lesion delivery times and

low CF levels would result in the opposite. With each configuration of desired CF and FTI, a similar profile was generated with an expected and predictable deviation.
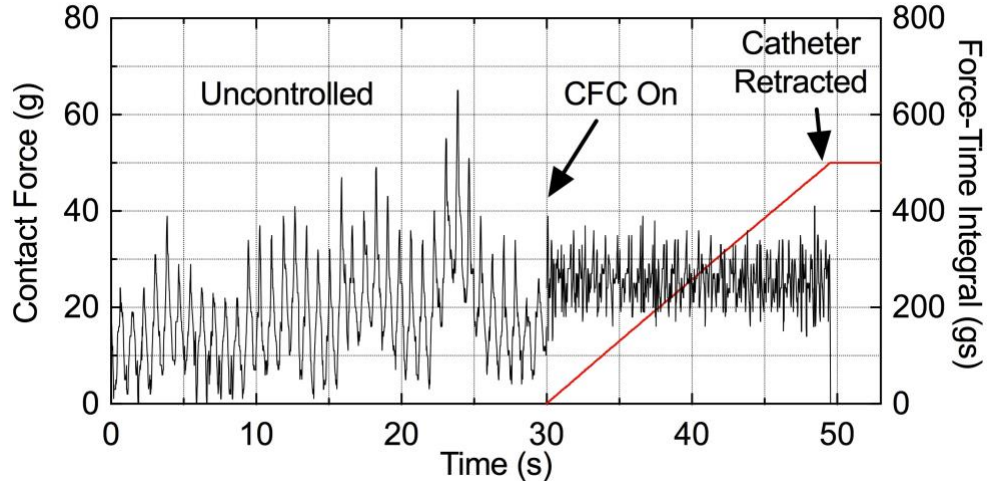
Figure 2.10. Interval 0-30 s, the catheter was in contact with the phantom while the CFC was disabled. Interval 30-49.5 s, the CFC was engaged to deliver 500 gs at 25 g. Interval 49.5-55 s, the tip of the catheter retracted into the sheath once the desired FTI (red) had been reached. The motion profile depicted here is profile #15 from **Figure 2.8D**.

2.5 Discussion

We have presented a novel and easy-to-use tool that regulates the CF imparted by standard ablation catheters on moving tissue regardless of the type of motion imposed. The compact hand-held device is used with commercially available force-sensing ablation catheters and steerable sheaths, which are widely used in modern EP labs. The presented CFC utilizes the same tools and information available to the interventionalist but grants the ability to regulate CF and FTI.

While CF measurement (at the tip of an ablation catheter) has been available to the EP for some time, it has been used primarily as a visual guide to determine if adequate contact has been made or if there is a risk of tissue perforation. The CFC has been demonstrated to control the force at the tip of the catheter to within a few grams of a prescribed force level.

The CF profiles, recorded during clinical ablation procedures, used to impart clinically relevant motion for evaluating the CFC and shown in **Figure 2.8** demonstrate some of the problems associated with ablation delivery. For example, profile #16 (**Figure 2.8A**) represents a lesion where negligible force existed between the catheter tip and the wall during most of the time RF power was being delivered; when the CFC was engaged the mean CF was increased to 25 g, as prescribed. Similarly, the scenario depicted in **Figure 2.8B** demonstrates large variations in CF (manual) due to motion, which is corrected via the use of the CFC, reducing the RMSE (about 25 g) from 15.1 to 5.5 g. Even when a tight distribution of forces is achieved manually, as in **Figure 2.8C**, the mean CF may not be at a level sufficiently high for the delivery of a transmural lesion – use of the CFC, in this case, shifts the distribution of CF from being centred about 15 g to being centred about 25 g. Consistently narrow, and symmetric, distributions of CF were also achieved for different prescribed CF levels (**Figure 2.9**, **Table 2.1**).

Successful control of CF over the duration of lesion "delivery" also enabled control of FTI. Automatic engagement and retraction of the catheter for specified FTI at the desired CF has the potential to become a fundamental and powerful tool in the EP lab. While FTI has been proposed as a useful measure in predicting lesion transmurality and volume, without a device like the CFC, FTI cannot be easily used as a metric clinically or in preclinical studies aimed at optimizing lesion delivery parameters.

The study evaluating the performance of the CFC under conditions of rapidly varying motion have also demonstrated that the use of the CFC clinically has the potential to minimize tissue damage due to excessive force. The CFC was able to compensate for changes in CF as fast as 700 g/s and maintain CF within 15 g of the prescribed values. These results are significant because they indicate that using the CFC, forces able to perforate tissue [23] would never be achieved.

The CFC was designed as a hand-held device that would enable the interventionalist to engage it at any point during a complete ablation procedure but is free to perform all other tasks as is done under current clinical practice. The CFC can easily be removed from the catheter and sheath assembly to ensure optimal catheter steerability and be re-clamped when a target location has been reached, just prior to RF power delivery. The device is versatile and can be used as a stand-alone CF control aid or can be incorporated with catheter robotic navigation systems for further improvements in position and force control. Ongoing *in vitro* and *in vivo* studies aim to demonstrate the full effectiveness of the CFC in controlling lesion volume.

2.6   Limitations

Despite the extremely promising results, it is important to note that the study is limited by the fact that the motion of an *in vitro* dynamic phantom was used as a surrogate for contact force measured at the catheter tip during CFC evaluation; the limitation is manifested in two ways. First, using a strain gauge positioned behind tissue-simulating silicone to provide CF measurements introduced damping of the CF that would have been measured at the tip of the catheter (i.e. at the interface of the catheter and silicone). Implementation of the CFC with a force-sensing catheter would require re-tuning of the control parameters to account for the different dynamics. Second, for the phantom based experiments, the acquired CF data were implemented as linear motion profiles with the catheter placed perpendicular to the surface of the tissue. This experimental design assumed that the catheter was oriented the same way during the acquisition of the clinical data. If clinically, the catheter tip was oriented at an oblique angle, larger motion profiles would correspond to the measured forces. All tested force profiles were collected in different parts of the left atrium within a single patient. This has implications as the phantom has a perpendicular only approach and may not simulate the catheter extended at an angle or with a curve. It is likely, however, that the exact characteristics of cardiac tissue motion will contain the same

frequency components as the profiles used in this study, which ultimately does not affect the implemented control system of the CFC.

All CF profiles used to evaluate the CFC were acquired from patients undergoing pulmonary vein isolation ablation therapy and may not be representative of the CF profiles measured during ablation therapies of the left ventricle. During left ventricular ablation procedures CF may change more rapidly due to systolic motion. The safety experiments performed as part of the present study contained CF waveforms with high changes of CF, larger than would be expected in ventricular ablations, and these preliminary tests provide confidence that the CFC will be able to control force even during ventricular ablations.

In all experiments, the distance between the tip of the catheter and the tip of the sheath was limited to less than 30 mm. Based on interviews with cardiac electrophysiologists, when using a steerable sheath, it is uncommon to exceed this distance. The performance of the CFC has not been tested with greater distances. Furthermore, it is important to note that the CFC will only work correctly when the catheter is adequately supported by the sheath at the distal tip. As such, significant catheter deflection and extension may compromise CFC performance.

2.7   Conclusions

This study represents the first demonstration of contact force control using a versatile hand-held catheter contact force controller, which can be coupled to any force-sensing ablation catheter and steerable sheath combination. The demonstrated control of contact force under varying motion conditions is promising and suggests that – when implemented in combination with a force-sensing catheter – the CFC can deliver prescribed ablation lesions.

2.8 References

[1]   L. Di Biase *et al.*, "Relationship Between Catheter Forces, Lesion Characteristics, "Popping," and Char Formation: Experience with Robotic Navigation System," *J Cardiovasc Electrophysiol,* vol. 20, no. 4, pp. 436-440, 2009

[2]   H. Nakagawa and W. M. Jackman, "The Role of Contact Force in Atrial Fibrillation," *Journal of Atrial Fibrillation,* vol. 7, no. 1, pp. 79-84, 2014

[3]   K. Yokoyama *et al.*, "Novel contact force sensor incorporated in irrigated radiofrequency ablation catheter predicts lesion size and incidence of steam pop and thrombus," *Circ Arrhythm Electrophysiol,* vol. 1, no. 5, pp. 354-362, 2008

[4]   M. R. Afzal *et al.*, "Use of Contact Force Sensing Technology During Radiofrequency Ablation Reduces Recurrence of Atrial Fibrillation: A Systematic Review and Meta-Analysis," *Heart Rhythm,* vol. 12, no. 9, pp. 1990-6, 2015

[5]   A. Natale *et al.*, "Paroxysmal AF Catheter Ablation With a Contact Force Sensing Catheter - Results of the Prospective, Multicenter SMART-AF Trial," *J Am Coll Cardiol,* vol. 64, no. 7, pp. 647-656, 2014

[6]   V. Y. Reddy *et al.*, "The relationship between contact force and clinical outcome during radiofrequency catheter ablation of atrial fibrillation in the TOCCATA study," *Heart Rhythm,* vol. 9, no. 11, pp. 1789-95, 2012

[7]   J. Kautzner *et al.*, "EFFICAS II: optimization of catheter contact force improves outcome of pulmonary vein isolation for paroxysmal atrial fibrillation," *Europace,* vol. 17, no. 8, pp. 1229-35, 2015

[8]   W. Ullah *et al.*, "Target indices for clinical ablation in atrial fibrillation: insights from contact force, electrogram, and biophysical parameter analysis," *Circ Arrhythm Electrophysiol,* vol. 7, no. 1, pp. 63-8, 2014

[9]   D. C. Shah, H. Lambert, H. Nakagawa, A. Langenkamp, N. Aeby, and G. Leo, "Area under the real-time contact force curve (force-time integral) predicts radiofrequency lesion size in an in vitro contractile model," *J Cardiovasc Electrophysiol,* vol. 21, no. 9, pp. 1038-43, 2010

[10]   A. Thiagalingam *et al.*, "Importance of catheter contact force during irrigated radiofrequency ablation: evaluation in a porcine ex vivo model using a force-sensing catheter," *J Cardiovasc Electrophysiol,* vol. 21, no. 7, pp. 806-11, 2010

[11]   M. C. Wong *et al.*, "Characterization of catheter-tissue contact force during epicardial radiofrequency ablation in an ovine model," *Circ Arrhythm Electrophysiol,* vol. 6, no. 6, pp. 1222-8, 2013

[12]   S. Kumar *et al.*, "Effect of respiration on catheter-tissue contact force during ablation of atrial arrhythmias," *Heart Rhythm,* vol. 9, no. 7, pp. 1041-1047, 2012

[13]   M. D. Hutchinson *et al.*, "Efforts to enhance catheter stability improve atrial fibrillation ablation outcome," *Heart Rhythm,* vol. 10, no. 3, pp. 347-53, 2013

[14]   L. Di Biase *et al.*, "General anesthesia reduces the prevalence of pulmonary vein reconnection during repeat ablation when compared with conscious sedation: results from a randomized study," *Heart Rhythm,* vol. 8, no. 3, pp. 368-72, 2011

[15]   S. B. Kesner and R. D. Howe, "Force Control of Flexible Catheter Robots for Beating Heart Surgery," in *IEEE Int Conf Robot Autom*, 2011, pp. 1589-94.

[16]   C. Piorkowski *et al.*, "Steerable sheath catheter navigation for ablation of atrial fibrillation: a case-control study," *Pacing Clin Electrophysiol,* vol. 31, no. 7, pp. 863-73, 2008

[17]   C. Piorkowski *et al.*, "Steerable versus nonsteerable sheath technology in atrial fibrillation ablation a prospective, randomized study," *Circ Arrhythm Electrophysiol,* vol. 4, no. 2, pp. 157-165, 2011

[18]   S. B. Kesner and R. D. Howe, "Force control of flexible catheter robots for beating heart surgery," in *ICRA*, Shanghai, 2011: IEEE, pp. 1589-1594.

[19]   M. A. Tavallaei, Y. Thakur, S. Haider, and M. Drangova, "A magnetic-resonance-imaging-compatible remote catheter navigation system," *IEEE: Transactions on Biomedical Engineering,* vol. 60, no. 4, pp. 899-905, 2013

[20]   M. Xu *et al.*, "Development of a PID controller for a novel robotic catheter system," in *International Conference on Complex Medical Engineering*, 2011: IEEE, pp. 64-8.

[21]   S. B. Kesner and R. D. Howe, "Position Control of Motion Compensation Cardiac Catheters," *IEEE Trans Robot,* vol. PP, no. 99, pp. 1-11, 2011

[22]   B. D. Tyreus and W. L. Luyben, "Tuning PI controllers for integrator/dead time processes," *Industrial & Engineering Chemistry Research,* vol. 31, no. 11, pp. 2625-8, 1992

[23]   F. Perna, E. K. Heist, S. B. Danik, C. D. Barrett, J. N. Ruskin, and M. Mansour, "Assessment of catheter tip contact force resulting in cardiac perforation in swine atria using force sensing technology," *Circ Arrhythm Electrophysiol,* vol. 4, no. 2, pp. 218-24, 2011

3 Eliminating the Effects of Motion during RF Ablation Delivery

This chapter is adapted from *"Eliminating the Effects of Motion during Radiofrequency Lesion Delivery using a Novel Contact-Force Controller."*[2]

My contribution to this chapter involved (i) integrating technologies, (ii) developing novel control systems, (iii) designing and developing phantoms, (iv) designing and conducting experiments, (v) collecting and analyzing data, and (vi) writing manuscripts.

3.1 Introduction

Catheter-tissue contact force is a major determinant of catheter ablation lesion size uncertainty during radiofrequency (RF) power application [1-5]. Insufficient contact force results in inadequate lesion production and increased AF recurrence rates [6-8], while excessive contact force is associated with tissue over-heating, increased incidence of steam pops, perforation, thrombus formation, and collateral tissue damage to the esophagus and phrenic nerve [2, 9-13]. In addition to the average force, contact-force variability has been shown to be an essential parameter in determining RF lesion formation [14]. Improving

---

[2]Gelman D, Skanes AC, Jones DL, Timofeyev M, Baron T, Drangova M. "Eliminating the Effects of Motion during Radiofrequency Lesion Delivery using a Novel Contact-Force Controller," *Journal of Cardiovascular Electrophysiology* (Accepted).

contact-force stability enables RF power to be effectively deposited within the tissue and not the surrounding blood pool, and this, in turn, could be critical to achieving long-term success [15].

A recent meta-analysis, summarizing all randomized controlled trials investigating contact force in AF ablation, reports that contact force variability, rather than average force alone, has emerged as a critical element that governs lesion size and ablation outcomes [16]. The EFFICAS II trial demonstrated durable PVI using a contact-force target of 20 g, with a narrow range between 10 g and 30 g [4]. Similarly, the SMART-AF trial showed an increase in clinical success when more time was spent within a pre-defined force range (*i.e.* reduced force variability) [15]; operators who stayed within a selected range for more than 80% of the time during RF applications were more than 4 times more likely to have clinical success in comparison to those who did not. In further studies, Ullah *et al.* [17] showed that, for the same accumulated FTI, RF ablation lesions delivered with contact-force variation less than 5 g significantly increased impedance drops and achieved higher maximums compared to lesions with greater variation [17]. The authors of this study suggest that improving force stability rather than merely delivering more FTI can produce more effective lesions. In a similar study, Makimoto *et al.* [18] found that a relative standard deviation less than 30% of the mean force (*e.g.* 10 ± 3 g or 20 ± 6 g) correlated with a reduction in reconnection gaps during PVI [18]. Both of these studies identified regional locations typically associated with AF reconnection, such as the LA roof, with parameters demonstrating high contact-force variability.

Despite this evidence, in clinical practice, it is virtually impossible to maintain sufficient average contact force and reduce contact-force variability reliably [18-22]. The adjustments made by an operator are limited by human factors (perception and reaction time) and system delays (including time required to average and display a mean force level), making it impossible to compensate for force variability in real-time and

highlighting the clear need for new technology to control catheter-tissue contact force and optimize catheter ablation techniques.

In our previous work [23], we developed and evaluated a catheter contact-force controller (CFC) that monitors catheter-tissue contact force in real-time and simultaneously adjusts the position of the ablation catheter within a sheath to compensate for variations in contact force that occur due to cardiorespiratory motion. Preliminary lab-bench tests demonstrated that using the CFC resulted in significant improvement in the stability and control of catheter-tissue contact force on moving tissue-mimicking material.

The aim of the present study was to demonstrate the ability of the CFC to maintain a set level of force *in vivo* and determine the device's impact on lesion production when compared to manual intervention. In the first part of the study, the device was tested in a porcine model *in vivo*, where an experienced electrophysiologist attempted to maintain a set force level with and without the assistance of the CFC. In the second part of the study, an *in vitro* contractile bench model tested the hypothesis that the CFC helps deliver prescribed and reproducible ablation lesions despite the presence of clinically relevant tissue motion under fixed conditions of RF power and duration. In these experiments, the sizes of lesions delivered to moving tissue samples with and without the CFC were compared to lesions delivered to stationary tissue.

3.2   Methods

3.2.1   Catheter Contact-Force Controller

The CFC is a simple add-on to a conventional force-sensing catheter used in conjunction with a steerable sheath, as described in detail in Chapter 2 [23]. Briefly, the CFC actuation unit is clamped onto the back-end of a steerable sheath near the hemostatic seal (**Figure 3.1**); a linear motor clamped onto the catheter shaft via a locking adaptor adjusts catheter motion with respect to the sheath. The CFC's embedded electronics monitor the CF in real-

time and use 1 of 2 control algorithms to adjust the catheter position within the sheath in order to maintain constant force at the catheter tip.
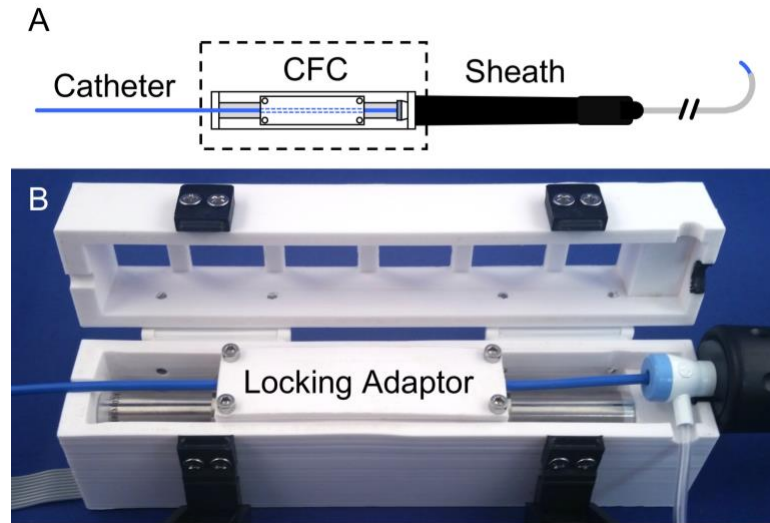
Figure 3.1. Schematic diagram **A** and photograph **B** of the CFC actuation unit attached to an ablation catheter and steerable sheath. A locking adaptor clamps the CFC to a linear actuator (shown in **B**), which enables the catheter to be displaced axially within the sheath.

First, a model-based adaptive control system [24] was implemented to assist in cases where gradual changes in CF are required (*e.g.* respiratory motion). However, such adaptive algorithms perform poorly in the presence of large, rapid fluctuations of CF, such as those caused by systolic-diastolic motion. To address this, an additional control system, which uses repetitive control [25], was implemented. Specifically, the repetitive control system uses the heart rate, derived from the ECG, as *a priori* information to improve disturbance-rejection performance during the presence of fast-moving periodic cardiac motion. In the current implementation, the user selected the control mode (adaptive versus repetitive) based on the observed CF profile. Further detail about the two control systems is presented in Appendix C.

3.2.2   Force Control Performance *In Vivo*

Animal studies were performed in accordance with institutional and national guidelines and approved by the University of Western Ontario Animal Use and Care Committee (Protocol #2013-064, Appendix D). Two male farm pigs weighing approximately 35 kg were used for the study.
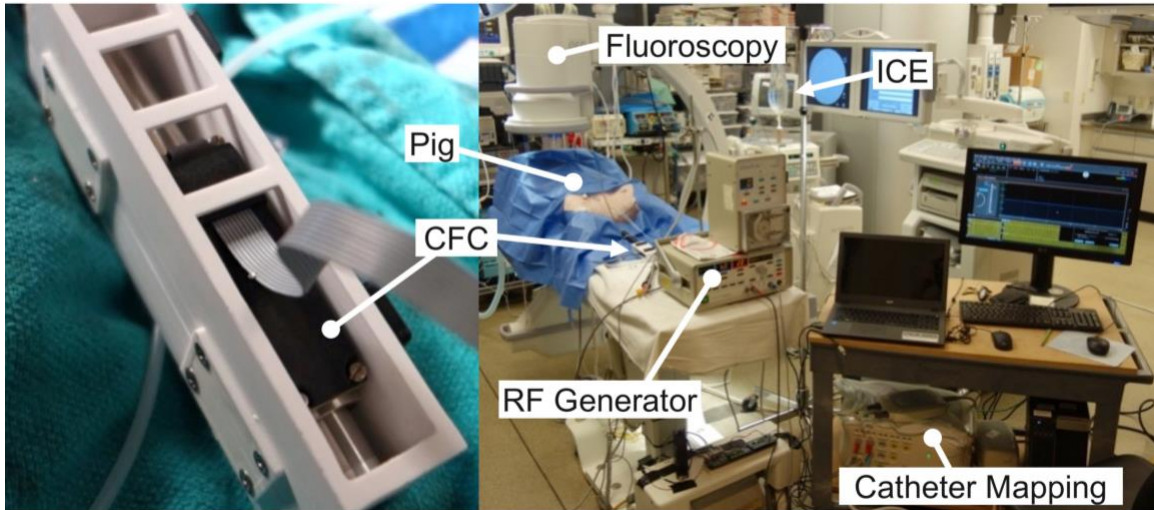
Figure 3.2. Photograph of the CFC, left, and the *in vivo* experimental setup, right.

Using standard procedures, each pig was anesthetized and prepared for catheterization [26]. Each pig was intubated, and the ventilation rate was set for 20 BPM. A research-based electro-anatomical catheter mapping system (CARTO® 3, Biosense Webster, Irvine, CA), mobile C-arm fluoroscopic x-ray unit (OEC 9900 Elite, General Electric, Boston, MA), and intracardiac echocardiography system (Acuson Sequoia, Seimens, Munich, Germany) were used to assist catheter navigation (**Figure 3.2**). A steerable sheath (Agilis™ NxT, Abbott Laboratories, St. Paul, MN) and a force-sensing ablation catheter (THERMOCOOL® SMARTTOUCH™, Biosense Webster, Irvine, CA) with the CFC attached were inserted into the heart via right femoral access. A pace-making lead attached to an external generator was introduced via the right jugular vein and placed in the superior RA to provide cardiac pacing at 115 BPM throughout the experiment. A shaped trans-

septal needle (Brockenbrough, Medtronic, Minneapolis, MN) was introduced via the left femoral vein and used to gain access to the left side of the heart, under the guidance of an intracardiac echocardiography catheter (Acuson AcuNav, Seimens, Munich, Germany).

A skilled electrophysiologist (A.C.S.) manipulated the catheter and steerable sheath to target locations in the LA, RA and LV. At each location, the physician attempted to maintain 20 g for 30 seconds with manual catheter intervention. The CFC was then enabled and set to maintain the force at 20 g. For all interventions, the catheter tip was maintained perpendicular to the surface of the tissue to mimic ideal ablation conditions and maximize motion-related force variability; a catheter-tissue incidence angle of between 0° and 45° from normal was considered perpendicular, as defined by Ullah *et al.* [17]. The electro-anatomical mapping system continuously displays the force angle, and experiments were performed only when perpendicular catheter angle was achieved. It is important to note that the anatomy of the pig LA is quite different from the human. Most importantly, the PV region is often a confluence with minimal musculature. Also, the LA appendage is very large and makes up a large portion of the surface area. Sites in the LA were targeted as follows; after transseptal access was obtained the catheter was advanced to the LA appendage, withdrawn to the LA roof and turned posteriorly to the posterior LA wall to allow sampling of several sites within the LA.

Contact-force profiles of manual and CFC-assisted interventions were recorded and compared. The average contact force and variation were calculated for manual and contact-force-controlled experiments. Variability in contact force and was calculated as contact-force variation (CFV) [17] – *i.e.* the difference between the mean trough and peak forces – as well as the relative standard deviation (RSD) or the coefficient of variation [18]. Calculations were performed using a custom script in MATLAB (MathWorks).

Several CFC-assisted ablations were also delivered within the RA and LA to ensure the delivery of power did not affect the performance of the CFC. Visual inspection of the lesions after the pigs were euthanized was performed only to confirm that power was indeed delivered.

3.2.3 Lesion Formation Under Contact-Force Control

3.2.3.1 *In Vitro* Setup
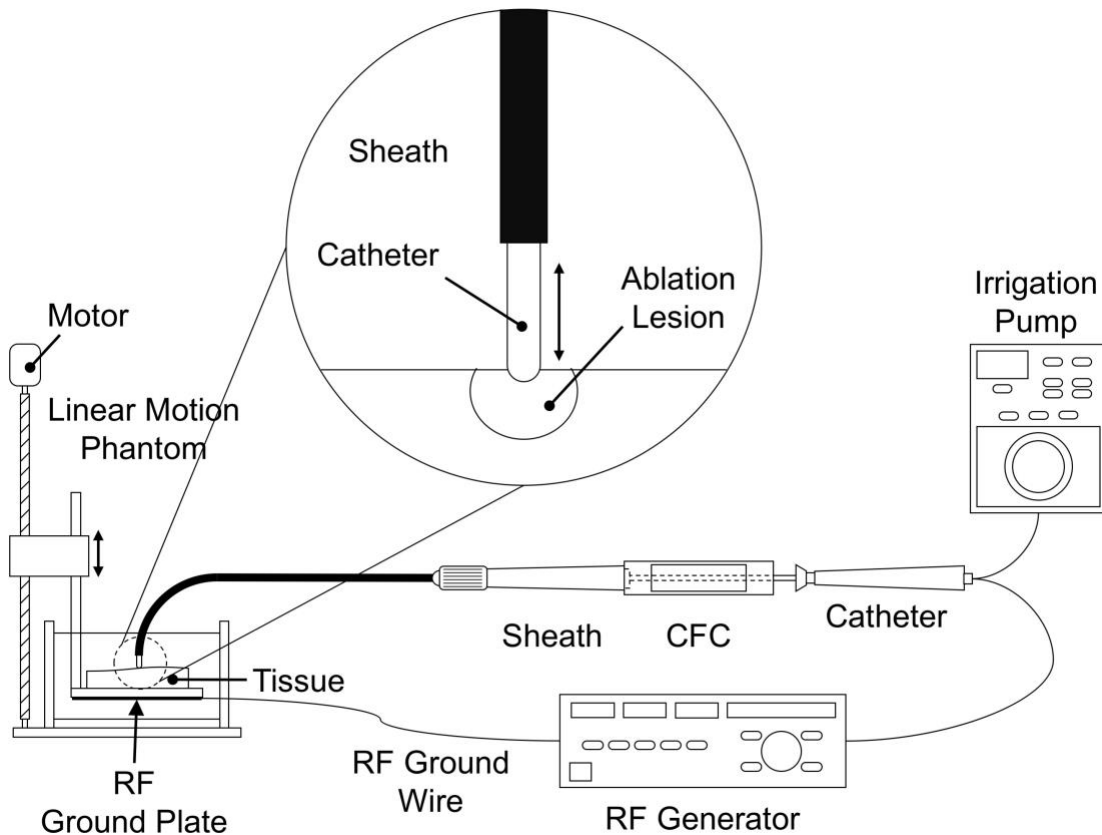
Figure 3.3. Setup for the *in vitro* ablation experiments. A linear motion phantom capable of producing clinically relevant myocardial motion moves bovine tissue within a saline bath. The CFC is attached to a force-sensing ablation catheter and steerable sheath, enabling the delivery of RF lesions to moving tissue under force control.

The impact of the CFC on lesion production was evaluated using an *in vitro* model simulating the beating heart, adapted from the experimental setup and protocol of Shah *et al.* [14]. Illustrated in **Figure 3.3**, the distal portion of a steerable sheath, housing a force-

sensing ablation catheter, was deflected 90° and mounted over a Delrin platform submerged within an acrylic tank filled with 0.7% saline at room temperature. The platform was fixed to a custom-built linear motion stage, which could be raised and lowered by a gear motor. An RF generator (EP Shuttle, Stockert GmbH, Munich, Germany) in power-control mode delivered RF energy between the catheter-tip electrode and a ground plate fixed underneath the platform. Slabs of bovine muscle, 20-30 mm thick, were placed on the platform. A peristaltic pump (CoolFlow®, Biosense Webster, Irvine, CA) connected to the irrigation port of the catheter, delivered 0.7% saline during RF delivery.

The linear motion phantom was driven in 1 of 2 modes, either reproducing CF measurements recorded by force-sensing catheters during RF delivery in patients [23] or simulating empirically derived cardiorespiratory motion profiles (**Figure 3.4**). For the simulated motion profiles, the respiratory component resembled typical tidal lung volume profiles, while the cardiac component replicated either intermittent or variable contact profiles. Simulated cardiac and respiratory motion waveforms with user-defined amplitudes and frequencies were used to reproduce scenarios of intermittent catheter-tissue contact, induced patient apnea, and various combinations of dominant respiratory or cardiac motion. Simulated motion was used to isolate tissue motion, without the introduction of artifacts potentially introduced by a physician operation or the force sensor itself (*e.g.*, noise).
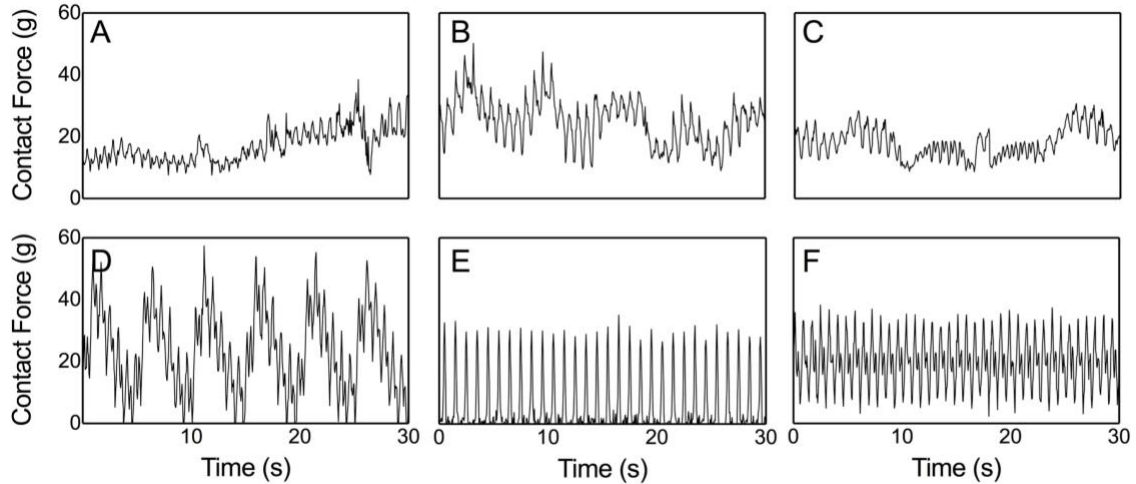
Figure 3.4. Sample CF profiles measured as the linear motion phantom moves tissue against a fixed catheter. The CF profiles in **A** through **C** simulate force generated during patient ablations. The profiles in **D** through **F** represent examples of simulated profiles: **D** combination of cardiac and respiratory motion (cardiac: 75 BPM, 15 g peak-to-peak; respiration: 12 BPM, 30 g peak-to-peak; offset: 10 g), **E** intermittent cardiac motion (cardiac: 75 BPM, 30 g peak-to-peak; respiration: none; offset: none), and **F** variable cardiac motion (cardiac: 75 BPM, 30 g peak-to-peak; respiratory: none; offset: 20 g).

3.2.3.2   Protocol

RF energy was delivered to the tissue at 20 W for 30 seconds; the irrigation flow rate was at 17 ml/min. First, CFC-assisted ablation lesions were delivered to stationary tissue at 4 force levels (5 g, 15 g, 25 g, and 35 g). These lesions were used as "control lesions" – *i.e.* created in the absence of motion. The same set of ablation protocols was then repeated, but the motion stage was set to execute randomly selected motion profiles with the CFC enabled to maintain the force constant at 1 of the 4 force levels. Lastly, to mimic lesion production during manual intervention, lesions were delivered to moving tissue while the CFC was disabled. For all experimental conditions, CF profiles were recorded, and the mean, CFV and RSD were calculated.

3.2.3.3   Lesion Measurement

Once lesions were delivered, the tissue slabs were sliced along the centre of each lesion using a scalpel to expose the cross-section. Photographs of sectioned lesions were taken with a camera mounted in a 3D-printed custom bracket to ensure that the cross-section of the lesion was centred and parallel to the aperture of the camera; a constant distance between the camera and lesion surface enabled calibration of the images. The photographs were randomized prior to analysis by a blinded observer. The dimensions of the necrotic zone within each lesion were measured using digital callipers in the image-analysis software ImageJ [27]. The maximum diameter, maximum depth, and depth at the maximum diameter for each lesion were measured (**Figure 3.5**). Lesion volumes were calculated using the formula for a truncated oblate spheroid:

$$V_{Lesion} = V_{Spheroid} - V_{Spheroidal\ Cap} = \frac{4\pi a^2 c}{3} - \frac{\pi a^2 h^2 (3c - h)}{3c^2}$$

where a = *Maximum Diameter / 2*, c = *Maximum Depth - Depth at Maximum Diameter*, and h = c - *Depth at Maximum Diameter*. Similar ellipsoidal modelling of lesion volume has been used previously [14].
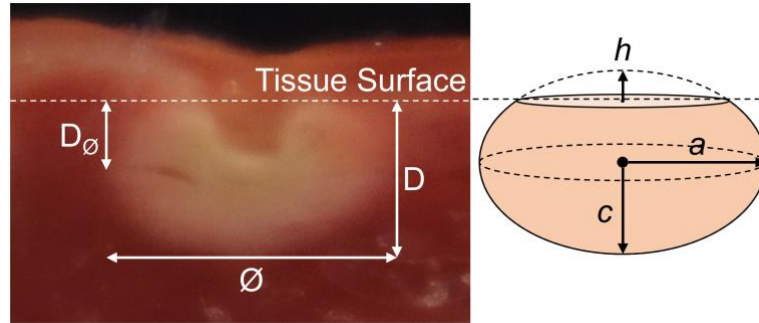
Figure 3.5. Photograph of a cross-section through an ablation lesion (left) illustrating the locations where measurements were made in order to calculate lesion volume: maximum diameter (Ø); maximum depth (D); and depth at maximum diameter ($D_\varnothing$). The truncated oblate spheroid approximation (right) was used to measure volume, characterized by dimensions a, c, and h. The indentation left by the catheter tip pushing into the tissue was included in lesion volume calculation.

3.2.3.4   Statistical Analysis

Statistical analysis was performed using Prism 7 (GraphPad Software, USA). Two-way analysis of variance (ANOVA) was performed for both lesion volume and lesion depth to determine if the set-force level effect on lesion size was statistically significant. Means at each set force level were compared and the Sidak multiple comparison test was used to test the hypothesis that the volume and depth of CFC-controlled lesions delivered to moving tissue do not differ from those of lesions delivered to stationary tissue. A p-value of < 0.05 was considered statistically significant.

3.3   Results

3.3.1   *In Vivo* Experiments

Fourteen CF-control experiments were performed, 8 in the LA, 5 in the RA, and 1 in the LV. Of these, 12 experiments were performed with the CFC set to repetitive control mode using the heart rate determined from ECG and 2 with the CFC set for adaptive control mode (the results below are averages of all 14 experiments). Representative examples of the CF profiles achieved when using repetitive control and adaptive control are provided in **Figure 3.6A** through **Figure 3.6C** and **Figure 3.6D**, respectively. Through manual

catheter intervention, the interventionalist was able to maintain an average force level of 24.6 ± 6.4 g, which was larger than the target of 20 g; the smallest average force was 14.9 g, and the largest average was 30.5 g. In contrast, for all CFC-assisted interventions, with a set force of 20 g, the average CF was 19.9 ± 0.3 g [range 18.9 g to 20.1 g]. When compared to manual intervention, CFC-assistance resulted in a reduction in CFV from 31.6 ± 15.9 g to 4.6 ± 1.1 g (p < 0.0001) and RSD from 53 ± 24 % to 20 ± 7 % (p = 0.005).
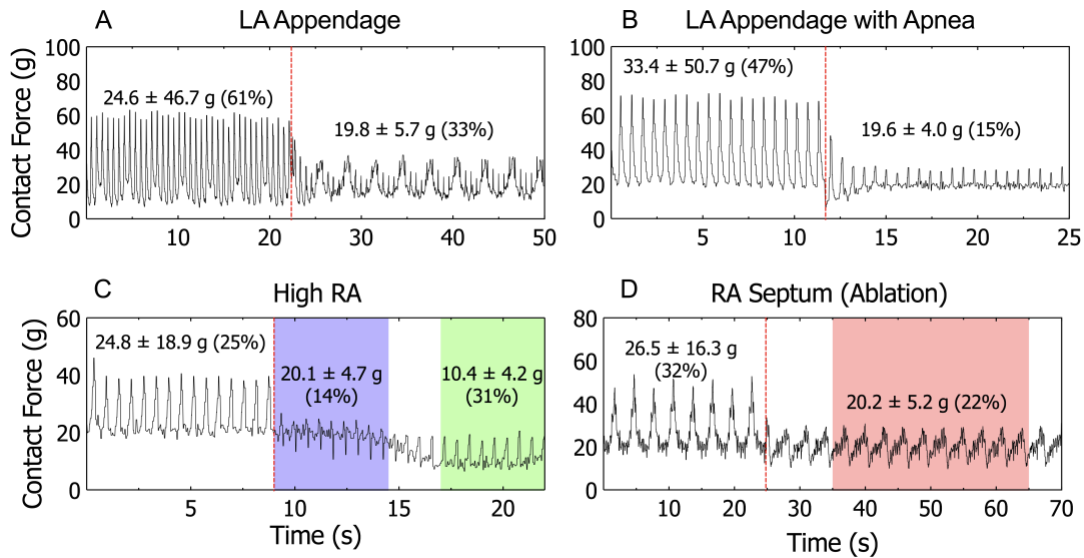
Figure 3.6. Results from four experiments performed in various locations in the LA and RA. Each CF profile begins with manual intervention prior to CFC engagement (red line). The regions targeted were: LA appendage without **A** and with apnea **B**; high RA with apnea **C** while changing the set level of force from 20 g (blue area) to 10 g (green area); **D** while delivering a lesion (red area) to the RA septum. The mean CF ± CFV (RSD) during manual and CFC-assisted intervention is reported. Note: the CFC was able to compensate for myocardial motion greater than that observed in humans (**A** and **B**), where the CFC was capable of reducing spikes of over 50 g at a heart rate over 110 BPM down to negligible disturbances. Note the difference in time and force scales.

Analyzing CFC-assisted performance on a regional level, no significant difference in CFV between the LA (4.9 ± 1.2 g, n = 8) and RA (4.0 ± 0.6 g, n = 5) was observed (p = 0.161). While testing the CFC in the LV, catheter engagement induced premature ventricular contractions (PVC). The presence of PVC caused the repetitive control system to

temporally lose synchrony with the cardiac motion of the pig heart, resulting in poor performance. In the single case where PVCs were not induced (**Figure 3.7**), the CFV was reduced from 32.9 g to 8.6 g when the CFC was engaged. Importantly, the maximum force measured did not exceed 50 g in any of the cases when the CFC was engaged (all three chambers) and was lower than the maximum measured during manual intervention.
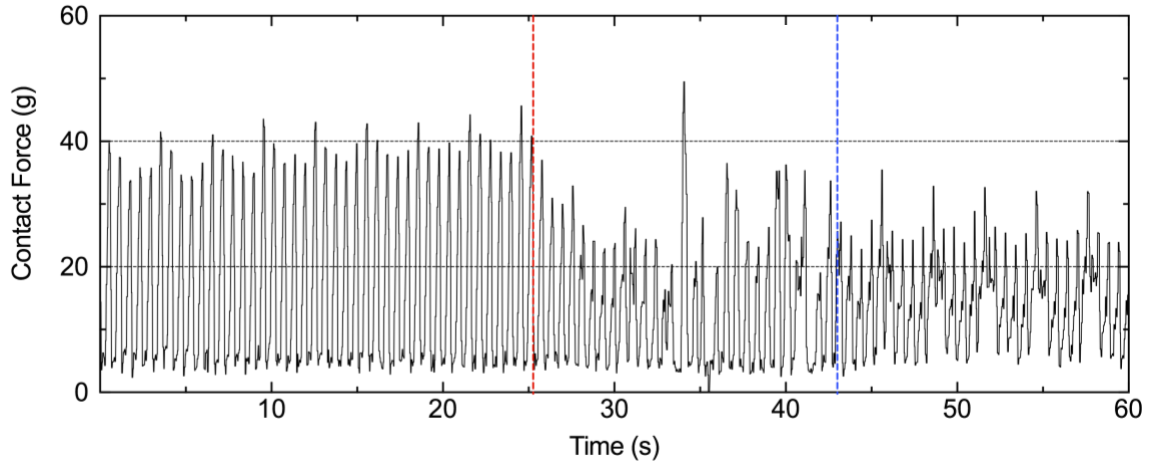
Figure 3.7. An example experiment of the CFC employed in the LV. Interval A reveals significant cardiac motion. Engaging the CFC in repetitive control mode (red line) induced PVCs resulting in poor force control performance. The CFC was able to resynchronize with the heartbeat, likely due to the disappearance of PVCs (blue line), resulting in improved control, Interval C.

3.3.2   Contact-Force Control *In Vitro*

The mean, CFV and RSD of the CF profiles recorded during CFC-assisted ablation-lesion delivery for the 3 sets of experiments (CFC-assisted lesion delivery to stationary tissue, CFC-assisted lesion delivery to moving tissue, and manual lesion delivery to moving tissue) are shown in **Table 3.1**. Similar to the *in vivo* results, the average CF remained within 1 g of the set level, and the CFV reduced to less than 5 g on average for all set levels of the CFC. Specifically, CFC-assisted intervention reduced CFV from 19.4 ± 10.2 g to 4.0 ± 1.0 g ($p < 0.0001$) and RSD from 64 ± 39 % to 25 ± 14 % ($p < 0.0001$). When setting the CFC with a modest set force (15 g and greater), the resulting RSD improved to 17 ± 7 %.

Versus manual intervention, employing the CFC narrowed the distribution of contact forces and centred in on the set force, improving precision and accuracy. Furthermore, the range (the difference between maximum and minimum) of contact forces was reduced by at least a factor of 2.

	n	Mean (g)	Nadir (g)	Peak (g)	Range (g)	CFV (g)	RSD (%)
Stationary Tissue							
5 g	6	4.9 ± 0.03	1.7 ± 0.3	8.2 ± 0.2	6.5 ± 0.4	1.7 ± 0.1	21 ± 1
15 g	6	14.9 ± 0.02	11.1 ± 0.5	18.9 ± 0.5	7.8 ± 1.0	1.7 ± 0.1	8 ± 0
25 g	6	24.9 ± 0.03	20.5 ± 0.7	29.4 ± 0.6	8.9 ± 1.2	1.8 ± 0.1	5 ± 0
35 g	6	34.9 ± 0.03	30.4 ± 1.0	39.8 ± 0.7	9.4 ± 1.4	1.8 ± 0.1	4 ± 1
Moving Tissue							
CFC-Assisted							
5 g	6	5.1 ± 0.1	-2.8 ± 0.7	13.0 ± 2.0	15.8 ± 2.9	3.0 ± 0.4	47 ± 8
15 g	9	14.7 ± 0.3	6.4 ± 1.8	26.1 ± 5.0	19.7 ± 6.7	4.1 ± 1.1	22 ± 5
25 g	6	25.0 ± 0.1	12.2 ± 2.2	39.1 ± 5.1	23.5 ± 2.7	4.7 ± 1.2	19 ± 3
35 g	7	34.4 ± 0.6	26.6 ± 1.1	44.1 ± 1.0	17.5 ± 1.5	4.1 ± 0.8	9 ± 0
Manual	15	15.9 ± 7.3	0.02 ± 6.0	42.9 ± 12.0	42.9 ± 13.4	19.4 ± 10.2	64 ± 39

Table 3.1. Characteristics of CF profiles recorded during CFC-assisted and manual ablation delivery. Comparison of generated CF profiles with and without (i.e., manual intervention) the CFC on stationary and moving tissue. Values are expressed as mean ± standard deviation. Note that for manual lesion deliver to moving tissue, there was no desired force actively compensated for.

It is important to note that these results include several ablation experiments performed while the motion phantom was driven to reproduce variability that resembles patient, catheter, or unpredictable cardiorespiratory motion. Even in these irregular motion cases, CFV was reduced to less than 5 g (and RSD to below 30%) when the CFC was used. Comparative example force profiles achieved with the CFC when the motion was irregular are shown in **Figure 3.8**.
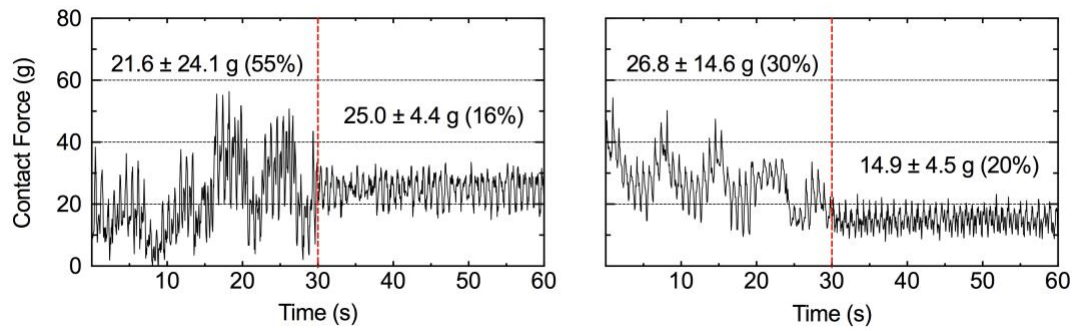
Figure 3.8. Results from two experiments performed in vitro where the phantom was driven to reproduce motion profiles based on force measurements obtained from force-sensing catheters during RF delivery in patients. The beginning of each experiment shows tissue motion characteristic of unpredictable respiration. With the absence of significant periodic tissue motion, the adaptive control mode of the CFC was engaged (red line) with a set force level of 25 g (left) and 15 g (right). Average contact force ± CFV (RSD) are reported.

3.3.3   Lesion Production With and Without Force Control

Representative example photographs of cross-sections of delivered lesions are provided in **Figure 3.9**. The measured depths and calculated volumes of the CFC-assisted ablation lesions on stationary and moving tissue, as well as lesions delivered to mimic manual intervention (without the CFC), are presented in **Figure 3.10**. As determined by two-way ANOVA, statistically significant differences were observed between lesion depth and volume for lesions delivered to stationary or moving tissues at different set force levels ($p < 0.0001$). Most importantly, motion during lesion delivery (while employing the CFC) had no effect on lesion depth or volume ($p = 0.82$ and 0.78, respectively) compared to stationary lesions. On the other hand, manual intervention delivered to moving tissue resulted in highly inconsistent lesion depth and volume. Multiple comparison analysis revealed a small difference in lesion depth (not volume) between stationary and moving tissue when the set level was 5 g.
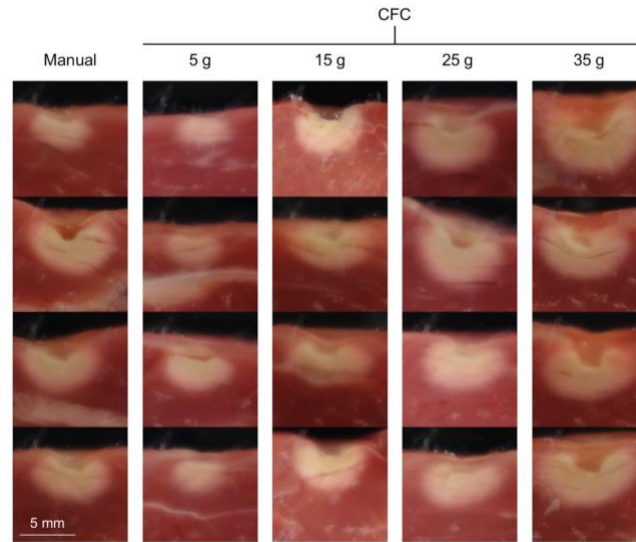
Figure 3.9. Photographs of the cross-sections of delivered ablation lesions to moving tissue. Representative examples of ablation sizes while the CFC is disabled, representing manual intervention, and while the CFC is set to desired forces of 5 g, 15 g, 25 g, and 35 g (organized in columns). Lesions delivered during manual intervention vary in size, while prescribed CFC-assisted ablation lesions are precise and reproducible, despite myocardial motion.
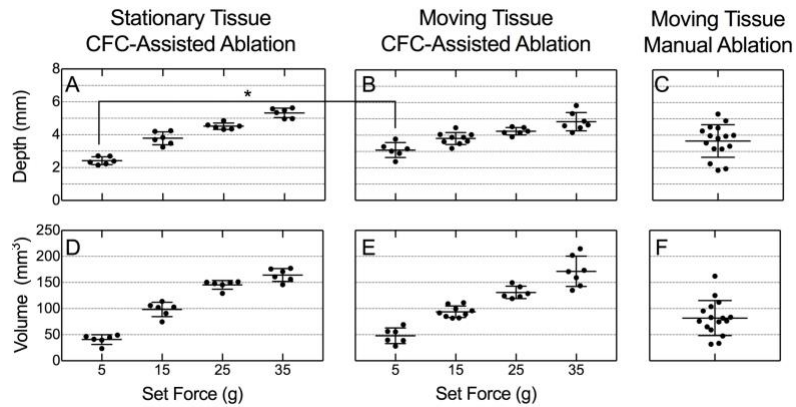
Figure 3.10. Measured lesion depth and volume are presented for CFC-assisted lesion creation on stationary tissue (**A** and **D**) and on moving tissue (**B** and **E**). For comparison depth and volume are also presented in panels **C** and **F** for lesions created under manual intervention (i.e. no control); these lesions were generated while the phantom was moving with the same motion profile as the controlled lesions generated in **B** and **E**. For the same set force, no statistical differences between lesions volumes delivered to moving tissue and lesions delivered to stationary tissue were observed. Note that retrospectively analyzed average force values for the manually delivered ablations (**C** and **F**) demonstrated a similar relationship between depth/volume and achieved contact force, as expected; however, unlike the CFC-assisted case, the force level could not be set prospectively by the operator.

3.4   Discussion

In this study we demonstrated that: a) on average, the CFC can consistently control force to within 1 g of the set level; b) the variation in contact force dropped below 5 g when using the CFC – a 5-fold improvement over manual intervention; c) when using the CFC, the catheter tip never lost contact with the tissue and never approached dangerous force levels; d) delivered ablation lesions were reproducible regardless of myocardial motion, and finally, e) delivered lesions to moving tissue were of the same depth and volume as lesions delivered in the absence of tissue motion. Recalling the clinical studies performed by Ullah *et al*. [17] and Makimoto *et al.* [18], which respectively report that a CFV of less than 5 g ensures a maximum impedance drop and RSD less than 30% is correlated with more durable lesions, our results suggest that using the CFC can assist clinicians in achieving these previously unattainable goals.

During the *in vitro* ablation experiments, on average a 2-fold reduction was observed between the standard deviations of lesion volume (and depth) of CFC-assisted and manually delivered lesions. This indicates improved precision and accuracy in lesion production over manual intervention while the tissue was moving. More importantly, regardless of tissue motion, lesions delivered were reproducible and statistically identical in size compared to lesions delivered to stationary tissue, indicating that lesions were delivered to moving tissue as if no motion was present. The slightly significant difference in lesion depth noted at the 5-g level is attributed to the likelihood that at low force levels, lesion production is more vulnerable to variation in force – improving the control performance of the CFC may prevent this.

During *in vivo* evaluation in the porcine model, the CFC demonstrated the ability to compensate for significant cardiac tissue motion, greater than those observed in humans. The CFC was capable of reducing spikes of 50 g caused by the systolic-diastolic motion of the heart at over 110 BPM to negligible disturbances (**Figure 3.6A** and **Figure 3.6B**). This

performance was achieved in all target locations in the LA and RA. However, in the LV, we observed poorer performance, likely due to the occurrences of PVCs and the fact that the repetitive controller was optimized for atrial use. Further development of the CFC control system, which may involve fine-tuning of the repetitive controller or utilizing the adaptive controller, is required before a more extensive evaluation in the LV.

A primary concern of using the CFC is the possibility of perforating the tissue while the CFC is engaged. For this reason, the CFC is programmed to continuously monitor contact force and automatically retract the catheter back into the sheath and disable the force control algorithm if the force level exceeds a user-defined limit of 80 g. It is important to note that for all CFC-interventions performed during the *in vivo* and *in vitro* experiments, the force never exceeded 50 g. Demonstrated in Chapter 2, the CFC has shown to effectively react to large and sudden changes in tissue displacement that would otherwise result in large spikes of contact force and potentially cause tissue damage.

The development of two different control systems (adaptive and repetitive) was required to handle types of motion typically observed during patient therapy. Different controllers were required to compensate for the delay, sampling rate and noise characteristics of the force sensor incorporated on the catheter tip. The repetitive control system can be used to eliminate fast systolo-diastolic force variations when they are the most dominant component, but strictly requires that tissue motion is periodic (i.e. normal sinus rhythm). The current version of the repetitive control system is unable to effectively handle the non-periodic disturbances observed in patients in AF or instances of mechanically-induced PVCs but was able to compensate for motion associated with heart-rate drifts up to $\pm 7\%$. On the other hand, the adaptive control system ignores fast disturbances caused by cardiac motion and can only reject gradual changes in force variations and is suitable for most interventions where the largest motions are caused by respiration or involuntary movement. The adaptive controller may, therefore, be ideally suited for use during arrhythmias, where

cardiac-induced motion is expected to be smaller. Lastly, in the cases where both cardiac and respiratory motion is large, both control algorithms will have reduced benefit; however, such cases are rare.

The benefit of the CFC is dependent on the angle between the catheter tip and the surface of the tissue, with the highest improvement achieved during perpendicular contact, when the effect of motion is greatest. On the other hand, when the catheter is nearly parallel to the tissue, such as during CTI ablation, the CFC is expected to have little benefit. In this study, the CFC was evaluated at angles up to 45°; however, a significant reduction of force variability has been observed at angles as large 60° from the normal (data not shown). Additional studies are required to determine a threshold angle beyond which using the CFC will not provide benefit.

Systolo-diastolic cardiac motion and respiration are the primary contributors to variability in contact force [19, 21, 28]. Clinical techniques used to mitigate their effect include rapid atrial pacing, high-frequency jet ventilation (HFJV), and induced apnea [28-33]. Rapid pacing has been shown to reduce the standard deviation in force by less than 1 g compared to its non-paced counterpart, and its effectiveness is dependent on regional anatomical location within the LA [29]. In a study examining almost 30,000 RF applications, HFJV only reduced force variability index by 0.06 on average in comparison to normal ventilation [33]. In contrast, to achieve optimal force variability based on the variability criteria of CFV (less than 5 g [17]) and RSD (less than 30% [18]), the CFC reduced standard deviation in the force profiles by 6.3 g on average and the force variability index by 0.21. Importantly, the CFC is a device that can be used independently to compensate for the effect of motion or to supplement one of these techniques. In particular, the combination of induced apnea and the CFC working in repetitive-control mode would be an extremely effective way to control force (**Figure 3.6B**).

Emerging catheter ablation techniques in treating AF include delivering RF energy with high-power (typically 70-90 W) for 4-8 seconds. In pre-clinical porcine studies, high-power short-duration (HP-SD) ablation have been shown to successfully isolate the pulmonary veins [34, 35]. However, in these studies, HP-SD in swine have demonstrated that CF values between 10 g and 20 g resulted in successful ablation [34] while fluctuating forces exceeding 40 g caused steam pops [35]. For clinical applications of HP-SD, the EP would need to maintain CF within the guidelines set out by these studies, which may be difficult to achieve reliably. These preclinical studies indicate the importance of controlling CF and minimizing variability, regardless of the method of RF delivery. Further studies evaluating the role of CF variability in HP-SD lesion production is needed.

3.5   Study Limitations

While the study demonstrates that the CFC can reduce the effects of motion on contact force during ablations *in vivo* and *in vitro* in a limited set of experiments, more comprehensive studies of the device are required (*e.g.* in the LV) before the real impact of using the CFC can be determined.

Typical CF profiles observed in the clinical setting are dominated by respiration; CF disturbances caused by cardiac motion are often negligible in most targets. Surprisingly, the opposite relationship was observed in the porcine model, where for most target locations, disturbances were dominated by systolo-diastolic cardiac motion, while disturbances caused by respiration were smaller in comparison. As a result, the primary control mode that was tested *in vivo* was the repetitive control system. While the adaptive control system could not be extensively evaluated *in vivo,* this control mode was thoroughly tested in the *in vitro* experiments.

Lesion production in the *in vitro* study does not directly reflect lesion production in humans. Our experimental set up did not mimic blood and tissue temperature and did not

model convective and perfusive cooling. However, all experimental conditions remained consistent from lesion-to-lesion, and the results generated from these experiments were solely dependent on tissue motion and CF. The measured reference impedance (75-85 Ω, achieved by titrating the salinity to 0.7%) was low compared to clinical levels but was chosen to enable the generation of measurable lesions at clinically relevant CF levels and duration. Finally, lesion volume was measured only by a single observer and was based on measurements of the necrotic area. Systematic bias was avoided by cropping, anonymizing, and randomizing the photographed tissue samples, thereby blinding the observer to the ablation protocol used for each lesion.

3.6   Conclusions

Monitoring catheter-tissue force has become an important tool for RF catheter ablation in patients and has become a standard-of-care. Until this work, CF information has been strictly used for visual guidance and navigation. The CFC uses this available information and optimizes lesion production on moving tissue by controlling catheter-tissue CF. In this study, we demonstrated the ability for the CFC to significantly improve catheter-tissue CF profiles and their impact on lesion production in moving tissue. The results obtained in this study suggest that the CFC can be a valuable add-on tool available to electrophysiologists to optimize lesion delivery techniques and ultimately improve patient outcomes.

3.7   References

[1]   H. Nakagawa and W. M. Jackman, "The Role Of Contact Force In Atrial Fibrillation Ablation," *J Atr Fibrillation,* vol. 7, no. 1, p. 1027, 2014

[2]   K. Yokoyama *et al.*, "Novel contact force sensor incorporated in irrigated radiofrequency ablation catheter predicts lesion size and incidence of steam pop and thrombus," *Circ Arrhythm Electrophysiol,* vol. 1, no. 5, pp. 354-362, 2008

[3]   H. Calkins *et al.*, "2017 HRS/EHRA/ECAS/APHRS/SOLAECE expert consensus statement on catheter and surgical ablation of atrial fibrillation," *Heart Rhythm,* vol. 14, no. 10, pp. e275-e444, 2017

[4]   J. Kautzner *et al.*, "EFFICAS II: optimization of catheter contact force improves outcome of pulmonary vein isolation for paroxysmal atrial fibrillation," *Europace,* vol. 17, no. 8, pp. 1229-35, 2015

[5]   P. Neuzil *et al.*, "Electrical reconnection after pulmonary vein isolation is contingent on contact force during initial treatment: results from the EFFICAS I study," *Circ Arrhythm Electrophysiol,* vol. 6, no. 2, pp. 327-33, 2013

[6]   S. Haldar *et al.*, "Contact force sensing technology identifies sites of inadequate contact and reduces acute pulmonary vein reconnection: a prospective case control study," *Int J Cardiol,* vol. 168, no. 2, pp. 1160-6, 2013

[7]   J. B. le Polain de Waroux *et al.*, "Low contact force and force-time integral predict early recovery and dormant conduction revealed by adenosine after pulmonary vein isolation," *Europace,* vol. 17, no. 6, pp. 877-83, 2015

[8]   B. J. Tofig *et al.*, "Recurrence after pulmonary vein isolation is associated with low contact force," *Scand Cardiovasc J,* vol. 52, no. 1, pp. 28-33, 2018

[9]   B. Avitall, K. Mughal, J. Hare, R. Helms, and D. Krum, "The effects of electrode-tissue contact on radiofrequency lesion generation," *Pacing Clin Electrophysiol,* vol. 20, no. 12 Pt 1, pp. 2899-910, 1997

[10]   A. Thiagalingam *et al.*, "Importance of catheter contact force during irrigated radiofrequency ablation: evaluation in a porcine ex vivo model using a force-sensing catheter," *J Cardiovasc Electrophysiol,* vol. 21, no. 7, pp. 806-11, 2010

[11]   C. Pappone *et al.*, "Atrio-esophageal fistula as a complication of percutaneous transcatheter ablation of atrial fibrillation," *Circulation,* vol. 109, no. 22, pp. 2724-6, 2004

[12]   D. C. Shah and M. Namdar, "Real-time contact force measurement: a key parameter for controlling lesion creation with radiofrequency energy," *Circ Arrhythm Electrophysiol,* vol. 8, no. 3, pp. 713-21, 2015

[13]   A. Ikeda *et al.*, "Relationship between catheter contact force and radiofrequency lesion size and incidence of steam pop in the beating canine heart: electrogram amplitude, impedance, and electrode temperature are poor predictors of electrode-tissue contact force and lesion size," *Circ Arrhythm Electrophysiol,* vol. 7, no. 6, pp. 1174-80, 2014

[14]   D. C. Shah, H. Lambert, H. Nakagawa, A. Langenkamp, N. Aeby, and G. Leo, "Area under the real-time contact force curve (force-time integral) predicts radiofrequency lesion size in an in vitro contractile model," *J Cardiovasc Electrophysiol,* vol. 21, no. 9, pp. 1038-43, 2010

[15]   A. Natale *et al.*, "Paroxysmal AF catheter ablation with a contact force sensing catheter: results of the prospective, multicenter SMART-AF trial," *J Am Coll Cardiol,* vol. 64, no. 7, pp. 647-56, 2014

[16]   N. Ariyarathna, S. Kumar, S. P. Thomas, W. G. Stevenson, and G. F. Michaud, "Role of Contact Force Sensing in Catheter Ablation of Cardiac Arrhythmias: Evolution or History Repeating Itself?," *JACC Clin Electrophysiol,* vol. 4, no. 6, pp. 707-723, 2018

[17]   W. Ullah *et al.*, "Factors affecting catheter contact in the human left atrium and their impact on ablation efficacy," *J Cardiovasc Electrophysiol,* vol. 26, no. 2, pp. 129-36, 2015

[18]   H. Makimoto *et al.*, "Incidence and anatomical locations of catheter instability during circumferential pulmonary vein isolation using contact force," *Int Heart J,* vol. 55, no. 3, pp. 249-55, 2014

[19]   S. Kumar *et al.*, "Prospective characterization of catheter-tissue contact force at different anatomic sites during antral pulmonary vein isolation," *Circ Arrhythm Electrophysiol,* vol. 5, no. 6, pp. 1124-9, 2012

[20]   R. De Ponti, R. Marazzi, L. A. Doni, J. Marazzato, C. Baratto, and J. A. Salerno-Uriarte, "Optimization of catheter/tissue contact during pulmonary vein isolation: the impact of atrial rhythm," *Europace,* vol. 20, no. 2, pp. 288-94, 2018

[21]   A. Sarkozy *et al.*, "Contact force variability during catheter ablation of atrial fibrillation: the role of atrial rhythm and ventricular contractions: co-force AF Study," *Circ Arrhythm Electrophysiol,* vol. 8, no. 6, pp. 1342-50, 2015

[22]   H. Matsuda *et al.*, "Atrial rhythm influences catheter tissue contact during radiofrequency catheter ablation of atrial fibrillation: comparison of contact force between sinus rhythm and atrial fibrillation," *Heart Vessels,* vol. 31, no. 9, pp. 1544-52, 2016

[23]   D. Gelman, A. C. Skanes, M. A. Tavallaei, and M. Drangova, "Design and Evaluation of a Catheter Contact-Force Controller for Cardiac Ablation Therapy," *IEEE Trans Biomed Eng,* vol. 63, no. 11, pp. 2301-7, 2016

[24]   P. Jain and M. J. Nigam, "Design of a Model Reference Adaptive Controller Using Modifited MIT Rule for a Second Order System," *Advance in Electronic and Electric Engineering,* vol. 3, no. 4, pp. 477-484, 2013

[25]   W. Qing-Guo, Z. Han-Qin, Y. Yong-Sheng, Z. Yong, and Z. Yu, "Modified Smith predictor design for periodic disturbance rejection," in *Asian Control Conference*, 2004, vol. 2: IEEE, pp. 1145-50.

[26]   Y. Thakur, D. L. Jones, A. Skanes, R. Yee, and M. Drangova, "Right-side RF ablation using remote catheter navigation: experimental results in vivo," *J Cardiovasc Electrophysiol,* vol. 23, no. 1, pp. 81-7, 2012

[27]   C. A. Schneider, W. S. Rasband, and K. W. Eliceiri, "NIH Image to ImageJ: 25 years of image analysis," *Nat Methods,* vol. 9, no. 7, pp. 671-5, 2012

[28]   S. Kumar *et al.*, "Effect of respiration on catheter-tissue contact force during ablation of atrial arrhythmias," *Heart Rhythm,* vol. 9, no. 7, pp. 1041-1047.e1, 2012

[29]   A. Aizer *et al.*, "Pacing Mediated Heart Rate Acceleration Improves Catheter Stability and Enhances Markers for Lesion Delivery in Human Atria During Atrial Fibrillation Ablation," *JACC Clin Electrophysiol,* vol. 4, no. 4, pp. 483-90, 2018

[30]   J. S. Goode, Jr., R. L. Taylor, C. W. Buffington, M. M. Klain, and D. Schwartzman, "High-frequency jet ventilation: utility in posterior left atrial catheter ablation," *Heart Rhythm,* vol. 3, no. 1, pp. 13-9, 2006

[31]   N. Elkassabany *et al.*, "Anesthetic management of patients undergoing pulmonary vein isolation for treatment of atrial fibrillation using high-frequency jet ventilation," *J Cardiothorac Vasc Anesth,* vol. 26, no. 3, pp. 433-8, 2012

[32]   M. D. Hutchinson *et al.*, "Efforts to enhance catheter stability improve atrial fibrillation ablation outcome," *Heart Rhythm,* vol. 10, no. 3, pp. 347-53, 2013

[33]   B. Sivasambu *et al.*, "Initiation of a High-Frequency Jet Ventilation Strategy for Catheter Ablation for Atrial Fibrillation: Safety and Outcomes Data," *JACC Clin Electrophysiol,* vol. 4, no. 12, pp. 1519-1525, 2018

[34]   M. Barkagan, F. M. Contreras-Valdes, E. Leshem, A. E. Buxton, H. Nakagawa, and E. Anter, "High-power and short-duration ablation for pulmonary vein isolation: Safety, efficacy, and long-term durability," *J Cardiovasc Electrophysiol,* vol. 29, no. 9, pp. 1287-96, 2018

[35]   E. Leshem *et al.*, "High-Power and Short-Duration Ablation for Pulmonary Vein Isolation: Biophysical Characterization," *JACC Clin Electrophysiol,* vol. 4, no. 4, pp. 467-79, 2018

4 Remote Catheter Navigation and Contact-Force Control

This chapter is adapted from "*Remote Catheter Navigation and Contact-Force Control: Design and Evaluation of a Novel Steerable Sheath and Catheter Robotic Navigation System.*"[3]

My contribution to this chapter involved (i) designing and developing all components of the robotic navigation system, (ii) designing and developing phantoms, (iii) preparation and conducting experiments, (iv) collecting and analyzing data, and (v) writing manuscripts.

4.1 Introduction

Radiofrequency (RF) catheter ablation is a widely used therapy to permanently treat atrial fibrillation (AF) – the most common form of cardiac arrhythmia. Delivering contiguous transmural ablation lesions is crucial for improving clinical outcomes by increasing first-procedure efficacy rates [1]. Unfortunately, 40% to 70% of patients experience a recurrence of AF symptoms due to electrical reconnections of isolated pulmonary veins [2-

---

[3]Gelman D, Skanes AC, Drangova M. "Remote Catheter Navigation and Contact-Force Control: Design and Evaluation of a Novel Steerable Sheath and Catheter Robotic Navigation System," *IEEE Transactions on Biomedical Engineering* (In Preparation).

4]. AF ablation strategies are complex, technically challenging, require a high degree of dexterity and physical effort.

To this end, over the past two decades, three remote catheter navigation systems (both robotic [RNS] and magnetic navigation systems [MNS]) have been developed, approved by the FDA, and introduced clinically. The Amigo™ RNS developed by Catheter Precision facilitates control of a single conventional ablation catheter by loading it into an electromechanical manipulator providing full-range of its functions (insertion, withdrawal, deflection, and rotation) operated by a hand-held remote. However, the system lacks a steerable sheath, thereby significantly reducing the degrees-of-freedom (DOF) associated with catheter manipulation. Steerable sheaths are widely used as they improve maneuverability, stability, and catheter-tissue contact, collectively resulting in better clinical outcome [5-8]. The Sensei® X RNS developed by Hansen Medical (acquired by Auris Health), solves this problem by robotically steering two concentric sheaths, through which any catheter can be introduced. The entire assembly is manipulated within the heart using pull-wires actuated by a robotic arm controlled by a 3D joystick [9]. Early reports of high incidence of clinical complication, steep learning curve, and the inability to navigate within the left ventricle and the coronary sinus due to the large 14 Fr outer sheath are reported shortcomings of this system [9-12]. Lastly, the NIOBE® MNS developed by Stereotaxis uses a specialized magnetic catheter, which can be navigated to target locations by changing the orientation of two permanent magnets positioned on each side of the patient's body. The weak magnetic field (0.08 T) and flexible catheter ensures a safe procedure. However, it results in relatively low catheter-tissue contact force, which is associated with ineffective lesion production and increased rates of AF recurrence [13-16]. The magnetic catheter is not responsive in real-time as motions require mechanical movement of external magnets followed by electromechanical actuation. However, the primary shortcoming among MNS is the inability of the magnetic catheter to detect real-

time catheter-tissue contact force used clinically to guide and assess lesion deliver in real-time. Robotic and magnetic navigation systems have shown to reduce radiation exposure, physician exhaustion, and RF duration [17]. However, none of these systems has demonstrated better clinical outcome versus the manual catheter intervention, and the potential advantages of these systems are offset by additional costs for the systems itself, consumables and maintenance contracts. Emerging technologies must not only provide the ability to precisely place lesions but also optimize lesion production.

Among all factors that influence lesion production, the catheter-tissue contact force (CF) is one of the most critical [18-21]. As such, the incorporation of novel force-sensing ablation catheters into standard practice has become the cornerstone for RF ablation therapy, as it has demonstrated improved clinical outcome [22-24]. Higher levels of force, although delivering larger lesions, can result in tissue perforation, intramural boiling, and collateral tissue damage [20, 25-28]. Lesions delivered with insufficient force produce ineffective superficial lesions [16] and have a higher risk of intermittent contact [29]. Recent literature also highlights the importance of CF variability on lesion production, not merely just CF quantity [21, 30, 31]. Unfortunately, current tools and techniques to improve the stability of CF are limited and reliably achieving an optimal CF profile is virtually impossible.

Our group has developed a novel RNS, enabling remote navigation of a conventional steerable sheath and force-sensing ablation catheter. The Steerable Sheath and Catheter Robotic Navigation System (SSC-RNS) allows for full-range manipulation of a conventional steerable sheath (insertion, withdrawal, rotation, and deflection) in 3-DOF, as well as insertion and withdrawal of a force-sensing ablation catheter within the sheath in 1-DOF. The 4-DOF SSC-RNS also incorporates a catheter contact-force controller – a compact device, which has been independently evaluated previously [32, 33]. The force controller improves the catheter-tissue CF profile and can deliver optimal and reproducible

ablation lesions, even in the presence of cardiac tissue motion. The device maintains an average CF to within 1 gram (g) of the set level and reduces CF variability to less than 5 grams – a variability considered optimal for lesion production [31].

The purpose of this study is to evaluate the SSC-RNS ability to enable remote navigation of a force-sensing ablation catheter. First, to evaluate the performance of the SSC-RNS, an electromagnetic tracking system was used to track the input device and the catheter tip during dynamic motion. Second, an *in vitro* contractile bench model representing a cardiac chamber was used to test the hypothesis that the SSC-RNS can navigate a catheter to specific target locations under the control of a skilled electrophysiologist (EP) and maintain a set amount of force on moving tissue-mimicking material, despite the presence of cardiorespiratory motion.

4.2   Steerable Sheath and Catheter Robotic Navigation System

The SSC-RNS comprises three distinct components: an intuitive master input device, where the EP interfaces to control the robotic system, a robotic system, which is responsible for positioning the catheter and sheath according to the changes in motion of the input device, and finally, the catheter contact-force controller – a device incorporated within the robotic system – which employs closed-loop CF control between the catheter tip and moving tissue.

4.2.1   Master Input Device

The input device to the SSC-RNS, which has been validated in previous work [34], provides an interface to the user to control the robotic system. The input device embodies a repurposed steerable sheath handle (Agilis™ NxT, Abbott Laboratories, St. Paul, MN) fitted with 3D-printed inserts that extend to support walls mounted with two optical encoders (**Figure 4.1**). One optical encoder (HEDS 5600, Infineon Technologies,

Neubiberg, Germany) detects the rotation of the sheath handle, and another encoder is used to detect the deflection mechanism of the sheath. The entire assembly is then mounted on a linear rail fitted with a rack, where a third encoder coupled to a pinion detects insertion and withdrawal of the sheath handle.
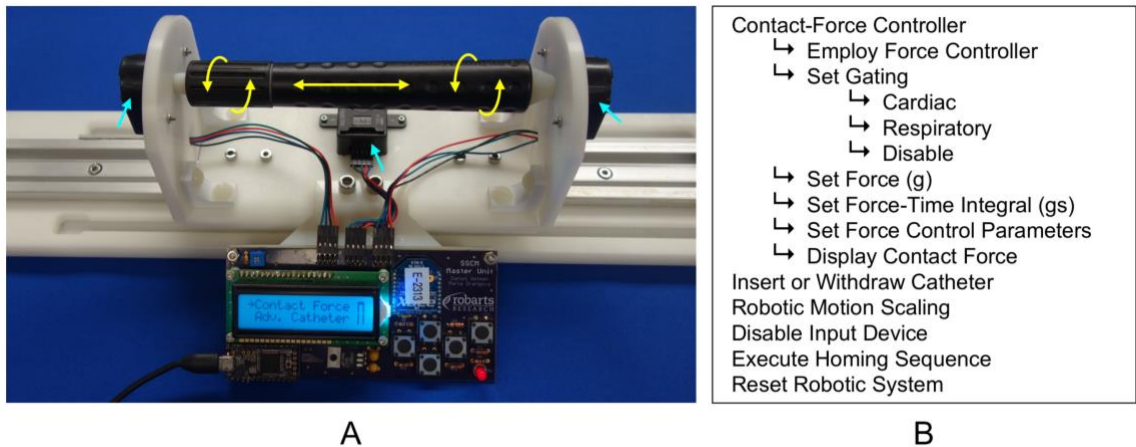
Figure 4.1. Photograph of the input device to the robotic system **A**. Three optical encoders (blue arrows) detect all motion from a steerable sheath handle (insertion, withdrawal, rotation, and deflection indicated by yellow arrows). A digital user interface programmed with a menu system provides the user full control of all features of the robotic system **B**.

A microcontroller-powered (Teensy, PJRC, Sherwood, OR) electronics system, mounted onto the assembly, is responsible for quadrature encoding and transmitting the position information to the robotic system using a wireless transceiver (XBee, Digi International, Minnetonka, MN). The electronics also provide a digital user interface (LCD with tactile buttons), which allows the EP to set parameters of the SSC-RNS including: inserting and withdrawing the catheter through the sheath; setting robotic motion scaling; disabling the input device, and home the robotic system (**Figure 4.1B**). Importantly, the interface allows the user to configure the parameters for the force controller including setting the desired level of force and force-time integral (a metric used in the clinic to access lesion production) and other parameters such as cardiac or respiratory gating.

4.2.2   Robotic System
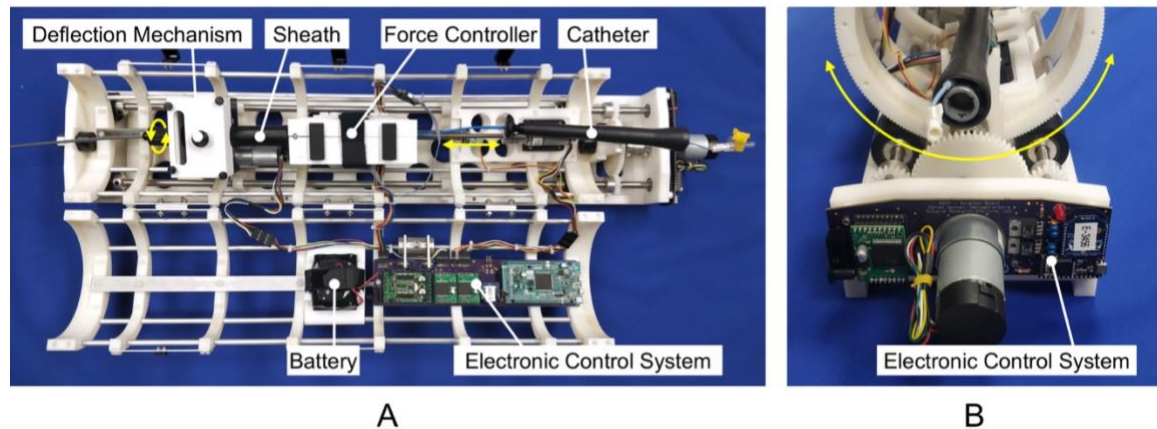
Figure 4.2. The robotic system takes the form of a cylindrical gantry, which opens along its long axis, **A**. Within the gantry; battery-powered electronics receive position data from the input device to insert and withdraw the catheter and sheath as well as deflect the sheath tip using a deflection mechanism (indicated with yellow arrows). The electronics also receives force information and processes a control algorithm to drive the force controller. While in a closed position, the gantry sits on two pairs of rollers driven by a DC motor affixed to the back of the unit, **B**. A separate electronics control system received rotational position data from the input device to rotate the catheter and sheath.

The robotic system (**Figure 4.2**) incorporates a cylindrical gantry with hinges allowing it to open up along its long axis. Within the gantry, two carriages sitting on linear guide rail are driven by a lead screw mechanism coupled to a DC motor (9.7:1 25D Gearmotor, Pololu, Las Vegas, NV). One of the carriages houses a sprocket and chain mechanism powered by another DC motor (47:1 25D Gearmotor, Pololu, Las Vegas, NV) designed to actuate the deflection mechanism of the sheath handle. An electronic control system and battery are mounted within the gantry. An ARM-based microcontroller (Arduino Due, Arduino, Turin, Italy) uses a wireless transceiver to receive position data from the input device and process two proportional-integral (PI) controllers: 1) to control the lead screw mechanism resulting insertion and withdrawal the catheter and steerable sheath; and 2) to control the deflection mechanism to deflect the tip of the steerable sheath. Generated pulse-width modulated (PWM) control signals are received and amplified by motor drivers

(VNH5019 Motor Driver Carrier, Pololu, Las Vegas, NV) before driving each corresponding motor.

While in a closed position, the gantry sits securely on two pairs of rollers, which are driven by a final DC motor (131:1 37D Gearmotor, Pololu, Las Vegas, NV) affixed on the back of the unit (**Figure 4.2B**). An electronic control system receives wireless position data from the input device and processes a PI control algorithm to generate a PWM signal. The control signal is then received and amplified by a motor driver, resulting in rotational tracking of the sheath and catheter. The robotic system measures approximately 86 cm long, 16 cm wide, and 20 cm tall.

4.2.3   Catheter Contact-Force Control

The force controller is an independent compact device, which monitors real-time CF measurements and autonomously adjusts the position of a force-sensing ablation catheter (THERMOCOOL® SMARTTOUCH™, Biosense Webster, Irvine, CA) within a steerable sheath thereby maintaining the force level set by the EP. The device, described in detail in Chapter 2 and Chapter 3, is clamped onto the back-end of a steerable sheath (Agilis™ NxT, Abbott Laboratories, Chicago, IL) near the hemostatic seal; a linear DC servomotor (LM 2070, MICROMO, Clearwater, FL) clamped onto the catheter shaft via a locking adaptor adjusts catheter motion with respect to the sheath (**Figure 4.3**). The force-sensing catheter, steerable sheath and contact-force control device are placed and secured onto the two carriages within the gantry of the SSC-RNS. The electronics control system (within the gantry) receives real-time CF measurements transmitted by a separate microelectronics system; this stand-alone system receives, parses, and transmits incoming force information through a local area network connection with a research-based catheter mapping system (CARTO® 3, Biosense Webster, Irvine, CA). The SSC-RNS electronics process a control algorithm and generate a PWM signal, which sent to a separate motor controller and driver (MCLM 3003, MICROMO, Clearwater, FL). The signal directly adjusts the catheter

position within the sheath to maintain constant force at the catheter tip under closed-loop control. The force controller of the SSC-RNS uses similar control algorithms described in Appendix C.
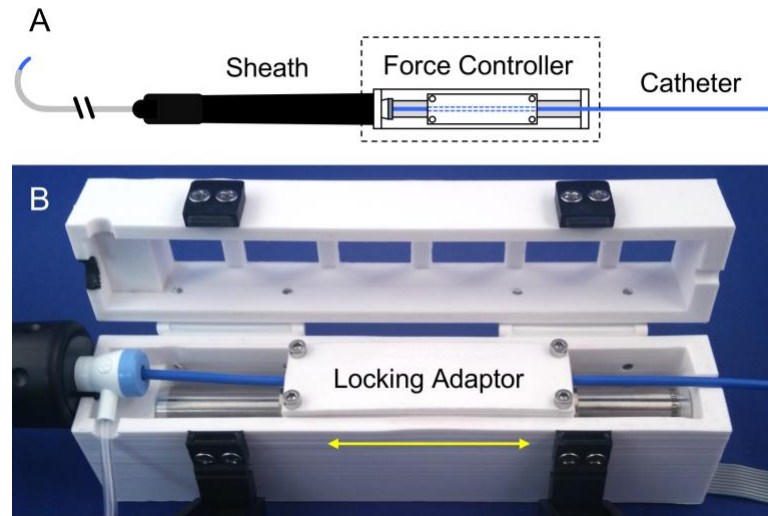
Figure 4.3. Line drawing **A** and photograph **B** of the force controller attached to a force-sensing ablation catheter and steerable sheath. A locking adaptor clamps the catheter to a linear actuator (shown in **B**), which enables the catheter to be inserted and withdrawn within the sheath.

4.3   Evaluation

4.3.1   SSC-RNS Catheter Positioning

Prior to performing *in vitro* evaluation of the system, the tracking performance of the SSC-RNS was quantified using an electromagnetic tracking system (Aurora®, Northern Digital, Waterloo, ON, Canada). An electromagnetic field generator captured the location of a 5-DOF sensor, which was fed through the steerable sheath to the distal tip (in place of the catheter). A second 5-DOF sensor was fixed to the repurposed sheath handle of the input device. A series of six 10-second dynamic motion profiles were performed on the input device (three insertion and withdrawal, three rotation) and mimicked by the robotic system; position coordinates of both sensors were recorded in real-time. Root-mean-squared error (RMSE) with respect to the reference position and angle of the input device was calculated.

Additionally, steady-state error and lag between the input device and the robotic system were determined.

4.3.2   *In Vitro* **Experimental Setup**

A lab-bench motion phantom representing a beating heart was designed and developed (**Figure 4.4**). The phantom comprises a 60-cm long Tygon tube, which enters a 3D-printed hollow truncated 10-cm diameter sphere with 18 6-mm diameter divots scattered on the outside of the shell. The opening of the stationary sphere leads to a frame affixed to the linear motion stage, which was driven to reproduce cardiorespiratory motion. To mimic tissue compliance, a rubber sheet was stretched within the frame. Described in detail in our previous work, the linear stage can reproduce both cardiac and respiratory motion, whereby the frequency and relative amplitude of each component is user-defined [33].

The phantom was scanned using a mobile CT scanner (O-Arm™ 1000 Imaging System, Medtronic, Littleton, MA) and the volume image was imported into the catheter mapping system (CARTO® 3, Biosense Webster, Irvine, CA). A force-sensing ablation catheter (THERMOCOOL® SMARTTOUCH™, Biosense Webster, Irvine, CA) was manually placed within the centre of five divots on the outside of the phantom, enabling a five-point landmark registration to be performed to register the phantom to the reference coordinates of the catheter mapping system. The coordinates of the remaining divots were then acquired in the same way – these points represent the "target locations."
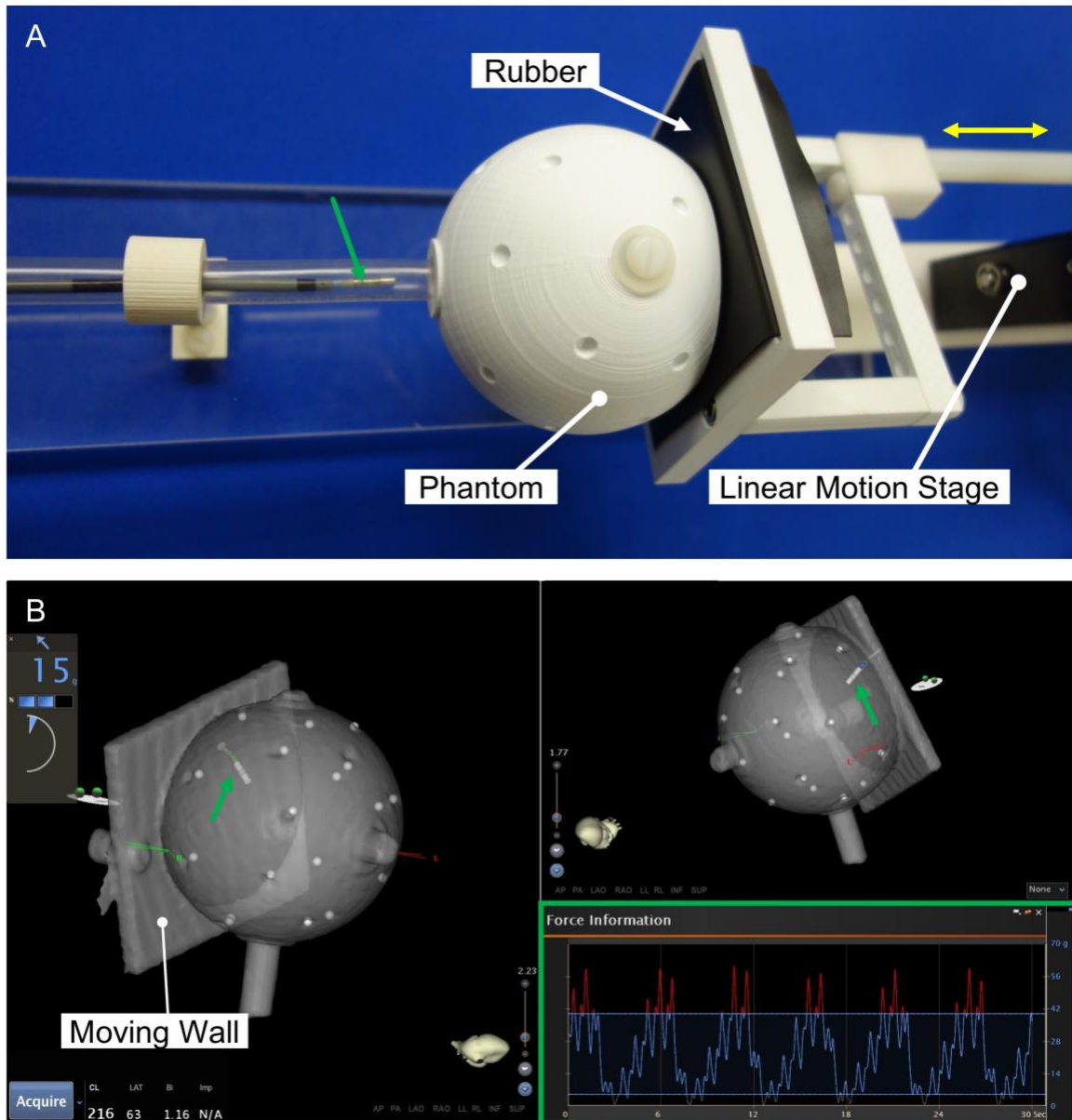
Figure 4.4. Photograph (top-down perspective) of the *in vitro* motion phantom representing a beating heart chamber **A**. The phantom was CT-scanned and imported into the catheter mapping system **B**, where the phantom was registered, and target location (white spheres) were acquired. **B** shows the catheter (green arrows) inside the phantom in contact with a rubber sheet mounted on a moving wall resulting in a CF profile (green square) due to the cardiorespiratory motion reproduced by the linear motion stage.

4.3.3   *In Vitro* Protocol

Comparison between manual and remote navigation was performed. A skilled EP (A.C.S.) was instructed to navigate a catheter tip (in conjunction with a steerable sheath) to eight

stationary target locations using traditional catheter manual intervention. The EP manipulated the catheter to each target location between two and six times, resulting in 27 total navigational tasks. Once the EP reached each target location, the final position of the catheter tip was acquired, and the duration of the task was recorded. Between each task, the catheter was retracted back to the starting position within the Tygon tubing.

The EP was then instructed to navigate to two targets on the moving wall – one with a 90° catheter-rubber incidence angle and the other with a 45° angle. The linear stage was programmed to execute cardiorespiratory motion with randomly selected but clinically relevant amplitudes and frequencies for both cardiac and respiratory components. The EP was instructed to maintain 15 g of CF between the catheter tip and moving wall for 30 seconds; the resulting CF profile was recorded. This was repeated three times, each with the linear motion stage set to different cardiorespiratory motion parameters.

The above protocol was repeated by the same EP using the SSC-RNS. The EP was given a brief introduction to the user interface of the input device and 5-10 minutes of training. The operator was encouraged to use all functions of the SSC-RNS such as catheter insertion and withdrawal within the sheath as well as robotic motion scaling. The EP robotically manipulated the remote catheter to the same eight stationary targets between one and three times, resulting in 22 total navigational tasks (**Figure 4.5**). During robotically assisted CF control experiments on moving targets, the EP was instructed to use to the input device to employ the force controller set for 15 g of force.

The coordinates of the final catheter tip position and their corresponding target location were exported from the catheter mapping system, and the relative distance between those coordinates was calculated. It is important to note that 0.635 mm separate the inner wall of the phantom from the acquired target locations (center of the divot); this value was subtracted from each distance measurement. Distances achieved, duration of each task, and

recorded CF profiles using manual and robotically assisted intervention were compared with one another using a paired t-test to determine significance. The overall interaction time by the EP with the SSC-RNS was also recorded.
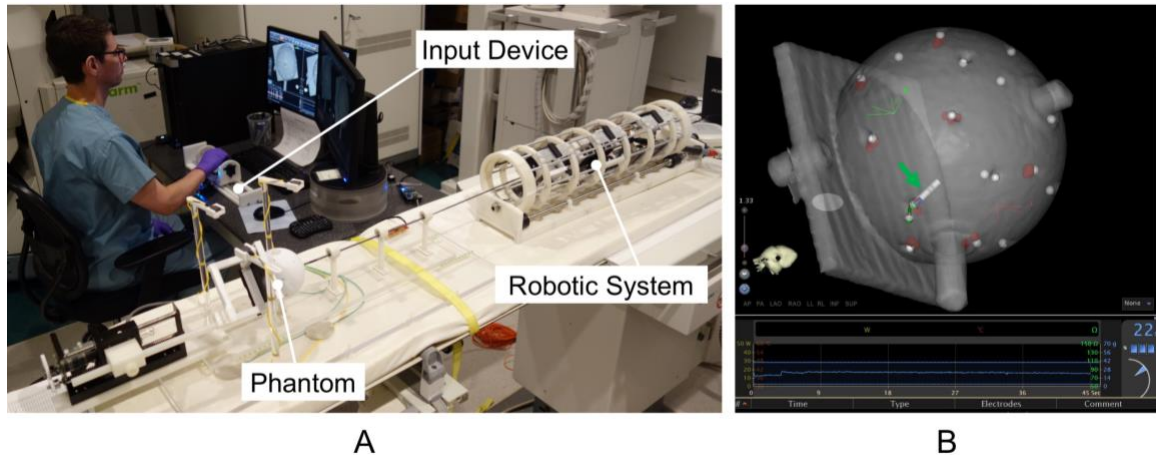
Figure 4.5. Photograph of the electrophysiologist using the SSC-RNS to navigate a remote catheter tip within the *in vitro* phantom **A**. The catheter tip (green arrow), stationary target locations (white spheres), and final catheter tip position (red spheres) are captured and recorded by the catheter mapping system **B**.

In this study, contact-force variability (CFV) was defined as the difference between the mean trough and peak forces. CFV of less than 5 g significantly increased impedance drops and achieved higher maximums compared to lesions with greater variation [31]. Other metrics have previously been shown to be important for lesion delivery [31, 35, 36]. Specifically, the relative standard deviation (RSD) [36] or the coefficient of variation, defined as the ratio between the standard deviation of CF to its mean. RSD less than 30% (*e.g.* 10 ± 3 g or 20 ± 6 g) correlated with a reduction in reconnection gaps during PVI [36]. CFV and RSD were calculated using a custom script in MATLAB (MathWorks, Natick, MA).

Statistical analysis was performed using Prism 8 (GraphPad Software, San Diego, CA). Two-way analysis of variance (ANOVA) was performed to determine if the intervention method (manual or SSC-RNS) and catheter angle (90° or 45°) had a significant effect on

the force profile. The average CF, CFV and RSD were compared and the Sidak multiple comparison test was used to test the hypothesis that robotically assisted intervention resulted in improved force profile that is independent of catheter angle. A p-value of less than 0.05 was considered statistically significant.

4.4   Results

4.4.1   SSC-RNS Tracking Performance

The SSC-RNS is capable of accurately navigating a catheter remotely, with the following specification. While dynamically inserting and withdrawing the catheter and sheath, the steady-state error of 0.5 ± 0.4 mm, RMSE of 1.53 ± 0.25 mm and a lag of 24 ± 6 ms was observed. While rotating the catheter and sheath, the steady-state error was $2.2 \pm 1.9°$, RMSE of $7.54 \pm 0.27°$ and lag of 63 ± 12 ms (**Figure 4.6**).
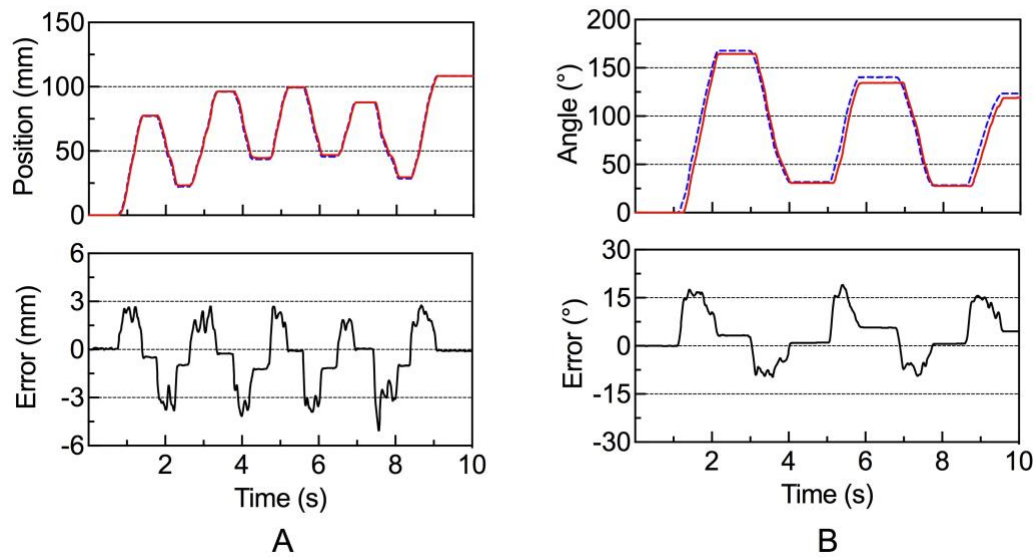
Figure 4.6. Example experiments demonstrating the tracking performance of the SSC-RNS. **A** illustrates the insertion and withdrawal of the input device (blue) and corresponding motion of the sheath tip (red), resulting in a minimal error. **B** illustrates rotational tracking and error.

4.4.2   Catheter Navigation and Contact-Force Control *In Vitro*

All navigation tasks were performed successfully. During manual catheter navigation, the EP was an average distance of 2.5 ± 0.9 mm from the target location and took 28.7 ± 9.9 seconds to complete each task. In contrast, while using the SSC-RNS, the EP was an average distance of 1.7 ± 0.8 mm from the target location and required 53.1 ± 19.3 seconds to complete each task (**Figure 4.7**). There was a significant difference in the distances to the corresponding targets achieved ($p = 0.003$) as well as the time duration to accomplish navigational tasks ($p < 0.0001$) between manual and robotic intervention. These results suggest that there is a higher level of accuracy when using the SSC-RNS over the manual approach. Including instruction to the SSC-RNS and performing all navigation tasks, the EP's interaction time with the SSC-RNS was approximately 63 minutes.
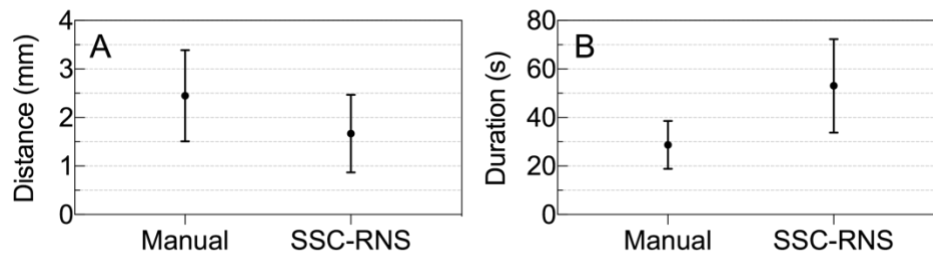
Figure 4.7. Distances between target locations and the catheter tip position **A** and their task durations **B** using manual (n = 27) and robotic intervention (n = 22). Within an hour of using the SSC-RNS, the EP was completing tasks in a time comparable to the manual approach.

Through manual catheter invention, the EP was able to maintain an average force level of 16.8 ± 3.9 g. In contrast, for all robotically assisted interventions, with a set force of 15 g, the average CF was 14.9 ± 0.2 g ($p = 0.1919$) (**Figure 4.8**). Robotically assisted force control resulted in a reduction in CFV from 19.6 ± 11.2 g to 4.7 ± 1.9 g ($p = 0.0024$), and RSD from 48 ± 20 % to 26 ± 3 % ($p = 0.007$). The above results represent the average of four experiments performed with the contact-force controller set to cardiac gating and four experiments set to respiratory gating.
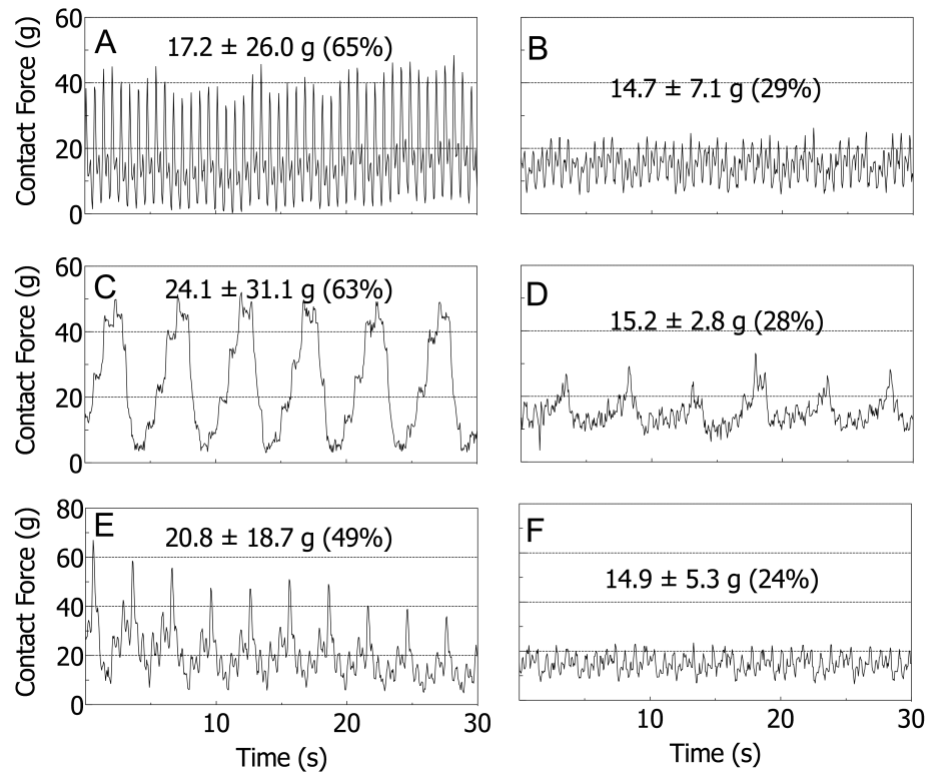
Figure 4.8. Results from three pairs of experiments, each performed with a different motion profile programmed into the linear motion stage. **A**, **C**, and **E** illustrates the resulting CF profile using the manual approach. Respectively, **B**, **D,** and **F** are the resulting CF profile using the force controller of the SSC-RNS. The linear motion stage was programmed with dominant cardiac motion, **A** and **B**, dominant respiratory motion, **C** and **D**, and typical cardiorespiratory motion combining both components, **E** and **F**. For all experiments, the force controller of the SSC-RNS was set for 15 grams of force (red line). Average CF ± CFV (RSD) is provided for each experiment.

With a 90° catheter-rubber incidence angle, throughout manual catheter intervention the EP achieved an average CF of 19.5 ± 3.7 g; larger than the target force level of 15 g. When the incidence angle was reduced to 45° the average force improved to 14.2 ± 1.6 g (p = 0.013), demonstrating better force control to the desired 15 g level. Importantly, by reducing incidence angle the EP was able to significantly reduce CFV from 28.5 ± 8.3 g to 10.7 ± 3.5 g (p = 0.0011), and RSD from 63.0 ± 10.7 % to 33.8 ± 15.8 % (p = 0.006). In contrast, during robotically assisted catheter intervention, no significant difference in average CF between incidence angles of 90° (14.9 ± 0.2 g) and 45° (15.0 ± 0.2 g) was

measured (p > 0.999). Similarly, there was no significant difference in CFV [90°: 4.7 ± 1.9 g, 45°: 4.8 ± 2.3 g, p > 0.999] and RSD [90°: 26.3 ± 2.6 %, 45°: 25.8 ± 3.5 %, p > 0.999] (**Figure 4.9**). Unlike manual catheter intervention, robotically assisted force control was not dependent on catheter incidence angle; consistent average CF at the set level, and reduced CFV and RSD, regardless of the angle tested.
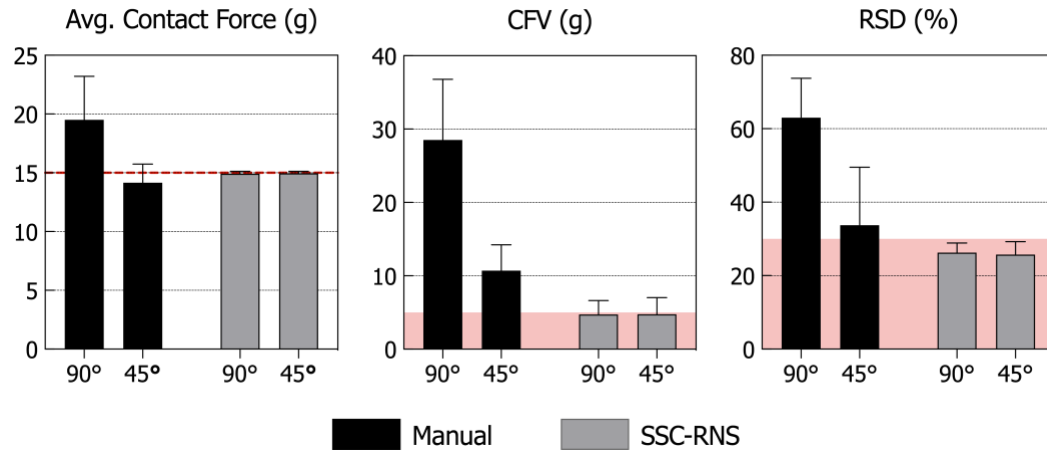
Figure 4.9. Comparison of force profiles while the catheter-rubber incidence angle is reduced from 90° (perpendicular) to 45°. Manual and robotically assisted catheter intervention are reported. Manual catheter intervention resulted in a slight improvement in the force profile. Using the SSC-RNS ensured the average force maintained to 15 g set level (left, red line), reduced CFV to less than 5 g (middle, red area) and RSD to less than 30 % (right, red area), regardless of catheter angle.

Results comparing the force control performance of the SSC-RNS *in vitro* with its simulation is provided in Appendix E.

4.5   Discussion

The design, development and evaluation of a novel robotic platform permitting remote navigation of a conventional steerable sheath and catheter and enabling catheter-tissue CF control was presented in this study. First, the tracking performance of the steerable sheath and catheter robotic navigation system was validated using an electromagnetic tracking system. Second, the SSC-RNS was also tested by a skilled operator using an *in vitro* model

representing a beating cardiac chamber. We demonstrated that the robotic system could track the input device as well as enabling remote navigation of a steerable sheath and catheter, while also providing the capability of maintaining a set force level between the catheter tip and moving tissue-mimicking material.

Measured steady-state errors using SSC-RNS to track the input device were minimal, and the lag between the input device and robotic system was negligible (average delay found to be no greater than 63 ± 12 ms). During the *in vitro* experiment, the EP was able to successfully reach all target locations using the robotic system with an accuracy significantly better in comparison to manual catheter intervention. Furthermore, the robotic system provides the ability to control catheter-tissue CF – a task virtually impossible to accomplish with manual the approach. The force control performance of the robotic system was similar to the results obtained in our previous work, where we evaluated the device independent from the SSC-RNS [32, 33]. Similar to the results discussed in detail in Chapter 3, force control of the SSC-RNS ensured that the average force is less than 1 g of the set level. Under force control, RSD reduced to less than 30% on average, implying more durable lesion delivery would occur in the clinic, according to Makimoto *et al.* [36]. CFV reduced to less than 5 g, implying that the force controller of the SSC-RNS would provide improved durability in PVI, according to Ullah *et al.* [31].

During manual catheter intervention, as demonstrated in this study, the EP can improve the CF profile by reducing the catheter-tissue incidence angle. The shallower incidence angle allows the distal catheter tip to deflect along with the displacement of tissue in a spring-like fashion. Achieving a shallow angle is often not possible, and controlling the amount of average CF is limited in this orientation [37]. Importantly, deeper lesions are achieved when the catheter tip is perpendicular to the tissue (*i.e.* 90° incidence angle) [38]. However, as demonstrated in this study, perpendicular orientation results in more CF instability.

Unlike the manual approach, robotically assisted force control ensured that the CF profile is optimal and independent of catheter incident angle.

One of the features of the SSC-RNS includes robotic motion scaling. This feature allows scaling of the motion of the robotic system in relation to the input device. For instance, if a motion scaling setting of four were to be used, an advancement of the input device of 10 cm would result in 2.5 cm advancement of the remote catheter and sheath; the same principle is applied for rotation and deflection. During the experiments, the EP robotically guided the catheter to the general area of the target location, then enabled motion scaling (set to two) to adjust the catheter tip position to the target location finely; the EP found this feature to be very useful in getting the catheter tip closer to target. The authors suspect this contributed to the improved accuracy in comparison to manual catheter intervention.

The EP acknowledged that the robotic system greatly enhanced the stability of the catheter. Since the SSC-RNS always holds the remote catheter and sheath, it allows the EP to focus on slight adjustments to hit the target location – this implies that the robotic system would be ideal for line or "drag" ablation strategies. Furthermore, engaging the force controller without the need of manually holding the catheter and sheath position throughout an RF application (30-60 seconds) is a considerable advantage over the manual approach as it improves catheter stability and reduces operator fatigue.

Through formative studies our group performed prior to this study, the majority of EPs manipulate the steerable sheath to guide the catheter tip to a target and dial in the force by advancing or retracting the catheter within the sheath. The operator involved in this study manipulated the instruments differently, whereby the catheter (rather than the sheath) is manipulated for most of the procedure. The SSC-RNS was designed for operators who use the former strategy. Because the EP interacted with the SSC-RNS for approximately an hour, the amount of time required to complete each navigational task remotely was greater

than that required for manual intervention. However, it is expected that subsequent sessions, with minimal additional practice, would result in faster navigation times. Additional studies with multiple users need to be performed to evaluate the learning curve of the SSC-RNS. We suspect that other EPs who use the former strategy would require less training due to the intuitive input device and the principal design of the SSC-RNS. A primary limitation in this work is that only one EP was involved in this study. Involving more operators, particularly EPs who manipulate the steerable sheath and catheter using the former strategy, may affect the reported results.

Several other issues relating to the design of the SSC-RNS were identified. First, the inability for the operator to rotate and deflect the ablation catheter independently of the sheath limits the degrees-of-freedom associated with catheter and sheath manipulation. Second, the loss of haptic feedback from the sheath handle prevents the EP from determining the sheath deflection angle in relation to its "neutral position" (*i.e.*, when the sheath tip is not deflected). Finally, a digital menu system for the user interface is cumbersome; changing parameters and operations of the robotic system should be easily accessible. Future iterations of similar catheter RNS must consider these design flaws.

4.6   Conclusion

Commercially available robotic and magnetic catheter navigation systems have been demonstrated to be safe and feasible in treating cardiac arrhythmia using catheter ablation techniques. Although they show to reduced reduce x-ray radiation exposure and fatigue to the EP, they have not yet demonstrated better first-procedure success rates over the manual approach. For clinical uptake of new technologies entering the market, it is critical that they demonstrate better clinical outcomes over the manual approach. One strategy is to develop technologies that do not merely mimic the manual intervention, instead provide a level of automation such as catheter-tissue CF control.

In the work presented in this study, we took advantage of robotic technology to optimize the CF profile between the catheter tip and moving tissue. The novel RNS uses available force information to improve lesion production by incorporating this feature. The results obtained in this study suggest that the SSC-RNS can be a valuable tool available to the EP to not only allow or remote catheter navigation but also optimize lesion delivery techniques and ultimately improve first-procedure efficacy rates.

4.7 References

[1] H. Calkins *et al.*, "2017 HRS/EHRA/ECAS/APHRS/SOLAECE expert consensus statement on catheter and surgical ablation of atrial fibrillation," *Heart Rhythm,* vol. 14, no. 10, pp. e275-e444, 2017

[2] R. A. Winkle, R. H. Mead, G. Engel, and R. A. Patrawala, "Long-term results of atrial fibrillation ablation: the importance of all initial ablation failures undergoing a repeat ablation," *Am Heart J,* vol. 162, no. 1, pp. 193-200, 2011

[3] R. Weerasooriya *et al.*, "Catheter ablation for atrial fibrillation: are results maintained at 5 years of follow-up?," *J Am Coll Cardiol,* vol. 57, no. 2, pp. 160-6, 2011

[4] M. Bhargava *et al.*, "Impact of type of atrial fibrillation and repeat catheter ablation on long-term freedom from atrial fibrillation: results from a multicenter study," *Heart Rhythm,* vol. 6, no. 10, pp. 1403-12, 2009

[5] M. W. Deyell *et al.*, "The impact of steerable sheaths on unblinded contact force during catheter ablation for atrial fibrillation," *J Interv Card Electrophysiol,* 2019

[6] C. Piorkowski *et al.*, "Steerable versus nonsteerable sheath technology in atrial fibrillation ablation a prospective, randomized study," *Circ Arrhythm Electrophysiol,* vol. 4, no. 2, pp. 157-165, 2011

[7] W. Ullah *et al.*, "Impact of steerable sheaths on contact forces and reconnection sites in ablation for persistent atrial fibrillation," *J Cardiovasc Electrophysiol,* vol. 26, no. 3, pp. 266-73, 2015

[8] T. Kimura *et al.*, "Operator-blinded contact force monitoring during pulmonary vein isolation using conventional and steerable sheaths," *Int J Cardiol,* vol. 177, no. 3, pp. 970-6, 2014

[9] B. L. Nguyen, J. L. Merino, and E. Gang, "Remote Navigation For Ablation Procedures - A New Step Forward In The Treatment Of Cardiac Arrhythmias," *European Cardiology Review,* vol. 13, no. 2, pp. 50-6, 2010

[10] L. Di Biase *et al.*, "Remote magnetic navigation: human experience in pulmonary vein ablation," *J Am Coll Cardiol,* vol. 50, no. 9, pp. 868-74, 2007

[11] A. Al-Ahmad, J. D. Grossman, and P. J. Wang, "Early experience with a computerized robotically controlled catheter system," *J Interv Card Electrophysiol,* vol. 12, no. 3, pp. 199-202, 2005

[12] A. Rillig *et al.*, "Manual Versus Robotic Catheter Ablation for the Treatment of Atrial Fibrillation: The Man and Machine Trial," *JACC Clin Electrophysiol,* vol. 3, no. 8, pp. 875-83, 2017

[13]   S. Haldar *et al.*, "Contact force sensing technology identifies sites of inadequate contact and reduces acute pulmonary vein reconnection: a prospective case control study," *Int J Cardiol,* vol. 168, no. 2, pp. 1160-6, 2013

[14]   J. B. le Polain de Waroux *et al.*, "Low contact force and force-time integral predict early recovery and dormant conduction revealed by adenosine after pulmonary vein isolation," *Europace,* vol. 17, no. 6, pp. 877-83, 2015

[15]   B. J. Tofig *et al.*, "Recurrence after pulmonary vein isolation is associated with low contact force," *Scand Cardiovasc J,* vol. 52, no. 1, pp. 28-33, 2018

[16]   K. Yokoyama *et al.*, "Novel contact force sensor incorporated in irrigated radiofrequency ablation catheter predicts lesion size and incidence of steam pop and thrombus," *Circ Arrhythm Electrophysiol,* vol. 1, no. 5, pp. 354-362, 2008

[17]   V. Y. Reddy *et al.*, "View-synchronized robotic image-guided therapy for atrial fibrillation ablation: experimental validation and clinical feasibility," *Circulation,* vol. 115, no. 21, pp. 2705-14, 2007

[18]   D. C. Shah, H. Lambert, H. Nakagawa, A. Langenkamp, N. Aeby, and G. Leo, "Area under the real-time contact force curve (force-time integral) predicts radiofrequency lesion size in an in vitro contractile model," *J Cardiovasc Electrophysiol,* vol. 21, no. 9, pp. 1038-43, 2010

[19]   H. Nakagawa and W. M. Jackman, "The Role Of Contact Force In Atrial Fibrillation Ablation," *J Atr Fibrillation,* vol. 7, no. 1, p. 1027, 2014

[20]   A. Ikeda *et al.*, "Relationship between catheter contact force and radiofrequency lesion size and incidence of steam pop in the beating canine heart: electrogram amplitude, impedance, and electrode temperature are poor predictors of electrode-tissue contact force and lesion size," *Circ Arrhythm Electrophysiol,* vol. 7, no. 6, pp. 1174-80, 2014

[21]   A. Natale *et al.*, "Paroxysmal AF catheter ablation with a contact force sensing catheter: results of the prospective, multicenter SMART-AF trial," *J Am Coll Cardiol,* vol. 64, no. 7, pp. 647-56, 2014

[22]   K. S. Hoffmayer and E. P. Gerstenfeld, "Contact force-sensing catheters," *Curr Opin Cardiol,* vol. 30, no. 1, pp. 74-80, 2015

[23]   J. Kautzner *et al.*, "EFFICAS II: optimization of catheter contact force improves outcome of pulmonary vein isolation for paroxysmal atrial fibrillation," *Europace,* vol. 17, no. 8, pp. 1229-35, 2015

[24]   P. Neuzil *et al.*, "Electrical reconnection after pulmonary vein isolation is contingent on contact force during initial treatment: results from the EFFICAS I study," *Circ Arrhythm Electrophysiol,* vol. 6, no. 2, pp. 327-33, 2013

[25] W. Ullah, R. J. Schilling, and T. Wong, "Contact Force and Atrial Fibrillation Ablation," *J Atr Fibrillation,* vol. 8, no. 5, p. 1282, 2016

[26] A. Thiagalingam *et al.*, "Importance of catheter contact force during irrigated radiofrequency ablation: evaluation in a porcine ex vivo model using a force-sensing catheter," *J Cardiovasc Electrophysiol,* vol. 21, no. 7, pp. 806-11, 2010

[27] C. Pappone *et al.*, "Atrio-esophageal fistula as a complication of percutaneous transcatheter ablation of atrial fibrillation," *Circulation,* vol. 109, no. 22, pp. 2724-6, 2004

[28] D. C. Shah and M. Namdar, "Real-time contact force measurement: a key parameter for controlling lesion creation with radiofrequency energy," *Circ Arrhythm Electrophysiol,* vol. 8, no. 3, pp. 713-21, 2015

[29] K. H. Kuck *et al.*, "A novel radiofrequency ablation catheter using contact force sensing: Toccata study," *Heart Rhythm,* vol. 9, no. 1, pp. 18-23, 2012

[30] N. Ariyarathna, S. Kumar, S. P. Thomas, W. G. Stevenson, and G. F. Michaud, "Role of Contact Force Sensing in Catheter Ablation of Cardiac Arrhythmias: Evolution or History Repeating Itself?," *JACC Clin Electrophysiol,* vol. 4, no. 6, pp. 707-723, 2018

[31] W. Ullah *et al.*, "Factors affecting catheter contact in the human left atrium and their impact on ablation efficacy," *J Cardiovasc Electrophysiol,* vol. 26, no. 2, pp. 129-36, 2015

[32] D. Gelman, A. C. Skanes, M. A. Tavallaei, and M. Drangova, "Design and Evaluation of a Catheter Contact-Force Controller for Cardiac Ablation Therapy," *IEEE Trans Biomed Eng,* vol. 63, no. 11, pp. 2301-7, 2016

[33] D. Gelman, A. C. Skanes, D. L. Jones, M. Timofeyev, T. Baron, and M. Drangova, "Eliminating the effects of motion during radiofrequency lesion delivery using a novel contact force controller: a pre-clinical study," *J Cardiovasc Electrophysiol,* 2019

[34] M. A. Tavallaei *et al.*, "Design, development and evaluation of a compact telerobotic catheter navigation system," *Int J Med Robot,* vol. 12, no. 3, pp. 442-52, 2016

[35] A. Sarkozy *et al.*, "Contact force variability during catheter ablation of atrial fibrillation: the role of atrial rhythm and ventricular contractions: co-force AF Study," *Circ Arrhythm Electrophysiol,* vol. 8, no. 6, pp. 1342-50, 2015

[36] H. Makimoto *et al.*, "Incidence and anatomical locations of catheter instability during circumferential pulmonary vein isolation using contact force," *Int Heart J,* vol. 55, no. 3, pp. 249-55, 2014

[37]   F. H. Wittkampf and H. Nakagawa, "RF catheter ablation: Lessons on lesions,"
       Pacing Clin Electrophysiol, vol. 29, no. 11, pp. 1285-97, 2006

[38]   N. Gallagher, E. C. Fear, I. A. Byrd, and E. J. Vigmond, "Contact geometry affects
       lesion formation in radio-frequency cardiac catheter ablation," *PLoS ONE,* vol. 8,
       no. 9, p. e73242, 2013

5 Conclusions and Future Work

5.1 Thesis Summary

The chapters in this thesis describe the individual steps required for the design, development, and evaluation of robotic technology that address problems associated with current cardiac catheter ablation therapy – specifically, the Catheter Contact-Force Controller (CFC) and Steerable Sheath and Catheter Robotic Navigation System (SSC-RNS). These systems were evaluated in several *in vitro* and *in vivo* experiments, which were designed to compare robotically assisted intervention to the manual approach.

Chapter 2 described the design, development, and *in vitro* evaluation of the CFC. This chapter also described the development and evaluation of a linear motion stage programmed to reproduce motion profiles corresponding to force profiles recorded during RF ablation in patients. The CFC was tested for its force control performance using the motion stage, which was fitted with a strain gauge to measure CF between the catheter tip and tissue-mimicking material in real-time. The control system of the CFC monitors the CF and processes a hybrid PID control algorithm to displace the catheter within sheath, thereby ensuring the set force level is always met. The CFC showed to be safe and effective in controlling CF. When using the CFC, the average force is within 1 g of the set level and variability is reduced to less than 5 (calculated as RMSE with respect to the set level) for each clinically appropriate force level tested (15 g, 25 g, and 40 g). In this study, the CFC also demonstrated to employ CF control at a set desired force level with a prescribed FTI.

The demonstrated control of contact force under varying motion conditions is promising and suggests that – when implemented in combination with a force-sensing ablation catheter – the CFC can deliver prescribed ablation lesions.

The CFC was then integrated with an EAM system fitted with specialized software allowing real-time CF measurements, detected by a force-sensing ablation catheter, to be continuously streamed to the CFC electronics in real-time. System integration enabled additional *in vitro* and *in vivo* evaluation, described in Chapter 3. Due to the characteristics of the force sensor incorporated on the catheter tip (*e.g.*, sampling time, dead-time, noise, *et cetera*), the design and implementation of two new control algorithms, replacing the existing hybrid PID control algorithm, were required. These algorithms were designed to compensate for different types of cardiorespiratory motion observed in the clinic. The force control performance of the CFC was first evaluated in an animal model, where a trained operator employed the CFC (set for 20 g) on moving targets in the RA, LA, and LV. The recorded CF profiles were compared to a repeat experiment whereby the operator attempted to maintain the desired force of 20 g using manual catheter intervention. An additional *in vitro* study was then performed to investigate CFC-assisted RF delivery to moving tissue, achieved by modifying the linear motion stage (described in Chapter 2) with a saline bath. CFC-assisted RF ablation lesions (set at different clinically relevant force levels) were delivered to moving tissue samples and were compared to lesions in the absence of motion. To compare to manual catheter intervention, a third set of RF lesions to moving tissue without the assistance of the CFC were delivered. For both *in vivo* and *in vitro* experiments, the CFC maintained an average force to within 1 g of the set level and significantly reduced both the contact-force variability (CFV) and relative standard of deviation (RSD). Specifically, in comparison to manual catheter intervention, CFC-assisted ablation reduced the average CFV by a factor of 6.0 to less than 5 g and reduced the average RSD by a factor of 2.5 to less than 30%. On average, the CFC reduced the

standard deviation of CFV and RSD by a factor of 13.1 and 2.5, respectively. These results reinforce the notion that CFC-assisted ablation delivery ensures a constant CF resulting in more durable lesion delivery [1, 2]. Importantly, CFC-assisted ablation lesions were reproducible in size despite the presence of randomly selected cardiorespiratory motion. These lesions were statistically identical in size (depth and volume) to lesions delivered to tissue absent of motion, indicating precise lesion delivery.

The CFC was then incorporated into a robotic platform enabling remote actuation of a steerable sheath. The novel SSC-RNS was designed to allow for full-range manipulation of a commercially available steerable sheath in 3-DOF (insertion, withdrawal, rotation, and deflection). Using the incorporated CFC, the SSC-RNS also allows for remote manipulation of the force-sensing ablation catheter through the sheath in 1-DOF (insertion and withdrawal), further enabling catheter-tissue CF control. An intuitive input device, designed around a repurposed steerable sheath handle fitted with embedded electronics, allows for wireless remote control of the robotic system. This design approach allows the operator to remotely navigate a catheter tip to target locations guided by an EAM system and employ CF control on moving targets. The SSC-RNS was first evaluated using an electromagnetic tracking system with sensors placed on the input unit and within the tip of the remote steerable sheath. This first test demonstrated sub-millimetre insertion and withdrawal error, a few degrees of rotational error, and negligible lag between the input device and robotic system of the SSC-RNS. The SSC-RNS was then evaluated *in vitro* using the linear motion stage (used in Chapter 2 and Chapter 3) modified to represent a beating heart phantom. Under EAM guidance, a skilled operator first navigated a remote catheter tip to several stationary and moving targets within the phantom. When engaging with moving targets, the operator employed CF control (set at 15 g) using the interface provided by the input device. Distances between the catheter tip and stationary target as well as the CF profiles generated between the catheter tip and moving targets were recorded

and compared to a repeated experiment using manual catheter intervention. Although navigational tasks took longer to complete, the catheter tip was significantly closer to the corresponding targets, demonstrating improved accuracy. Similar to the results obtained in Chapter 2 and Chapter 3, the SSC-RNS with the incorporated CFC, significantly improved the CF profile over manual catheter intervention.

5.2   Contributions

In current clinical practice, an EP would manipulate a catheter tip to a target and use the force information strictly as a visual guide. To the best of their abilities, the operator would make sure the catheter makes contact and does not exceed dangerous force levels. Whether or not stable CF is achieved, the EP would then deliver an RF lesion. These lesions are less safe, but more importantly, difficult to assess clinically – potentially increasing the risk of leaving reconnection gaps deep into the tissue, which may lead to early AF recurrence. As discussed in this thesis, the current tools and techniques available to the EP to address this problem is limited.

The introduction of the CFC allows the operator to ensure that RF ablations are delivered safely and prescribed for each application precisely, independent of its regional location in the heart and extent of motion. The CFC is the first device to use the available force information to implement a closed-loop system to enable CF control between the catheter tip and moving tissue, eliminating the effects of cardiorespiratory motion on lesion production. The CFC is also the first device to demonstrate the ability to deliver reliably reproducible and precise ablation lesions *in vitro*. The CFC is the first tool to use robotic technology to optimize point-point RF lesion production.

Clinically available robotic and magnetic navigation systems enable remote navigation of an ablation catheter. This design mainly provides ancillary benefits such as reduced fluoroscopic x-ray exposure and reduced operator fatigue. However, each of these systems

has its list of shortcomings that are not present in manual catheter intervention. Importantly, in the context of first-procedure success, none of these systems have demonstrated clear superiority over the manual approach. It is suspected that this is the primary reason for the lake of uptake of these systems into the clinic. Unless the benefits outweigh their shortcomings, it will be difficult for hospitals to justify purchasing and adopting these systems into clinical practice. Robotic systems for cardiac ablation therapy must limit their trade-offs and take advantage of robotic technology to improve ablation efficacy by implementing forms of automation.

The SSC-RNS is a promising example of such a system. The SSC-RNS uses of conventional catheters and steerable sheaths permitting access to all anatomical regions of the heart, preserve the natural hand-eye coordination of the operator by providing an intuitive input device, and importantly, implements an automatic feature of closed-loop CF control between the catheter tip and moving cardiac tissue. To this end, the SSC-RNS is the only device of its kind, in the context of RF catheter ablation, that enables remote catheter navigation with an autonomous catheter-tissue CF control. The SSC-RNS can be a valuable tool available to the EP to optimize the placement and production of RF ablation lesions, which can ultimately lead to improved first-procedure efficacy rates.

5.3   Future Research

Throughout this research project, several discussions with advisors, collaborators, and physicians sparked ideas of further development and evaluation of the CFC and SSC-RNS. Proposed research projects involving both robotic systems are described in detail in the following sections.

5.3.1   Fully Automated Catheter Intervention

Implementing functional automation designed to allow for automatic movement of the catheter to specific targets within the cardiac chamber under EAM guidance is the future

direction for the SSC-RNS. The proposed added feature to the SSC-RNS would enable an operator to select a target within the EAM system and employ the robotic system to automatically guide the steerable sheath to point to the selected target and engage force control. The input device to the SSC-RNS would be used for fine adjustment if necessary. This implementation allows for fully automated catheter delivery of reliably transmural RF ablation lesions.

Several robotic systems that allow for automatic catheter movements have been proposed and evaluated in academia. Design and evaluation of the CathROB RNS is described by Cercenelli *et al.* [3]. This system allows for remote navigation of an ablation catheter and implements an automatic repositioning algorithm to guide the catheter to preselected and memorized targets. It is assumed that this method actuates each DOF to the reference position previously acquired. This method is highly susceptible to external factors, including cardiac and patient motion, as well as a change in the position of the robot itself. Importantly, this method assumes the catheter is a rigid body. Due to the flexibility and compliance of the catheter, simply repositioning to a reference position will not reliably result in a tip position identical to when the reference position was acquired. Loschak *et al.* developed a more robust approach. The group developed a sophisticated 4-DOF RNS to manipulate intracardiac echocardiography (ICE) catheters [4, 5]. Briefly, the system uses an electromagnetic sensor to locate the position of the catheter tip and uses a kinematic model of a catheter within the control loop to robotically guide an ICE catheter along the pre-defined path [6, 7]. This solution enables closed-loop control of the catheter tip position and the ultrasound imaging plane. Other catheter kinematic models to enable automatic positioning of intracardiac catheters have been proposed [8, 9].

An automated version of the SSC-RNS would implement closed-loop control of the catheter tip position by developing a control system incorporating a kinematic model of the catheter and sheath. Since the sheath tip is (generally) not tracked by the EAM system,

the kinematic model must be derived while the catheter tip is in a fixed position relative to the sheath tip. For reliable control, this fixed position must be retained throughout automated navigation.
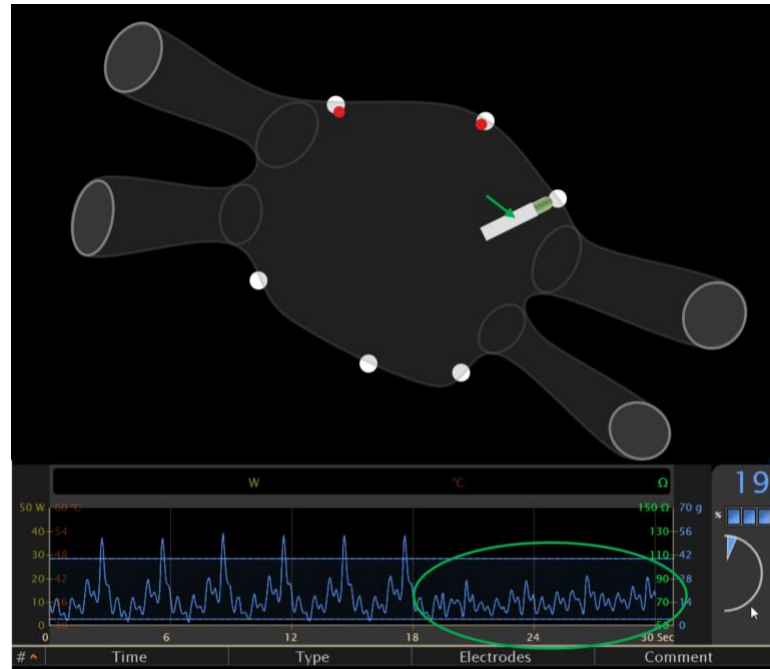
Figure 5.1. Illustration of an EAM of the animal's LA. The automated SSC-RNS actuates the steerable sheath (not shown) to point the tip towards one of six targets (white dots). The robotic system then advances the catheter tip (green arrow) forward and employs the force controller. Once an improved CF profile (green circle) is achieved, the final catheter tip position can be acquired (red dot).

An *in vivo* study to evaluate automated SSC-RNS can be performed in a porcine model in a similar approach described in Chapter 3. First, an adequate electro-anatomical map of a pig's LA is acquired (**Figure 5.1**) and registered correctly; a force-sensing ablation catheter can then be introduced into the cardiac chamber. The catheter and sheath can then be loaded into the SSC-RNS. Through the EAM, the EP can select the target location and the SSC-RNS will automatically navigate the sheath to point towards each corresponding target. The force controller with then advance the catheter forward, make initial contact with the moving tissue, and maintain a set force level of 15 g.

In comparison to the manual approach, we anticipate an improved accuracy and CF profile using the automated SSC-RNS. Like the results obtained in Chapter 4, the catheter tip will be closer to the corresponding target. Additionally, similar to the results obtained in Chapter 2 and Chapter 3, the automated SSC-RNS will enable improved CF control and reduction in CF variability. The SSC-RNS will allow the operator to engage targets accurately and safely in a fully automated process.

5.3.2   Further *In Vivo* Evaluation of CFC Impact

To further investigate the CFC's impact in lesion production, a series of additional *in vivo* experiments are proposed. The following section first describes a more representative method of performing *in vivo* evaluation for RF ablation experiments. This method will be used to investigate how the CFC can be utilized within existing lesion assessment techniques and emerging RF catheter technologies.

5.3.2.1   Thigh Muscle Preparation

In Chapter 3, the CFC was evaluated *in vivo* to examine its force control performance on a beating heart. During these experiments, RF ablation lesions were delivered to moving tissue with the CFC. These lesions were not quantified; instead, CFC-assisted lesion production was investigated *in vitro* to control for other factors that would have had unmeasurable influences on lesion production. The development of an RF-enabled contractile motion phantom allowed for the delivery of ablation lesions into tissue undergoing reproducible cardiorespiratory motion, while keeping other factors that influence lesion production consistent. Unfortunately, the experimental set up did not mimic blood and tissue temperature and did not model convective and perfusive cooling. Furthermore, the salinity of the water bath within the phantom was titrated to enable the generation of measurable lesions at the clinically relevant CF levels, RF duration, and RF

power. Thus, lesion production using this model does not directly reflect lesion production in humans.

Typically, a thigh muscle preparation using a porcine or canine model is used in such RF ablation experiments [10-15]. In comparison to cardiac tissue, a thigh model is a reasonable technique for evaluation of ablation catheter technology [16] (**Figure 5.2**). In this setup, an incision is made within the thigh of the animal, and a thick portion of the femoris muscle is exposed. The skin is raised to form a chamber overlying the thigh muscle. Arterial blood is collected from the femoral artery, heparinized, heated to 37°C, and circulated through an external pump (flow rate of 200 ml/min) introduced over the exposed muscle within the cavity of the femoral chamber. The linear motion stage, which was used extensively and modified throughout this thesis, can be fitted to the leg of the animal and employ cardiorespiratory motion profiles, resulting in motion of the thigh muscle. A lesion protocol, such as the protocol described in Chapter 3, can then be performed to the thigh muscle; motion can be introduced by merely engaging the linear motion stage. After each RF application, the catheter is moved to a new position along the muscle, the femoral chamber is emptied, and new heated heparinized blood is introduced. The thigh muscles can be harvested and placed in formaldehyde and stained with 2% triphenyl tetrazolium chloride in phosphate-buffered saline, which is used to differentiate the necrotic tissue from the untreated tissue accurately. Lesion measurement and statistical analysis can follow.

The thigh muscle preparation technique is a widely used and acceptable method for RF ablation experiments. Studies that adopt this experimental setup is considered to be more representative of lesion delivery in human. Several proposed studies, described in the following sections, should be performed using this technique to further evaluate the CFC and its effect on RF lesion production.
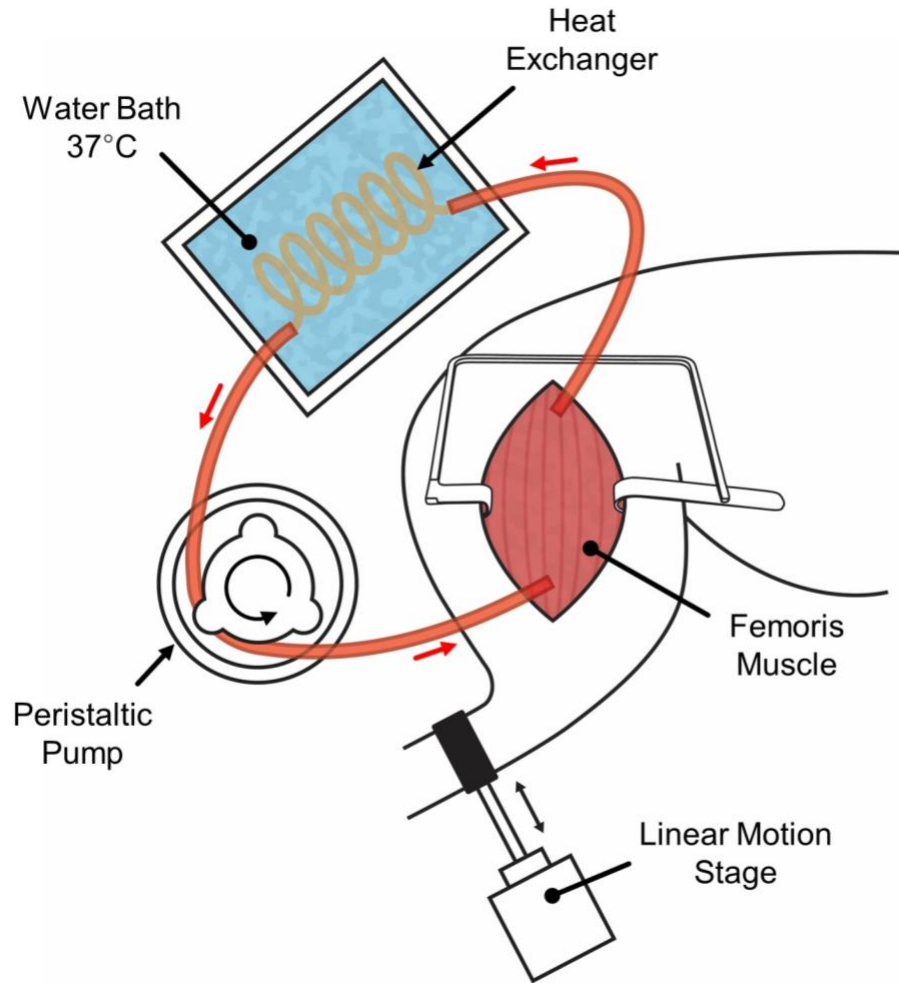
Figure 5.2. Illustration of thigh muscle preparation. Arterial blood, collected from the animal, is heparinized and pumped through a heat exchanger which is submerged in a water bath heated for 37°C. The blood is pumped over the femoris muscle within the chamber. A linear motion stage, attached to the leg of the animal, moves the femoris muscle resulting in cardiorespiratory motion. Illustrated was adapted from Leshem *et al*. [16].

5.3.2.2   **Force-Time Integral Prescribed Ablation**

Force-Time Integral (FTI), defined as the area under the CF curve with respect to time (represented in gs), is a real-time lesion assessment tool and is commonly used during RF ablation therapy (**Figure 5.3**). In the original study that introduced this metric, performed by Shah *et al*. [17], the group demonstrates that during a 60-second RF application (at fixed RF power and irrigation), the highest FTI occurred when CF remained constant, which

resulted in the largest and deepest lesions. However, this study did not attempt to examine whether FTI-prescribed lesion production is dependent on CF variability. In clinical practice, the intended use of FTI primarily involves stopping the RF application when the appropriate amount of FTI is accumulated. The value is then automatically annotated within the EAM system at each corresponding ablation point, which can be referenced and evaluated throughout the procedure. Generally, the EP does not take into account CF variability during FTI-prescribed RF application. In other words, it is unknown whether or not lesion size may vary with different CF profiles (average and variability), despite maintaining a constant FTI.
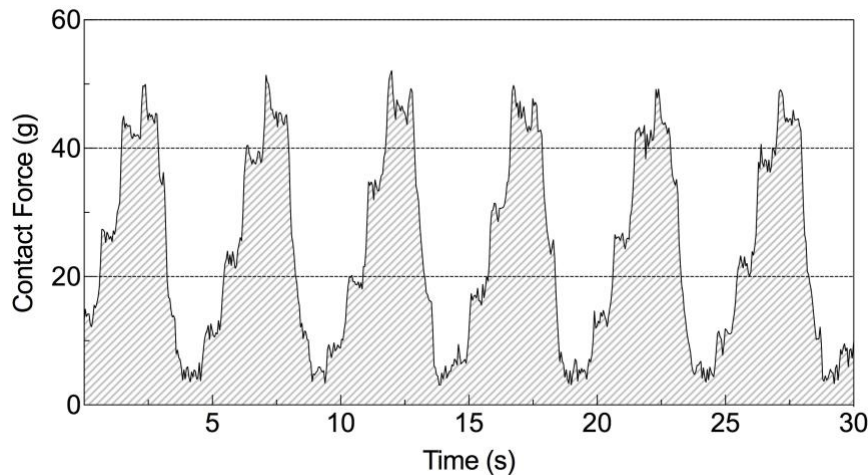
Figure 5.3. A representative example of a CF profile with 725 gs of FTI, indicated by the area under the CF curve with respect to time.

One study that demonstrates the importance of CF variability in the context of FTI is the work done by Ullah *et al.* [18]. The group demonstrated that with the same FTI, the presence of CF variability (greater than 5 g) is associated with lower impedance drop, which is a surrogate for poor lesion production. This study suggests that there is a profound negative impact of CF variability even when FTI remains the same. The authors suggest that EPs should actively improve CF variability rather than delivering more FTI. Other than this work, there is no published data describing the role of CF variability in lesion

production in the context of FTI. To this end, we propose an additional *in vivo* study to evaluate the effect of CF variability on FTI-prescribed lesion production.
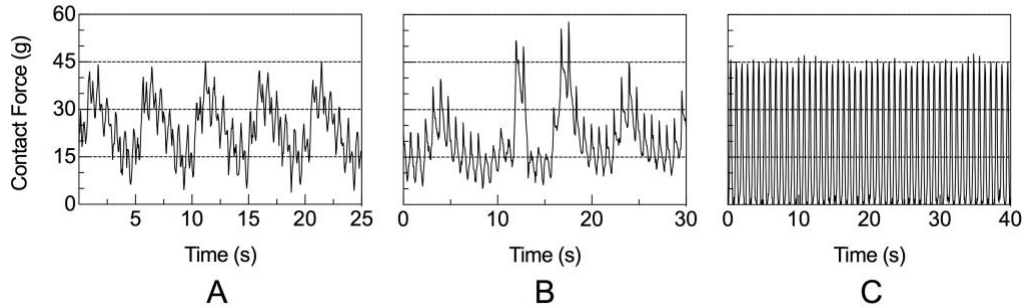
Figure 5.4. Representative CF profiles on moving tissue with approximately 600 gs FTI. **A** illustrates a CF profile caused by typical cardiorespiratory motion, **B** is a CF profile extracted from RF ablation during patient treatment, and **C** illustrates intermittent contact.
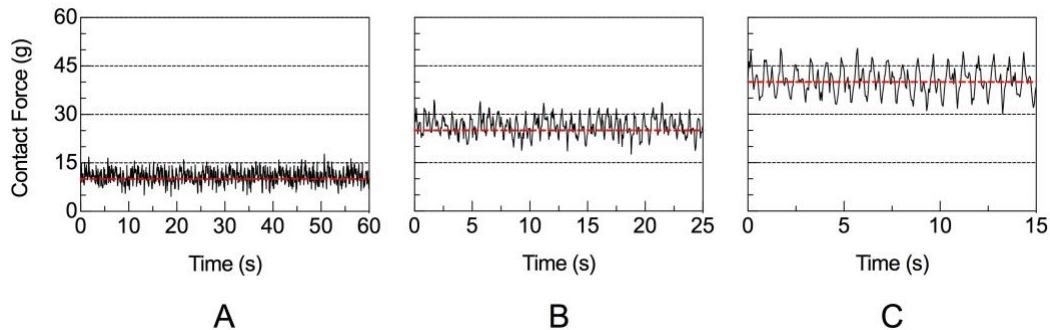
Figure 5.5. Simulated CF profiles during CFC-assisted intervention when the CFC is set to deliver 600 gs FTI at 10 g, 25 g, and 40 g set force levels, **A** to **C** respectively. Note: achieving 600 gs FTI with low set force level (10 g **A**) requires a longer lesion duration (over 60 s), and vice-versa (**C**: 40 g over 15 s).

Using the aforementioned thigh muscle preparation, sets of ablation lesions (similarly to the protocol described in Chapter 3) can be delivered with and without the CFC. All RF applications will accumulate a total of 600 gs FTI, which can be programmed into the CFC to automatically retract the catheter once a set FTI is reached, **Figure 2.10**. Representative examples of 600-gs CF profiles using the manual approach and assisted by the CFC is illustrated in **Figure 5.4** and **Figure 5.5**, respectively.

Although all lesions will be delivered with 600 gs, we suspect a variation in lesion sizes using the manual approach, as suggested by Ullah *et al*. [18]. Specifically, we anticipate a severe drop in lesion size in the presence of intermittent contact (**Figure 5.4C**). We also suspect that 600-gs CFC-assisted intervention will results in the reproducible lesion size, regardless of the presence of cardiorespiratory motion. Lastly, we hypothesize that 600-gs CFC-assisted lesions delivered with a higher set force will yield deeper lesions versus CFC-assisted lesions set at a lower force.

The results of this experiment would further demonstrate the importance of maintaining reduced variability in CF during RF application. Although there is an abundance of clinical data that suggest that CF variability is a crucial element to lesion production, there are no studies to date that show the importance of CF variability in lesion production in the context of FTI. Although FTI is a useful marker for lesion assessment, it may not tell the full story.

5.3.2.3   Catheter Stability Under Contact-Force Control

Maintaining spatiotemporal stability is critical for efficient transfer of RF energy into the tissue, resulting in a deeper, more durable RF ablation lesion. In the clinic, the stability of the catheter in relation to its target is affected by applied forces to the tip of the catheter, primarily caused by cardiorespiratory tissue motion. This results in the catheter sliding along the endocardium dispersing RF energy over a wider area, as illustrated in **Figure 5.6**.

Increased catheter drift is associated with reduced ablation efficacy [18]. Specifically, catheter drift of less than 3.5 mm is associated with a higher impedance drop, even if FTI remains constant. A 300-gs lesion with less than 3.5 mm drift has the same impedance drop in comparison to a 500-gs lesion with greater than 3.5 mm drift. Furthermore, FTI levels greater than 400 gs did not significantly increase the impedance drop if catheter drift exceeded 3.5 mm. However, a stable catheter tip showed a strong correlation between impedance drop and FTI levels up to 900 gs. Therefore, the authors suggest that achieving

more efficacy lesion production is ensuring greater spatiotemporal stability, rather than just ablate to a higher FTI.
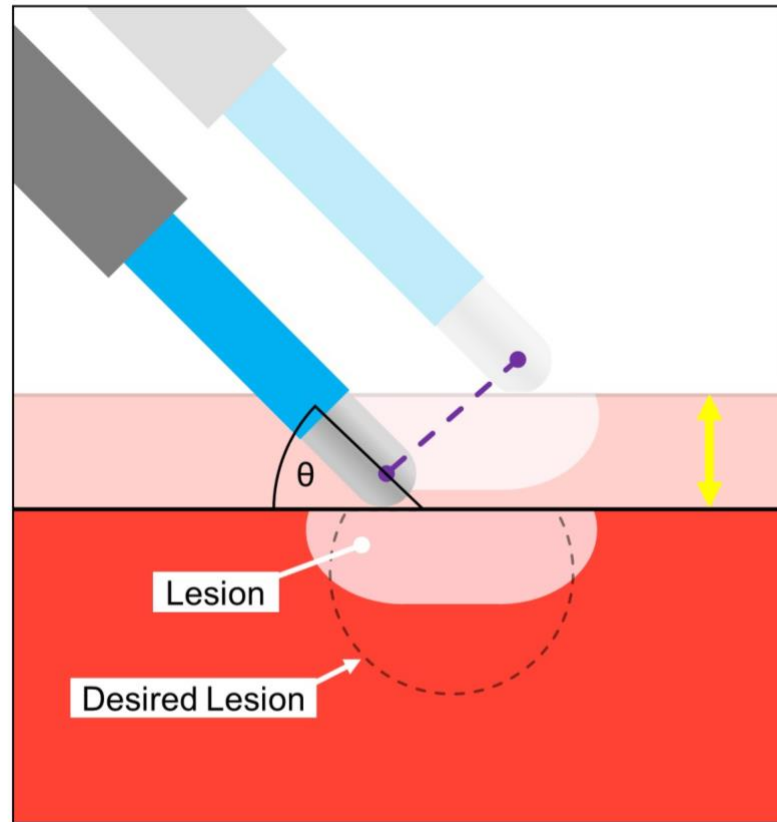
Figure 5.6. Cardiorespiratory tissue motion (indicated in yellow) causes the catheter tip to slide along the surface of the endocardium (indicated in purple). This results in a linear but shallow ablation lesion. This effect may depend on the catheter-tissue incident angle, θ.

The CFC enables CF control by adjusting the catheter within the sheath by reacting to the same applied external forces that cause catheter drift (cardiorespiratory motion). This suggests that the CFC may have an impact on catheter tip stability. In our original CFC studies (Chapter 2 and Chapter 3), CF control was of primary focus and catheter drift was not evaluated. To this end, we propose an additional *in vivo* study to evaluate if using the CFC will improve spatiotemporal stability.

The clinical techniques to measure catheter drift, performed by Ullah *et al*. [18], can be adopted *in vivo* within a thigh muscle preparation. Illustrated in **Figure 5.7**, a mapping catheter can be introduced and suspended in the blood pool within femoral chamber ensuring its position is not compromised by the moving tissue – this catheter will be used as the reference position for accurate calculation of catheter drift. Several sets of RF applications can be delivered to the tissue at different force levels and catheter-tissue incident angles. The coordinates of the tip of both ablation and mapping catheters can be recorded by the EAM system, which will be used to calculate the maximum relative drift. Statistical analysis will determine if using the CFC provides improved spatiotemporal stability over the manual approach and if either the set force level or incidence angle is significant.
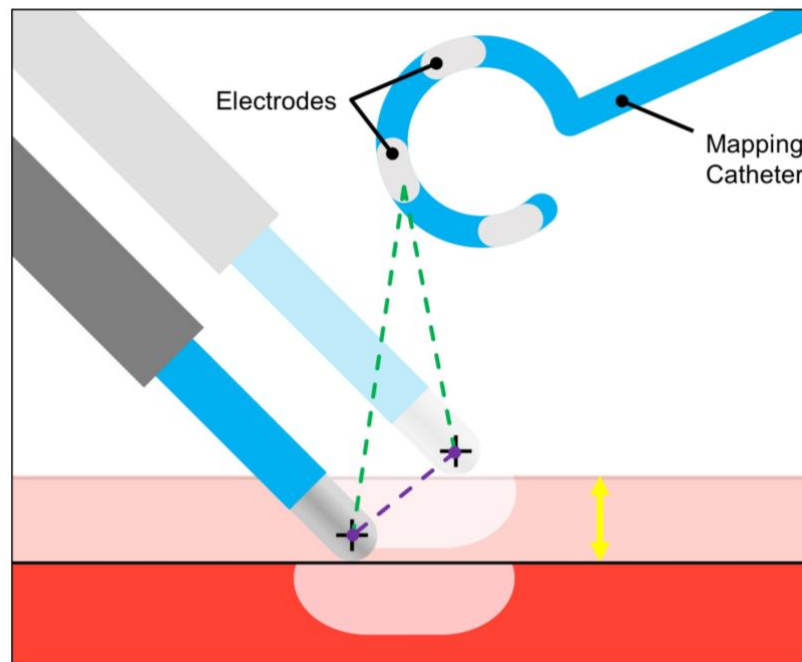

Figure 5.7. A secondary mapping catheter (in the form of a lasso), affixed to ensure it is not influenced by tissue motion (yellow), is used to track (green) the position of the RF electrode tip of the ablation catheter. The maximum catheter drift (purple) can be then determined.

It is hypothesized that CF control of the catheter tip will enhance spatiotemporal stability of the catheter tip. Therefore, the CFC-assisted ablation will likely improve spatiotemporal stability over the manual approach. The results from this experiment may suggest that CFC-assisted intervention may provide ancillary benefit in improving RF lesion production.

5.3.2.4   High-Power Short-Duration Ablation

Assessment of RF lesion production is a combination of CF, power, and duration. To this end, emerging RF catheter ablation techniques include delivering high-power RF energy (70-90 W) into the cardiac tissue for a short duration (4-8 seconds). The potential benefit of high-power short-duration (HPSD) ablation is to reduce the effects of lesion-to-lesion variability and catheter instability that cause partial-thickness lesion production. HPSD ablation results in improved linear continuity, shorter ablation time, and a safety profile comparable to conventional ablation. The less time the catheter is engaged with the tissue during an RF application, the less potential variability in lesion production.
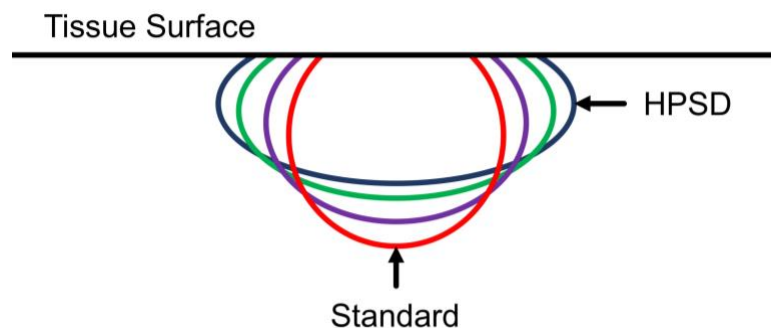
Figure 5.8. Overlay view of line drawings illustrating lesion geometries resulting from different RF lesion settings: 30 W 30 s (red), 50 W 13 s (purple), 60 W 10 s (green), 70 W 7 s (blue). The image was adapted from the original paper, published by Bourier *et al.* [19].

In comparison to standard RF ablation settings (20-35 W for 30-60 seconds), HPSD ablation results in similar lesion volumes but significantly different lesion geometries [19]. Illustrated in **Figure 5.8**, these lesions are generally shallower and with a larger diameter,

which may contribute to the better encirclement of PVs by reducing gaps between adjacent lesions and may suitable for PVI.

Successful ablation using HPSD application has been shown porcine models undergoing PVI [20-23]. In one study, HPSD applications were delivered with 90 W for 4 seconds with an average CF of 14 g $\pm$ 2.6 g, while maintaining an optimal CF range between 10 g and 20 g [20], resulting in successful ablation with no steam pops or adverse effects. In contrast, in a different study, HPSD ablations were delivered in swine using the same ablation settings and did experience steam pops [21]. In these events, HPSD applications delivered in the right side of the heart had an average CF between 40 g and 60 g, causing an audible steam pop within 3 seconds of RF application. Another group reported that achieving the desired CF was of prime priority and maintained CF of 10.3 $\pm$ 1.4 g [23]. Nonetheless, the group incurred steam pops in 11% of HPSD applications with settings of 80 W for 5 seconds. These preclinical studies suggest implications for HPSD in treating human patients, primarily, that EPs would need to maintain and follow stringent CF guidelines. However, as discussed in detail in the Introduction section of this thesis, EPs do not have sufficient tools and techniques to maintain a stable CF and regularly exceed force levels well beyond 40 g along a 4-second window. These studies also reported a range of lesion depths between 1 mm and 8 mm, analyzed over hundreds of HPSD applications [21, 22]. Importantly the variability of lesion depths achieved in HPSD applications is comparable to lesions delivered using standard RF settings. In an editorial written by Patel and Padanilam [24], they report that large standard deviations in HPSD lesion sizes may result in the same problems associated with conventional ablation therapy. Specifically, each lesion should be sized for a particular anatomical site – meaning – shallow lesions should be delivered to thin tissue, and deep lesions should be delivered to thick tissue. "The search for the perfect burn must continue." The results obtained in this thesis, specifically to the CFC, suggests that this technology may assist in HPSD ablation techniques.

No results have been reported, investigating CF variability in HPSD lesion production. However, it is evident that CF variability plays a significant role in the successful delivery of these lesions. To this end, we propose a final *in vivo* experiment to further investigate CF control and its impact on HPSD lesion production. Using a thigh preparation, several HPSD ablation sets can be delivered to moving tissue with and without the assistance of the CFC. Discussed in detail in the previous sections, similar ablation parameters, lesion measurement and analysis protocols can be followed to determine if CF variability plays a significant role in HPSD application and if the incorporation of the CFC provides a solution to ensuring reliable delivery of these lesions.

5.3.3   Clinical Evaluation of the CFC

The overarching goal to introduce the CFC to the clinic and perform the first-in-human clinical evaluation. The purpose of the first trial is to demonstrate the safety and efficacy of the CFC. A similar experimental protocol, outlined in Chapter 3 *in vivo* experiments, will be followed. The tip of a force-sensing ablation catheter guided with a steerable sheath will be navigated to targets in the RA. The CFC will then be employed at different set force levels typically desired for RA ablation strategies. CF profiles will be recorded and compared to the manual approach. In this first low-risk clinical trial, no RF applications will be delivered. Additional data including spatiotemporal stability will be collected to demonstrate the improved performance provided by the CFC.

To evaluate the CFC in a clinical setting, an authorization to perform investigational testing (issued by Health Canada) is required. Acquiring approval includes demonstrating safety and efficacy through extensive *in vitro* and *in vivo* experimentation. The preliminary data collected in this thesis provides a strong foundation to aid in this application. The additional preclinical experiments, proposed and outlined in the previous section, will provide further validation demonstrating that the device is safe and effective in maintaining a stable CF

between the catheter tip and moving tissue. These data will help meet the regulatory requirements to secure authorization and bring the CFC technology to clinical evaluation.

5.4   References

[1]   H. Makimoto *et al.*, "Incidence and anatomical locations of catheter instability during circumferential pulmonary vein isolation using contact force," *Int Heart J,* vol. 55, no. 3, pp. 249-55, 2014

[2]   A. Sarkozy *et al.*, "Contact force variability during catheter ablation of atrial fibrillation: the role of atrial rhythm and ventricular contractions: co-force AF Study," *Circ Arrhythm Electrophysiol,* vol. 8, no. 6, pp. 1342-50, 2015

[3]   L. Cercenelli, B. Bortolani, and E. Marcelli, "CathROB: A Highly Compact and Versatile Remote Catheter Navigation System," *Appl Bionics Biomech,* vol. 2017, no. 2712453, 2017

[4]   P. M. Loschak, A. Degirmenci, Y. Tenzer, C. M. Tschabrunn, E. Anter, and R. D. Howe, "A Four Degree of Freedom Robot for Positioning Ultrasound Imaging Catheters," *J Mech Robot,* vol. 8, no. 5, pp. 0510161-510169, 2016

[5]   P. M. Loschak, A. Degirmenci, Y. Tenzer, and R. D. Howe, "A 4-DOF Robot for Positioning Ultrasound Imaging Catheters," *Proc ASME Des Eng Tech Conf,* vol. 5A, 2015

[6]   P. M. Loschak, L. J. Brattain, and R. D. Howe, "Automated pointing of cardiac imaging catheters," in *Int Conf Robot Autom*, IEEE, 2013, pp. 5794-9.

[7]   P. M. Loschak, L. J. Brattain, and R. D. Howe, "Algorithms for Automatically Pointing Ultrasound Imaging Catheters," *IEEE Trans Robot,* vol. 33, no. 1, pp. 81-91, 2017

[8]   S. Hasanzadeh, F. Janabi-Sharifi, and P. Keenan, "Backlash characterization and position control of a robotic catheter manipulator using experimentally-based kinematic model," *Mechatronics,* vol. 44, pp. 94-106, 2017

[9]   Y. Ganji, F. Janabi-Sharifi, and A. N. Cheema, "Robot-assisted catheter manipulation for intracardiac navigation," *Int J Comput Assist Radiol Surg,* vol. 4, no. 4, pp. 307-15, 2009

[10]   H. Nakagawa *et al.*, "Comparison of in vivo tissue temperature profile and lesion geometry for radiofrequency ablation with a saline-irrigated electrode versus temperature control in a canine thigh muscle preparation," *Circulation,* vol. 91, no. 8, pp. 2264-73, 1995

[11]   C. Weiss *et al.*, "Transmembraneous irrigation of multipolar radiofrequency ablation catheters: induction of linear lesions encircling the pulmonary vein ostium without the risk of coagulum formation?," *J Interv Card Electrophysiol,* vol. 10, no. 3, pp. 199-209, 2004

[12]   C. Weiss, M. Antz, F. Thuneke, T. Meinertz, K. H. Kuck, and S. Willems, "Radiofrequency catheter ablation using long coiled electrodes: impact of irrigation on lesion dimensions and incidence of coagulum formation," *Pacing Clin Electrophysiol,* vol. 24, no. 6, pp. 933-8, 2001

[13]   J. Moreno *et al.*, "Morphological and thermodynamic comparison of the lesions created by 4 open-irrigated catheters in 2 experimental models," *J Cardiovasc Electrophysiol,* vol. 25, no. 12, pp. 1391-9, 2014

[14]   A. A. Hussein *et al.*, "Radiofrequency Ablation with an Enhanced-Irrigation Flexible-Tip Catheter versus a Standard-Irrigation Rigid-Tip Catheter," *Pacing Clin Electrophysiol,* vol. 38, no. 10, pp. 1151-8, 2015

[15]   D. Holmes *et al.*, "Contact sensing provides a highly accurate means to titrate radiofrequency ablation lesion depth," *J Cardiovasc Electrophysiol,* vol. 22, no. 6, pp. 684-90, 2011

[16]   E. Leshem, C. M. Tschabrunn, F. M. Contreras-Valdes, I. Zilberman, and E. Anter, "Evaluation of ablation catheter technology: Comparison between thigh preparation model and an in vivo beating heart," *Heart Rhythm,* vol. 14, no. 8, pp. 1234-40, 2017

[17]   D. C. Shah, H. Lambert, H. Nakagawa, A. Langenkamp, N. Aeby, and G. Leo, "Area under the real-time contact force curve (force-time integral) predicts radiofrequency lesion size in an in vitro contractile model," *J Cardiovasc Electrophysiol,* vol. 21, no. 9, pp. 1038-43, 2010

[18]   W. Ullah *et al.*, "Factors affecting catheter contact in the human left atrium and their impact on ablation efficacy," *J Cardiovasc Electrophysiol,* vol. 26, no. 2, pp. 129-36, 2015

[19]   F. Bourier *et al.*, "High-power short-duration versus standard radiofrequency ablation: Insights on lesion metrics," *J Cardiovasc Electrophysiol,* vol. 29, no. 11, pp. 1570-5, 2018

[20]   M. Barkagan, F. M. Contreras-Valdes, E. Leshem, A. E. Buxton, H. Nakagawa, and E. Anter, "High-power and short-duration ablation for pulmonary vein isolation: Safety, efficacy, and long-term durability," *J Cardiovasc Electrophysiol,* vol. 29, no. 9, pp. 1287-96, 2018

[21]   E. Leshem *et al.*, "High-Power and Short-Duration Ablation for Pulmonary Vein Isolation: Biophysical Characterization," *JACC Clin Electrophysiol,* vol. 4, no. 4, pp. 467-79, 2018

[22]   G. Rozen *et al.*, "Safety and efficacy of delivering high-power short-duration radiofrequency ablation lesions utilizing a novel temperature sensing technology," *Europace,* vol. 20, no. Fi_3, pp. f444-f450, 2018

[23]   A. Bhaskaran *et al.*, "Five seconds of 50-60 W radio frequency atrial ablations were transmural and safe: an in vitro mechanistic assessment and force-controlled in vivo validation," *Europace,* vol. 19, no. 5, pp. 874-80, 2017

[24]   P. J. Patel and B. J. Padanilam, "High-power short-duration ablation: Better, safer, and faster?," *J Cardiovasc Electrophysiol,* vol. 29, no. 11, pp. 1576-7, 2018

Appendices

A. Permissions for Reproduction of Scientific Articles

B.   CFC Motor Requirements: Velocity, Acceleration, and Torque

It is critical that the motor used in the CFC can exceed peak speed and acceleration of endocardial tissue. An abundant amount of information relating to this subject is available in the literature [1-5]. Myocardial velocities have been shown – using tissue Doppler imaging – not to exceed 10 cm/s, with less than 1000 cm/s^2.
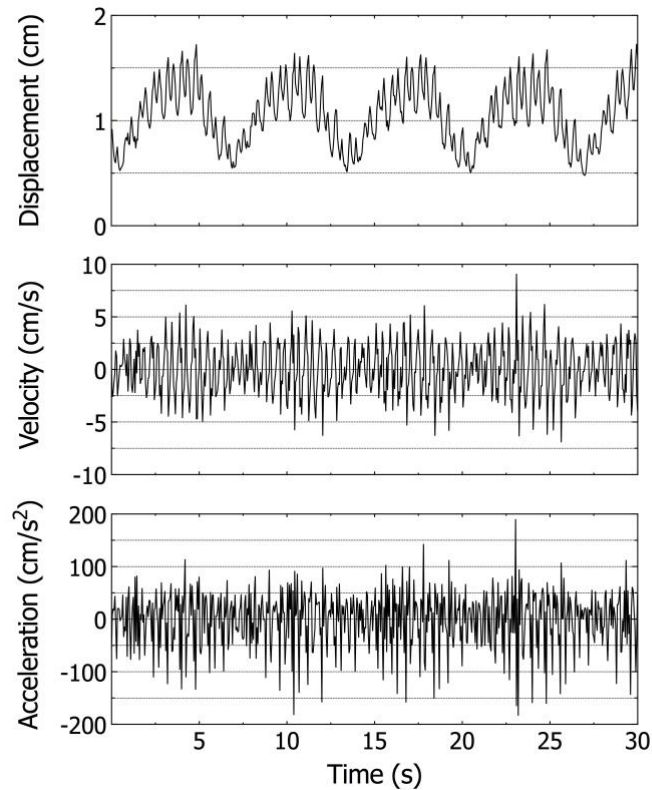
In addition to existing literature, I analyzed hundreds of contact-force profiles recorded during RF ablation in patients. These profiles were converted to position profiles based on Hooke's law. Specifically, the force profiles were empirically scaled down until the systolo-diastolic displacement matches those measured in human, typically between 3-6 mm peak-to-peak [6, 7]. The final "scaling" provided a conversion of 30 g to 1 cm. The derivative and second-derivatives provided velocity and acceleration profiles. A representative example is provided above; maximum displacement (top), velocity

(middle), and acceleration (bottom) are similar to the ones reported in the literature. These figures roughly provide maximum velocities and acceleration of tissue motion, and not necessarily true minimum requirements for the motor. The velocity/acceleration requirements for the motor should also consider the compliance of the catheter through the sheath (as it is not entirely rigid). The motor selected and used in this thesis has a maximum velocity of 230 cm/s and acceleration of 6570 cm/s^2 exceeding the requirements determined above.

For easy movement through the sheath, the motor must have torque capacity that overcomes the friction between the catheter and hemostatic seal and between the catheter shaft and the sheath itself. I used the setup, shown below, to measure the friction that must be overcome between the catheter and sheath components.
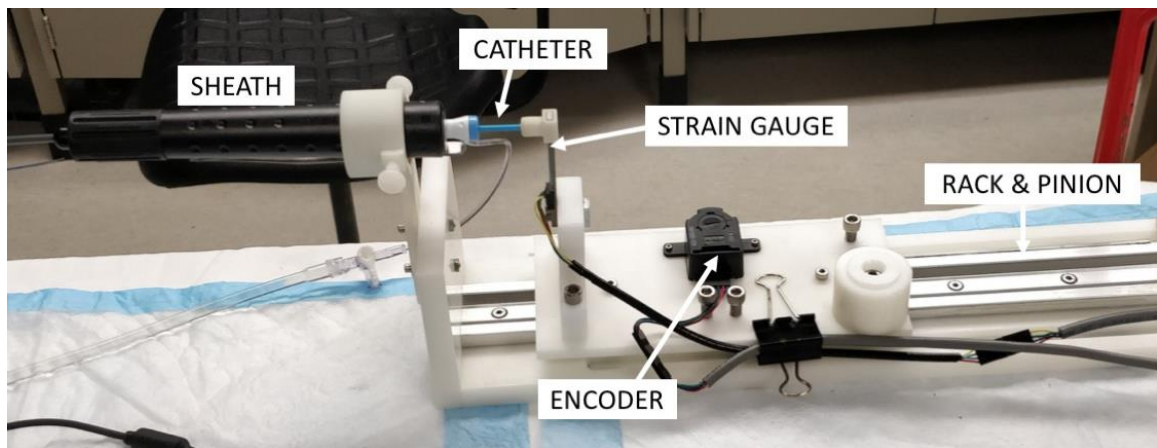
In this experiment, a strain gauge was fixed to a linear carriage which glides along a rail. The linear position of the carriage is detected using an encoder coupled to a rack and pinion mechanism. The carriage was moved back and forth rapidly, and the friction and velocity of the carriage were recorded by a microcontroller electronics system (not shown). Data were recorded while the sheath was in the neutral position (not deflected) as well as deflected to approximately 120°, illustrated below.
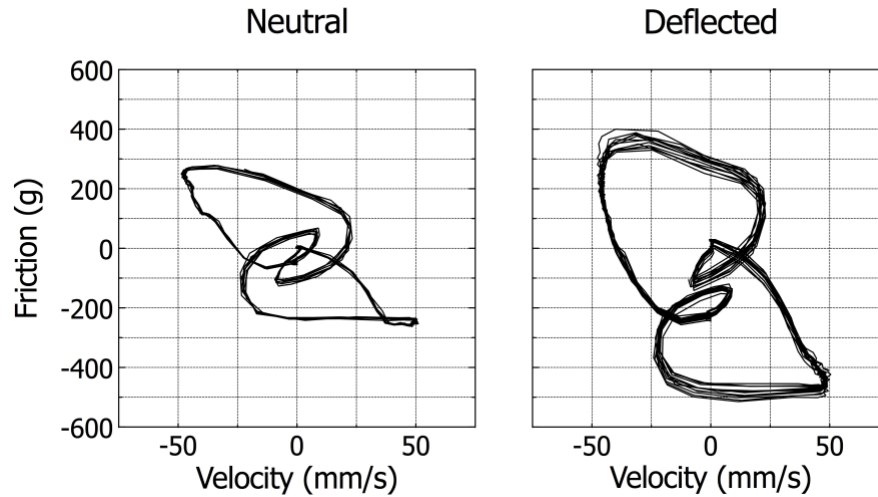
With the sheath in the neutral position, the amount of force required to move the catheter through the sheath did not exceed 250 g, illustrated below. While the sheath was deflected, the amount of force increased to 400 g. If the sheath is fully deflected to a maximum of 180° (not likely used in clinic), the required force can climb to 550 g. The amount of force required to translate the catheter through the sheath far exceeds the amount of force the catheter pushes onto the tissue (less 40 g).

In the clinic, physiological 0.9% saline is introduced into the irrigation port of the steerable sheath to provide passive irrigation to reduce the friction between the catheter and sheath. The above experiment was performed with this condition as well as repeated in the absence of any lubrication. In dry conditions, the maximum force increased by an additional 40 g. This was performed to ensure that the selected motor of the CFC can withstand the highest friction possible.

C.   CFC Control Systems

The CFC was integrated with a commercially available electro-anatomical catheter mapping system (CARTO® 3, Biosense Webster, Irvine, CA) to receive real-time force information from the tip of a force-sensing ablation catheter (THERMOCOOL®

SMARTTOUCH™, Biosense Webster, Irvine, CA). A local area network connection was used to establish communication between the mapping and CFC systems. Significant degradation in the measurement of real-time CF (*i.e.* slow 20 Hz sampling rate, long time-delay, noise, *et cetera*) was discovered. Because of this, two control systems were developed to provide compensation for a wide variety of variations in CF caused by cardiac and respiratory tissue motion, or patient and catheter motion.

The following sections briefly describe two control systems used in the CFC system. The *adaptive* and *repetitive* control systems were first implemented in MATLAB Simulink (Mathworks, Natick, MA) and their response to changes in CF was evaluated in a simulated environment. I implemented both control systems in the electronic hardware of the CFC as software code processed on an ARM-based microcontroller (Arduino Due, Arduino, Turin, Italy).

Adaptive Control System

The model reference adaptive control (MRAC) system is a direct adaptive strategy that uses an adjustment mechanism to adjust the response of the controller [8]. In comparison to standard simple-structured fixed-gain controllers, such as the proportional-integral-derivative (PID) controllers, adaptive controllers are very useful in handling the unknown variations in parameters and environmental changes (*e.g.* change in catheter angle, tissue compliance, deflection of sheath tip).

The MRAC, illustrated in the block diagram below, consists of two loops, a standard feedback loop and parameter adjustment loop. The adjustment mechanism uses the constant gain to reduce the cost function to zero in an iterative process. This strategy works on the principle of adjusting the controller parameters so that the output of the system plant (measured force), $P(s)$, tracks the output of a reference model, $R(s)$, having the same reference input (desired force). The reference input is first filtered by a low-pass filter, $S(s)$.

An adjustment mechanism uses a learning rate, γ, to reduce the cost function to zero. The controller, *C(s)*, takes the form of a standard integral (I) controller and generates a control signal which is sent to the linear motor of the force controller. All models were implemented as discrete-time transfer functions as software code on the microcontroller-based electronic system of the CFC.
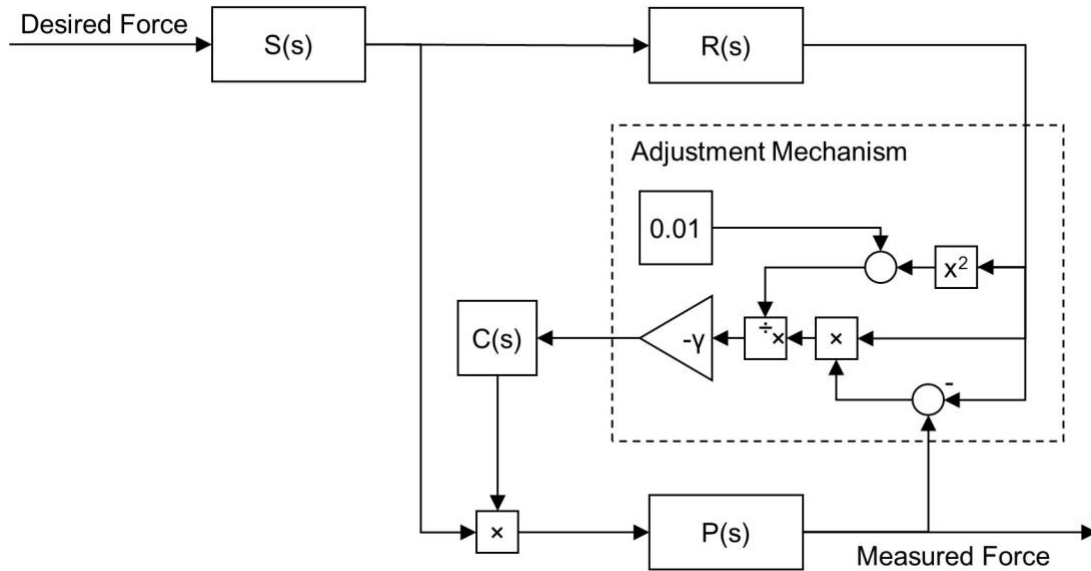
Through simulation, the MRAC was found to be an adequate controller to compensate for gradual disturbances in CF changes, such as those caused by respiration, patient and catheter motion. Additionally, this strategy is stable and does not increase the amplitude of higher frequency components (*i.e.* cardiac motion); a common problem associated with poorly sampled feedback closed-loop systems using standard PID controllers. The MRAC strategy provides no attempt to compensate for changes in cardiac motion.

Repetitive Control System

To compensate for substantial variation in CF caused by the systolo-diastolic motion of the heart, a repetitive control strategy was also implemented. The repetitive strategy is based on a Smith predictor, which is a predictive controller commonly used for systems with

significant time delay in the control loop [9, 10]. A Smith predictor is an appropriate solution for processes that have a dead-time (or time-delay) longer than the time constant, making it suitable for our force-control application, where the time constant is small (measured to be less than 35 ms).

A standard Smith predictor alone cannot compensate for large rapid fluctuations in CF. To address this, the standard Smith predictor was modified to enable repetitive control designed to reject *periodic* disturbances [11]. Illustrated in the block diagram below, the modified Smith predictor uses an added block to further delay the control loop by an appropriate amount in order to synchronize the feedback loop with the periodic disturbance. The known heart rate and modelled time-delay in the force sensor of the force-sensing ablation catheter are used to determine the additional delay required; this also can be used to eliminate CF variation caused by respiration. In the current implementation, the operator dials-in the desired frequency in beats per minute to eliminate CF fluctuations caused by cardiac motion, or, breaths-per-minute to eliminate respiratory motion.
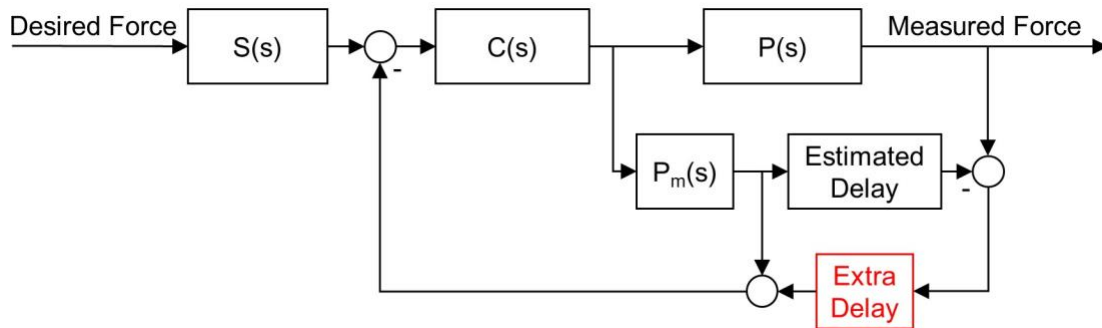
The modified Smith predictor, illustrated above, generates a control signal to the linear motor based on the controller, *C(s)*, which takes the form of a proportional-integral (PI) controller. This is based on the difference between the feedback measured force signal and the desired force, which is filtered by a low-pass filtered, *S(s)*. A delay-less model of the plant, $P_m(s)$, is a second-order transfer function modelling the real system plant, *P(s)*, to predict the force measurement ahead of time. The force sensor delay is estimated, and the

amount of extra delay (shown in red) needed to synchronize the force controller with periodic disturbance (cardiac or respiratory) is calculated by subtracting the estimated delay from the period of the disturbance. All models were implemented as discrete-time transfer functions as software code on the microcontroller-based electronic system of the CFC.

D.   Ethics Approval Notice

Western

AUP Number: 2013-064
PI Name: Drangova, Maria
AUP Title: Catheter Navigation Using A Remote Navigation System To Ablate Arrhythmic Sites In A Pig Model
Approval Date: 06/02/2014

Official Notice of Animal Use Subcommittee (AUS) Approval: Your new Animal Use Protocol (AUP) entitled "Catheter Navigation Using A Remote Navigation System To Ablate Arrhythmic Sites In A Pig Model" has been APPROVED by the Animal Use Subcommittee of the University Council on Animal Care. This approval, although valid for four years, and is subject to annual Protocol Renewal.2013-064::1

1. This AUP number must be indicated when ordering animals for this project.
2. Animals for other projects may not be ordered under this AUP number.
3. Purchases of animals other than through this system must be cleared through the ACVS office. Health certificates will be required.

The holder of this Animal Use Protocol is responsible to ensure that all associated safety components (biosafety, radiation safety, general laboratory safety) comply with institutional safety standards and have received all necessary approvals. Please consult directly with your institutional safety officers.

Submitted by: Copeman, Laura
on behalf of the Animal Use Subcommittee
University Council on Animal Care

E.   Comparison of Force Control: *In Vitro* to Simulation

The block diagram of the repetitive control loop illustrated in Appendix C (Repetitive Control System) was implemented in MATLAB Simulink (Mathworks, Natick, MA) to simulate the force control response of the SSC-RNS. A representative example comparing a robotically assisted force control experiment performed *in vitro* with its simulation is illustrated below.
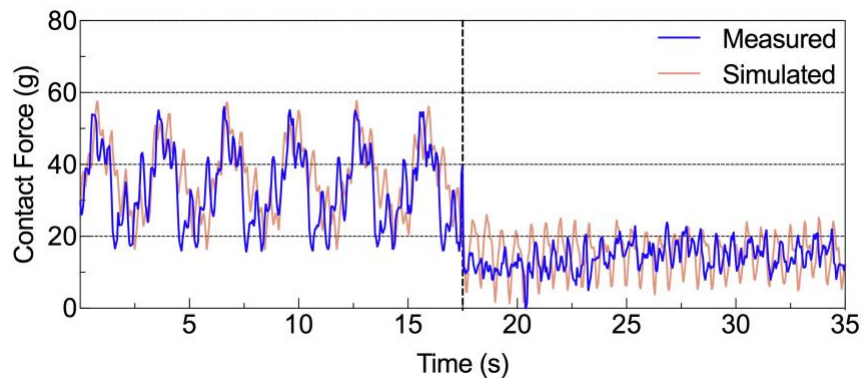
The SSC-RNS employed force control on the 17.5-second mark. For this example, the linear motion stage of the phantom was set to execute cardiac motion at 80 BPM and respiratory motion at 20 BPM with a 3:8 amplitude ratio. The motion was prescribed as the disturbance profile within the block diagram of the control loop (Appendix C, Repetitive Control System, added to the output of the plant, *P(s)*). To compensate for the dominant respiratory component, the SSC-RNS was set to respiratory gating, which synchronized the controller by further delaying the control loop by approximately one respiratory cycles period (20 BPM or 3 seconds). Respiratory gating was simulated by setting the extra delay with the control loop (Appendix C, Repetitive Control System, extra delay block in red) to the same amount. The measured CF profile and its simulated response demonstrated complete elimination of the large swings in force caused by respiration. In comparison to the simulation, the measured response demonstrated a slightly better CF control performance *in vitro*.

References

[1]   L. Thomas, K. Levett, A. Boyd, D. Y. Leung, N. B. Schiller, and D. L. Ross, "Changes in regional left atrial function with aging: evaluation by Doppler tissue imaging," *Eur J Echocardiogr,* vol. 4, no. 2, pp. 92-100, 2003

[2]   M. Duytschaever *et al.*, "Transthoracic tissue Doppler imaging of the atria: a novel method to determine the atrial fibrillation cycle length," *J Cardiovasc Electrophysiol,* vol. 17, no. 11, pp. 1202-9, 2006

[3]   I. Limantoro *et al.*, "Clinical correlates of echocardiographic tissue velocity imaging abnormalities of the left atrial wall during atrial fibrillation," *Europace,* vol. 16, no. 11, pp. 1546-53, 2014

[4]   N. Yoshida, M. Okamoto, and T. Fukuhara, "Left atrial wall motion velocity measured by the velocity profile method with tissue Doppler echocardiography in normal subjects: its relation to aging," *J Med Ultrason (2001),* vol. 31, no. 3, pp. 103-9, 2004

[5]   K. Mori, Y. Hayabuchi, Y. Kuroda, M. Nii, and T. Manabe, "Left ventricular wall motion velocities in healthy children measured by pulsed wave Doppler tissue echocardiography: normal values and relation to age and heart rate," *J Am Soc Echocardiogr,* vol. 13, no. 11, pp. 1002-11, 2000

[6]   H. Skulstad *et al.*, "Grading of myocardial dysfunction by tissue Doppler echocardiography: a comparison between velocity, displacement, and strain imaging in acute ischemia," *J Am Coll Cardiol,* vol. 47, no. 8, pp. 1672-82, 2006

[7]   A. Manouras *et al.*, "Are measurements of systolic myocardial velocities and displacement with colour and spectral Tissue Doppler compatible?," *Cardiovasc Ultrasound,* vol. 7, p. 29, 2009

[8]   P. Jain and M. J. Nigam, "Design of a Model Reference Adaptive Controller Using Modifited MIT Rule for a Second Order System," *Advance in Electronic and Electric Engineering,* vol. 3, no. 4, pp. 477-484, 2013

[9]   O. J. M. Smith, "Closed Control of Loops with Dead Time," *Chemical Engineering Process,* 1957

[10]   A. Ingimundarson and T. Hägglund, "Robust tuning procedures of dead-time compensating controllers," *Control Engineering Practice,* vol. 9, no. 11, pp. 1195-1208, 2001

[11]   W. Qing-Guo, Z. Han-Qin, Y. Yong-Sheng, Z. Yong, and Z. Yu, "Modified Smith predictor design for periodic disturbance rejection," in *Asian Control Conference*, 2004, vol. 2: IEEE, pp. 1145-50.

Curriculum Vitae

DANIEL GELMAN, PH.D

Robarts Research Institute
University of Western Ontario
1151 Richmond St. North
London, ON, Canada
N6A 5B7

EDUCATION

Sept. 2012 Present	**Doctor of Philosophy Candidate, School of Biomedical Engineering** University of Western Ontario, London, ON, Canada *Supervisor:* Maria Drangova, Ph.D. *Thesis:* Remote Navigation and Contact-Force Control of Radiofrequency Ablation Catheters
Sept. 2007 Apr. 2012	**Bachelor of Engineering, Electrical and Biomedical Engineering** McMaster University, Hamilton, ON, Canada *Supervisor:* Hubert de Bruin, Ph.D., P.Eng. *Thesis:* Responsive EMG Static Progressive Knee Split

WORK EXPERIENCE

May 2017 Present	**Aufero Medical Technologies, Inc.** President & CEO
May 2017 Aug. 2018	**Electronics Design Engineer** Archetype Medical
Sept. 2015 Dec. 2015	**Mechatronic Systems Engineer** Robarts Research Institute
May 2012 Sept. 2012	**Instrumentation Control Systems Engineer** Brockhouse Institute for Materials Research

PUBLICATIONS & CONFERENCES

Refereed Journal Manuscripts

1. **Gelman D**, Skanes AC, Drangova M, "Remote Catheter Navigation and Contact-Force Control: Design and Evaluation of a Novel Steerable Sheath and Catheter Robotic Navigation System," *IEEE Trans Biomed Eng*, 2019. (In Preparation)

2. **Gelman D**, Skanes AC, Jones DL, Timofeyev M, Baron T, Drangova M, "Eliminating the Effects of Motion during Radiofrequency Lesion Delivery using a Novel Contact-Force Controller," *J Cardiovasc Electrophysiol*, 2019. (Accepted)

3. **Gelman D**, Skanes AC, Tavallaei MA, Drangova M, "Design and Evaluation of a Catheter Contact-Force Controller for Cardiac Ablation Therapy," *IEEE Trans Biomed Eng*, vol. 63, no. 11, pp. 2301-7, 2016.

4. Tavallaei MA, **Gelman D**, Lavdas MK, Skanes AC, Jones DL, Bax JS, Drangova M, "Design, development and evaluation of a compact telerobotic catheter navigation system," *Int J Med Robot*, vol. 12, no. 3, pp. 442-52, 2015.

5. Tavallaei MA, Lavdas MK, **Gelman D**, Drangova M, "Magnetic resonance imaging compatible remote catheter navigation system with 3 degrees of freedom", *Int J Comput Assist Radiol Surg*, vol. 11, no. 8, pp. 1537-45, 2015.

Peer-Reviewed Published Conference Abstracts

1. **Gelman D**, Skanes AC, Jones DL, Drangova M, "Catheter Contact-Force Control during Cardiac Ablation Therapy: In Vivo Evaluation," *Cardiac Arrhythmia Network of Canada*, Halifax, NS, Canada, 2017.

2. **Gelman D**, Skanes AC, Jones DL, Drangova M, "Catheter Contact-Force Control during Cardiac Ablation Therapy: In Vivo Evaluation," *Imaging Network of Ontario*, London, ON, Canada, 2017.

3. **Gelman D**, Skanes AC, Jones DL, Drangova M, " Catheter Contact-Force Control during Cardiac Ablation Therapy: In Vivo Evaluation," *London Health Research Day*, London, ON, Canada, 2017.

4. Tavallaei MA, Lavdas MK, **Gelman D**, Drangova M, "MRI-Compatible Remote Catheter Navigation System", *iMRI 2016*, Baltimore, MD, USA, 2016.

5. **Gelman D**, Skanes AC, Tavallaei MA, Drangova M, "Catheter Contact-Force Control during Cardiac Ablation Therapy: In Vitro Evaluation," *Heart Rhythm*, San Fransico, CA, USA, 2016.

6. **Gelman D**, Skanes AC, Tavallaei MA, Drangova M, "Design and Evaluation of a Catheter Contact-Force Controller for Cardiac Ablation Therapy," *Imaging Network of Ontario*, Toronto, ON, Canada, 2016.

7. Tavallaei MA, Lavdas MK, **Gelman D**, Drangova M, "MRI-Compatible Remote Catheter Navigation System with 3-Degrees-of-Freedom", *Imaging Network of Ontario*, Toronto, ON, Canada, 2016.

8. **Gelman D**, Skanes AC, Tavallaei MA, Drangova M, "Design and Evaluation of a Catheter Contact-Force Controller for Cardiac Ablation Therapy," *London Health Research Day*, London, ON, Canada, 2016.

9. **Gelman D**, Lavdas MK, Drangova M, "Real-Time Three Degree-of-Freedom Measurement of Catheter Motion for Input to a Robotic Catheter Navigation System," *IUPESM: World Congress of Medical Physics and Biomedical Engineering*, Toronto, ON, Canada, 2015.

10. **Gelman D**, Lavdas MK, Drangova M, "An Instinctive 3-Degree-of-Freedom Master-Side Input Device to a Robotic Catheter Navigation System", *Imaging Network of Ontario*, London, ON, Canada, 2015.

11. Tavallaei MA, **Gelman D**, Lavdas MK, Skanes AC, Jones DL, Drangova M, "Design, Development and in vivo Evaluation of a Remote Catheter Navigation System with 3-Degrees-of-Freedom", *Imaging Network of Ontario*, Toronto, ON, Canada, 2015.

12. **Gelman D**, Tavallaei MA, Drangova M, "Towards Semi-Autonomous Remote Cardiac Catheter Navigation," *London Health Research Day*, London, ON, Canada, 2014.

Peer-Reviewed Oral Presentations (**presenting author*)

1. **Gelman D***, Skanes AC, Jones DL, Drangova M, "Catheter Contact-Force Control for Cardiac Ablation Therapy," *Society of Cardiac Robotic Navigation*, Chicago, IL, USA, 2017.

2. **Gelman D***, Skanes AC, Jones DL, Drangova M, "Catheter Contact-Force Control during Cardiac Ablation Therapy: In Vivo Evaluation," *Imaging Network of Ontario*, London, ON, Canada, 2017.

3. **Gelman D***, Skanes AC, Tavallaei MA, Drangova M, "Catheter Contact-Force Control during Cardiac Ablation Therapy: In Vitro Evaluation," *Cardiac Arrhythmia Network of Canada*, Calgary, AB, Canada, 2016.

4. Tavallaei MA, Lavdas MK, **Gelman D***, Drangova M, "MRI-Compatible Remote Catheter Navigation System with 3-Degrees-of-Freedom", *Imaging Network of Ontario*, Toronto, ON, Canada, 2016.

5. **Gelman D***, Lavdas MK, Drangova M, "Real-Time Three Degree-of-Freedom Measurement of Catheter Motion for Input to a Robotic Catheter Navigation System," *IUPESM: World Congress of Medical Physics and Biomedical Engineering*, Toronto, ON, Canada, 2015.

6. Tavallaei MA*, **Gelman D**, Lavdas MK, Skanes AC, Jones DL, Drangova M, "Design, Development and in vivo Evaluation of a Remote Catheter Navigation System with 3-Degrees-of-Freedom", *Imaging Network of Ontario*, Toronto, ON, Canada, 2015.

Peer-Reviewed Poster Presentations (**presenting author*)

1. **Gelman D***, Skanes AC, Jones DL, Drangova M, "Catheter Contact-Force Control during Cardiac Ablation Therapy: In Vivo Evaluation," *Cardiac Arrhythmia Network of Canada*, Halifax, NS, Canada, 2017.

2. **Gelman D***, Skanes AC, Jones DL, Drangova M, " Catheter Contact-Force Control during Cardiac Ablation Therapy: In Vivo Evaluation," *London Health Research Day*, London, ON, Canada, 2017.

3. **Gelman D***, Skanes AC, Tavallaei MA, Drangova M, "Catheter Contact-Force Control during Cardiac Ablation Therapy: In Vitro Evaluation," *Cardiac Arrhythmia Network of Canada*, Calgary, AB, Canada, 2016.

4. **Gelman D***, Skanes AC, Tavallaei MA, Drangova M, "Catheter Contact-Force Control during Cardiac Ablation Therapy: In Vitro Evaluation," *Heart Rhythm*, San Francisco, CA, USA, 2016.

5. **Gelman D***, Skanes AC, Tavallaei MA, Drangova M, "Catheter Contact-Force Control during Cardiac Ablation Therapy: In Vitro Evaluation," *Imaging Network of Ontario*, Toronto, ON, Canada, 2016.

6. **Gelman D***, Skanes AC, Tavallaei MA, Drangova M, "Catheter Contact-Force Control during Cardiac Ablation Therapy: In Vitro Evaluation," *London Health Research Day*, London, ON, Canada, 2016.

7. **Gelman D***, Lavdas MK, Drangova M, "An Instinctive 3-Degree-of-Freedom Master-Side Input Device to a Robotic Catheter Navigation System", *Imaging Network of Ontario*, London, ON, Canada, 2015.

8. Tavallaei MA*, **Gelman D**, Lavdas MK, Skanes AC, Jones DL, Drangova M, "Design, Development and in vivo Evaluation of a Remote Catheter Navigation System with 3-Degrees-of-Freedom", *Imaging Network of Ontario*, Toronto, ON, Canada, 2015.

9. **Gelman D***, Tavallaei MA, Drangova M, "Towards Semi-Autonomous Remote Cardiac Catheter Navigation," *London Health Research Day*, London, ON, Canada, 2014.

GRADUATE TEACHING ASSISTANTSHIP

University of Western Ontario, London, ON, Canada

Introduction to Electrical Instrumentation (MSE2201)
Mechatronics Engineering

Electrical Circuits and Electromechanics (ECE2274)
Electrical and Computer Engineering

Introduction to Medical Imaging (BME9513)
Biomedical Engineering

Introduction to Electronics for Mechanical Engineering (ECE3374)
Electrical and Computer Engineering

Programming Fundamentals for Engineers (ES1036)
Engineering Science

Introductory Engineering Design and Innovation Studio (ES1050)
Engineering Science

GRANTS

Feb. 2018

Commercialization Grant – $300,000
Cardiac Arrhythmia Network of Canada (CANet), Co-Applicant
Funds provided to accelerate the development of promising inventions originating from the university sector to promote their transfer into the Canadian healthcare environment. The Commercialization Grant provides funding to CANet Network Investigators and CHAT Members to support research and development projects with recognized technology transfer potential.

Mar. 2017

BURST – $70,000
TechAlliance, Awarded to Aufero Medical
Incubation program for high-potential medical technology start-ups intended to position London as a focal point for life science innovation.

Sept. 2016

CHAT Discovery Award – $25,000
Cardiac Arrhythmia Network of Canada
This award supported novel research ideas from CHAT (CANet HQP Association for Trainees) members. Funds were granted to the trainees to initiate their proposed research project under the supervision/mentoring of a CANet Network Investigator (Dr. Drangova). A single $25,000 award given annually.

SCHOLARSHIPS

Aug. 2019
Aug. 2021

Entrepreneurship-Accelerate Postdoctoral Fellowship – $110,000
Mitacs (Aufero Medical as Industry Partner)

May 2016
Apr. 2017

Ontario Graduate Scholarship – $15,000
University of Western Ontario

Sept. 2013
Sept. 2015

NSERC CREATE: CAMI – $24,000
University of Western Ontario

COMMITTEES & VOLUNTEER ACTIVITIES

Aug. 2017
Mar. 2018

2017/18 Proteus Innovation Competition
Aufero Medical
Technology featured as a part of the competition.

Apr. 2017
Present

CHAT Executive Committee
Cardiac Arrhythmia Network of Canada
Currently organizing and chairing a session on Pathway to Commercialization at 2019 CANet Annual Scientific Meeting.

Feb. 2015	**Recruitment Event: Robotic Catheter Systems** University of Western Ontario, School of Biomedical Engineering
Jan. 2015 *Jan. 2017*	**Pedagogy Committee** University of Western Ontario, School of Biomedical Engineering

PATENTS

July 2018	**Catheter Contact-Force Control Device** National Phase Submission CA3013270A US16/074,753 EP17746678.6A CN201780020658.0A JP2018558456A
Feb. 2017	**Catheter Contact-Force Control Device** PCT Application PCT/CA2017/050119
Feb. 2016	**Catheter Contact-Force Control Device** US Provisional US62/290,243

TECHNOLOGY TRANSFER

July 2018	**Licensing Agreement; Catheter Contact-Force Control** Aufero Medical
May 2017	**Aufero Medical Technologies, Inc.** Incorporation